Three-dimensional climatological distribution of tropospheric OH' Update and evaluation

C. M. Spivakovsk, J. A. Logan, S. A. Montzka, Yves Balkanski, M. Foreman-Fowler, D . B. A. Jones, L. W. Horowitz, a C Fusco, C. A. M. Brenninkmeijer, M. J. Prather, et al.

JOURNAL OF GEOPHYSICAL RESEARCH, VOL. 105, NO. D7, PAGES 8931–8980, APRIL 16, 2000

Three-dimensional climatological distribution of tropospheric OH: Update and evaluation

C. M. Spivakovsky,[1] J. A. Logan,[1] S. A. Montzka,[2] Y. J. Balkanski,[1,3] M. Foreman-Fowler,[1,4] D. B. A. Jones,[1] L. W. Horowitz,[1,5] A. C. Fusco,[1] C. A. M. Brenninkmeijer,[6] M. J. Prather,[7] S. C. Wofsy,[1] and M. B. McElroy[1]

Abstract. A global climatological distribution of tropospheric OH is computed using observed distributions of O_3, H_2O, NO_t (NO_2+NO+$2N_2O_5$+NO_3 +HNO_2+HNO_4), CO, hydrocarbons, temperature, and cloud optical depth. Global annual mean OH is 1.16×10^6 molecules cm^{-3} (integrated with respect to mass of air up to 100 hPa within ±32° latitude and up to 200 hPa outside that region). Mean hemispheric concentrations of OH are nearly equal. While global mean OH increased by 33% compared to that from *Spivakovsky et al.* [1990], mean loss frequencies of CH_3CCl_3 and CH_4 increased by only 23% because a lower fraction of total OH resides in the lower troposphere in the present distribution. The value for temperature used for determining lifetimes of hydrochlorofluorocarbons (HCFCs) by scaling rate constants [*Prather and Spivakovsky*, 1990] is revised from 277 K to 272 K. The present distribution of OH is consistent within a few percent with the current budgets of CH_3CCl_3 and HCFC-22. For CH_3CCl_3, it results in a lifetime of 4.6 years, including stratospheric and ocean sinks with atmospheric lifetimes of 43 and 80 years, respectively. For HCFC-22, the lifetime is 11.4 years, allowing for the stratospheric sink with an atmospheric lifetime of 229 years. Corrections suggested by observed levels of CH_2Cl_2 (annual means) depend strongly on the rate of interhemispheric mixing in the model. An increase in OH in the Northern Hemisphere by 20% combined with a decrease in the southern tropics by 25% is suggested if this rate is at its upper limit consistent with observations of CFCs and ^{85}Kr. For the lower limit, observations of CH_2Cl_2 imply an increase in OH in the Northern Hemisphere by 35% combined with a decrease in OH in the southern tropics by 60%. However, such large corrections are inconsistent with observations for ^{14}CO in the tropics and for the interhemispheric gradient of CH_3CCl_3. Industrial sources of CH_2Cl_2 are sufficient for balancing its budget. The available tests do not establish significant errors in OH except for a possible underestimate in winter in the northern and southern tropics by 15–20% and 10–15%, respectively, and an overestimate in southern extratropics by ~25%. Observations of seasonal variations of CH_3CCl_3, CH_2Cl_2, ^{14}CO, and C_2H_6 offer no evidence for higher levels of OH in the southern than in the northern extratropics. It is expected that in the next few years the latitudinal distribution and annual cycle of CH_3CCl_3 will be determined primarily by its loss frequency, allowing for additional constraints for OH on scales smaller than global.

1. Introduction

Ever since *Levy* [1971] presented a model of tropospheric chemistry with the hydroxyl radical as the key species, efforts have continued to estimate accurately its concentration in the troposphere [e.g., *McConnell et al.*, 1971; *Weinstock and Niki*, 1972; *Warneck*, 1974; *Wofsy*, 1976; *Singh*, 1977a, b; *Lovelock*, 1977; *Crutzen and Fishman*, 1977; *Fishman et al.*, 1979; *Makide and*

Paper number 1999JD901006.
0148–0227/00/1999JD901006$09.00

[1]Department of Earth and Planetary Sciences and Division of Engineering and Applied Sciences, Harvard University, Cambridge, Massachusetts.

[2]NOAA Climate Monitoring and Diagnostics Laboratory, Boulder, Colorado.

[3]Now at Laboratoire des Sciences du Climat et de l'Environnement, Gif-sur Yvette, France.

[4]Now at Steelhead Machine and Design Company, Albuquerque, New Mexico.

[5]Now at Atmospheric and Oceanic Sciences Program, Princeton University, Princeton, New Jersey.

[6]Max Planck Institute for Chemistry, Mainz, Germany.

[7]Department of Geoscience, University of California, Irvine.

Rowland, 1981; *Logan et al.*, 1981; *Chameides and Tan*, 1981; *Volz et al.*, 1981; *Crutzen and Gidel*, 1983; *Prinn et al.*, 1983, 1987, 1992, 1995; *Khalil and Rasmussen*, 1984; *Fraser et al.*, 1986; *Thompson and Cicerone*, 1986a, b; *Spivakovsky et al.*, 1990; *Thompson et al.*, 1990; *Crutzen and Zimmermann*, 1991; *Brenninkmeijer et al.*, 1992; *Mak et al.*, 1992, 1994; *Krol et al.*, 1998]. The abundance of OH determines lifetimes for CH_4, CO, and a variety of industrial pollutants, but the quest for accuracy has roots beyond the need to estimate the lifetimes of these gases. The chemistry of OH comprises tightly coupled, mutually compensating reactions which in effect provide a buffer against changes in precursors and rate constants. Decades apart, *Levy* [1971], *Logan et al.* [1981], and *Spivakovsky et al.* [1990] derived similar estimates for the abundance of OH in the troposphere despite considerable evolution in the understanding of both the chemical mechanism and the characterization of precursors. Errors of 15–25% in the global mean concentration of OH may signify major misconceptions about the chemistry or the abundance of precursors of OH in the troposphere. At the same time, testing global models for OH has been associated with uncertainties of a similar or larger magnitude intrinsic to deriving an estimate indirectly from budgets of species for which reaction with OH provides the dominant sink and the sources are believed to be known CH_3CCl_3 [e.g., *Singh*, 1977a, b; *Lovelock*, 1977; *Makide and Rowland*, 1981; *Logan et al.*, 1981; *Chameides and Tan*, 1981; *Khalil and Rasmussen*, 1984; *Fraser et al.*, 1986; *Prinn et al.*, 1983, 1987, 1992, 1995] and ^{14}CO [e.g., *Weinstock and Niki*, 1972; *Volz et al.*, 1981; *Brenninkmeijer et al.*, 1992; *Mak et al.*, 1992, 1994] (see *Thompson* [1994] for a review of studies of tropospheric OH through the early 1990s).

Significant recent developments have affected both direct and indirect methods for estimating the abundance of OH in the troposphere. Most notably, the budget of CH_3CCl_3 was modified by an 18% decrease in the calibration of CH_3CCl_3 [*Prinn et al.*, 1995], a decrease in the recommended rate constant for reaction with OH (by ~15% at 277 K) [*Talukdar et al.*, 1992] and the discovery of an ocean sink [*Butler et al.*, 1991]. Observations of *Brenninkmeijer et al.* [1992], *Brenninkmeijer* [1993] and *Mak et al.* [1992, 1994], together with earlier measurements of *Volz et al.* [1981], provided for the first time a comprehensive description of the tropospheric distribution of ^{14}CO. Initial interpretation of these measurements indicated significantly higher concentrations of OH than those predicted by models or inferred from the budget of CH_3CCl_3 at the time [*Mak et al.*, 1992]. In addition, lower concentrations of ^{14}CO in the Southern Hemisphere (SH) than in the Northern Hemisphere (NH) led to the suggestion that concentrations of OH are significantly lower in northern than in southern midlatitudes [*Brenninkmeijer et al.*, 1992], whereas most models predicted slightly higher concentrations of OH in the north [e.g., *Spivakovsky et al.*, 1990, *Crutzen and Zimmermann*, 1991]. Increasingly, however, it has been recognized that concentrations of ^{14}CO are as sensitive to rates of transport in the atmosphere as to the abundance of OH and that the initial interpretations of observations of ^{14}CO must be revised [*Spivakovsky and Balkanski*, 1994; *Mak et al.*, 1994; *Brenninkmeijer et al.*, 1999; P. Quay et al. (Atmospheric ^{14}CO: A tracer of OH concentration and mixing rates, submitted to *Journal of Geophysical Research*, 1999)].

Recent developments affecting the computation of tropospheric OH include the suggestion by *Michelsen et al.* [1994] of a nonnegligible quantum yield for $O(^1D)$ at wavelengths between 312 to 320 nm, confirmed by laboratory measurements [*Talukdar et al.*, 1998]. There have been changes in recommendations for other key rate constants [*DeMore et al.*, 1994, 1997], in particular, a decrease in the rate for reaction of OH with methane (19% at 277 K). New observational data afford a better definition of precursors for OH, such as O_3, NO_t (defined as $NO_2 + NO + 2N_2O_5 + NO_3 + HNO_2 + HNO_4$), CO, and H_2O. Reactions with nonmethane hydrocarbons (NMHC), omitted in earlier studies because of lack of observations, can now be included. The distribution of cloud cover, highly uncertain in the past, can now be constrained by a global climatology afforded by satellite observations, International Satellite Cloud Climatology Project (ISCCP) [*Rossow and Schiffer*, 1991].

Remarkable advances have been made in measuring concentrations of OH [e.g., *Eisele et al.*, 1997; *Mount et al.*, 1997; *Tanner et al.*, 1997l; *Mather et al.*, 1997; *McKeen et al.*, 1997; *Wennberg et al.*, 1994, 1998; *Brune et al.*, 1998]. Calculations of OH during the Tropospheric OH Photochemistry Experiment, constrained by concurrent measurements of precursors, yielded estimates in agreement with observed values within 30% for clean air conditions [*McKeen et al.*, 1997]. While these efforts lessen uncertainties in the current chemical mechanism and lead to its improvement, one has to rely on models to provide an integrated measure of the oxidative capacity of the atmosphere over large regions because of the extreme variability of OH in time and space.

The goal of this paper is to present an up-to-date global distribution of tropospheric OH (essentially an update of that provided by *Spivakovsky et al.* [1990], hereinafter referred to as S90) and to evaluate the computed distribution using available observations of tracers. Unlike studies that compute the distribution of OH as a byproduct of a fully coupled simulation of O_3, NO_x ($NO + NO_2$), CO, and hydrocarbons [e.g., *Muller and Brasseur*, 1995; *Roelofs and Lelieveld*, 1995; *Wang et al.*, 1998a, b, c; *Hauglustaine et al.*, 1998], which may suffer from imperfections in various aspects of the model, such as transport, deposition, and emissions, this study specifies distributions of precursors for OH based on observations, that is, according to our best present knowledge. The crudeness of the specified distributions is an inevitable disadvantage of our approach.

However, by relying on observations, we avoided correlation of errors expected in a fully coupled chemical tracer model (CTM) (e.g., an underestimate of NO_x resulting in an underestimate of O_3 and overestimate of CO). In some regions, as discussed below, lack of observations hinders equally efforts either to evaluate CTMs or to determine typical values for specification of precursors.

The distribution of OH, archived monthly with a resolution of 10° longitude, 8° latitude, and seven pressure levels (nine in the tropics), can be obtained in electronic form from the authors. This archive also includes concentrations of precursors for OH as well as computed distributions of key intermediate species and J values.

We begin by characterizing distributions of precursors for OH in section 2, describing the photochemical model in section 3 and presenting computed concentrations of OH in section 4. The sensitivity of OH to uncertainties in the specification of various precursors is discussed in section 5. In section 6 we update the procedure for estimating lifetimes by reference to known lifetimes of other species [*Prather and Spivakovsky*, 1990]. In section 7 we briefly describe the CTM used for simulations of CH_3CCl_3, CHF_2Cl (HCFC-22), ^{14}CO, C_2H_6, C_2Cl_4, and CH_2Cl_2 in the context of constraints observations of these gases pose for the computed distribution of OH. In section 8, observations of CH_3CCl_3 and HCFC-22 are used to test the global annual mean concentration of OH. We show that the present distribution of OH is consistent within a few percent with current budgets of these gases. In section 9 we continue to explore means to test computed distributions of tropospheric OH on scales smaller than global [e.g., S90; *Brenninkmeijer et al.*, 1992; *Mak et al.*, 1992, 1994; *Spivakovsky and Balkanski*, 1994; *Goldstein et al.*, 1995a] using observations of CH_3CCl_3, C_2H_6, C_2Cl_4, and CH_2Cl_2. The utility and limitations of observations of ^{14}CO for evaluating concentrations of OH are discussed in section 10. In section 11 we delineate the unique opportunities to test OH that may arise in the next few years due to phasing out emissions of CH_3CCl_3 [S90; *Ravishankara and Albritton*, 1995]. Section 12 summarizes the main conclusions.

2. Distributions of Precursors for OH

2.1. Ozone

We replaced zonal mean column densities of O_3 from Total Ozone Mapping Spectrometer (TOMS) Version 5 used in S90 with a two-dimensional (2-D) climatology derived from TOMS Version 7 for 1978–1992. Zonal means for the new values are 3% lower at midlatitudes. The consequent impact on global mean OH is less than 1%.

The global distribution of tropospheric O_3 was specified using the climatology developed by *Logan* [1999] for 1980–1993, incorporating ozonesonde data, tropospheric O_3 columns ("tropospheric residual") [*Fishman et al.*, 1990; *Fishman and Brackett*, 1997], and surface observations. The main improvement in the specification of O_3 (as compared to S90) is the resolution of longitudinal gradients in the tropics. The revised climatology reflects a prominent feature of the tropospheric residual, high concentrations of O_3 over a large area of the southern tropics during the biomass burning period. There is no indication in the observational data for a comparable increase in O_3 in the northern tropics, despite the fact that similar amounts of biomass are believed to be burned in the two regions [*Hao et al.*, 1990]. The sparseness of measurements for O_3 in the tropics does not allow for confirmation of the tropospheric column derived from the satellite data for the northern tropics [*Logan*, 1999]. The new climatology of O_3 results in an increase of 3% in mean tropospheric OH, as compared to S90.

2.2. Water Vapor

The distribution of water vapor was specified using monthly means from the European Centre for Medium-Range Weather Forecasts (ECMWF) archived at the National Center for Atmospheric Research (NCAR), averaged over 1986–1989 [*Trenberth*, 1992]. The ECMWF moisture fields for that period have undergone extensive comparisons with observations. *Liu and Tang* [1992] used radiosonde soundings from a global network, including 52 tropical stations, to evaluate the surface and column-integrated specific humidity. In addition, they compared the latter over oceans with 25 months of satellite observations from Special Sensor Microwave Imager (SSM/I) and found good agreement over most of the area. The mean and standard deviation of differences between the ECMWF and radiosonde data sets were 0.04 and 0.36 g cm^{-2}, respectively (the range of measurements was 0.5–7 g cm^{-2}). Significantly, the mean and standard deviation of differences between satellite and radiosonde data were similar in magnitude: −0.02 and 0.37 g cm^{-2}. Large discrepancies appear to be confined to relatively small areas off the west coast of continents, where the ECMWF values are higher than observational data by up to a factor of 2.

The column-integrated mean humidity reflects mainly the amount of water vapor in the lower troposphere. *Soden and Bretherton* [1994] evaluated ECMWF relative humidity fields integrated from 500 to 200 hPa using satellite observations from GOES for 60°S – 60°N and 150°W – 0° (the 6.7-μm channel spectral measurements attribute highest weight to values between 400 and 250 hPa). They report relative differences between the ECMWF values and those from GOES of "roughly 23% to 45% in the regions of subtropical subsidence, 0% to 23% over the northern and southern midlatitudes, and −23% to −45% over areas of deep tropical convection" [*Soden and Bretherton*, 1994, p. 1,206]. As discussed in section 5, concentrations of OH above 300 hPa depend little on specific humidity.

In comparison to this study, tropical humidity in S90 was too low below 800 hPa by 10–25% and too high by 20–30% at 700 hPa over the oceans. The change in global mean OH due solely to the revisions adopted for water vapor was small, however (~ 3% increase).

2.3. Nitrogen Oxides

The distribution of NO_t (Table 1) was based on an analysis of aircraft, shipboard and surface data for NO and NO_x [e.g., *Torres and Thompson*, 1993; *Carroll and Thompson*, 1995; *Emmons et al.*, 1997; *Bradshaw et al.*, 2000]. Profiles for NO_t in Table 1 were obtained using observations of NO, that is, by ensuring that the periodic solution of the system of kinetic equations representing the full chemical mechanism (with a period of 24 hours) provides NO values in agreement with daytime observations for NO. In the continental boundary layer in some regions, as described below, values for NO_t derived in this manner were replaced using observations of NO_x.

In deriving vertical profiles for NO, we used the analysis of *Bradshaw et al.* [2000] who gridded data from the NASA Global Tropospheric Experiment (GTE) and Airborne Arctic Stratospheric Experiment (AASE) aircraft campaigns, supplemented by measurements from other campaigns [e.g., *Drummond et al.*, 1988; *Kondo et al.*, 1993; *Rohrer et al.*, 1997]. Although these data are not sufficient in spatial or temporal extent to define a climatology for NO, they provide a series of "snapshots" that show some consistent patterns; for example, concentrations of NO in the marine boundary layer are low, a few parts per trillion by volume (pptv), those from 4 to 6 km tend to be in the range 10–40 pptv over both oceans and continents, while values for 10–12 km are generally in the range 10 to 150 pptv. Over the polluted continents, boundary layer concentrations are from 100 pptv to several parts per billion by volume (ppbv), and the profiles are C shaped [e.g., *Drummond et al.*, 1988], while in remote areas, such as the Amazon, concentrations are much lower, 10–40 pptv [*Torres and Buchan*, 1988]. Boundary layer concentrations in remote regions affected by biomass burning are elevated compared to those removed from such influence. Based on the features seen in the observations, we allowed for different profiles for NO over land and ocean, south and north of 30°N, and for a region in the southern tropics (0° – 24°S, 60°W – 45°E), with higher concentrations over the latter region in austral winter-spring using observations from the Transport and Atmospheric Chemistry Near the Equator–Atlantic (TRACE-A) mission. The standard "land" and "ocean" profiles are identical above 6 km.

The profiles selected for NO are compared in Figure 1 to observations in various parts of the world [*Bradshaw et al.*, 2000; GTE data archives, 1998]. In addition to the data shown in the figure (from which the selected profiles were largely derived), the ocean profile for 30°–90°N agrees well with measurements from Stratospheric Ozone Experiment (STRATOZ) III from the east coast of North America and the west coast of Europe in June 1984 [*Ehhalt and Drummond*, 1988; *Drummond et al.*, 1988]; mean NO values for 20°–70°N were only 20% larger than the standard profile in Figure 1a for 3–8 km, and were about a factor of 2 larger for 10–12 km. Measurements from the Tropospheric Ozone Experiment (TROPOZ) II in January 1991 [*Rohrer et al.*, 1997] close to Europe (not shown) were within a factor of 2 or less of the standard profile in Figure 1a, but downwind of North America were much higher, 100–300 pptv for 2–6 km. For 30°N–90°N over land (Figure 1b), in addition to the data included in the figure, *Ridley et al.* [1994] observed values for NO as low as 20 pptv at 4–6 km over New Mexico in summer, similar to those over the oceans, while values above 6 km were factors of 2–3 higher than those in Figures 1a and 1b, because of the bias in sampling near convective storms.

Table 1a. Distribution of NO_t

	90°S–30°N		30°N–90°N	
Pressure, hPa	Ocean	Land	Ocean	Land
1000	11	67	23	184
900	13	65	28	155
800	13	57	25	117
700	22	47	34	83
500	31	33	53	56
300	93	94	172	176
200	135	137	224	247
150	129	131	–	–
100	132	133	–	–

Except (1) for the continental boundary layer over industrial regions of Europe, North America and South-East Asia where 1 ppbv of NO_t was assumed in summer and 2 ppbv in winter, and (2) for tropical regions affected by biomass burning where Table 1b applies. Concentrations of NO_t are in pptv.

Table 1b. NO_t in Biomass Burning Regions

Pressure, hPa	Ocean[a]	Land[b]
1000	12	219
900	33	223
800	45	213
700	55	125
500	70	70
300	219	220
200	275	276
150	262	260
100	260	257

Concentrations of NO_t are in pptv.
[a]Over Atlantic (0°–24°S) in July-October.
[b]Over Africa and South America (0°–24°S) in July-October and over Africa (0°–16°N) in November-March.

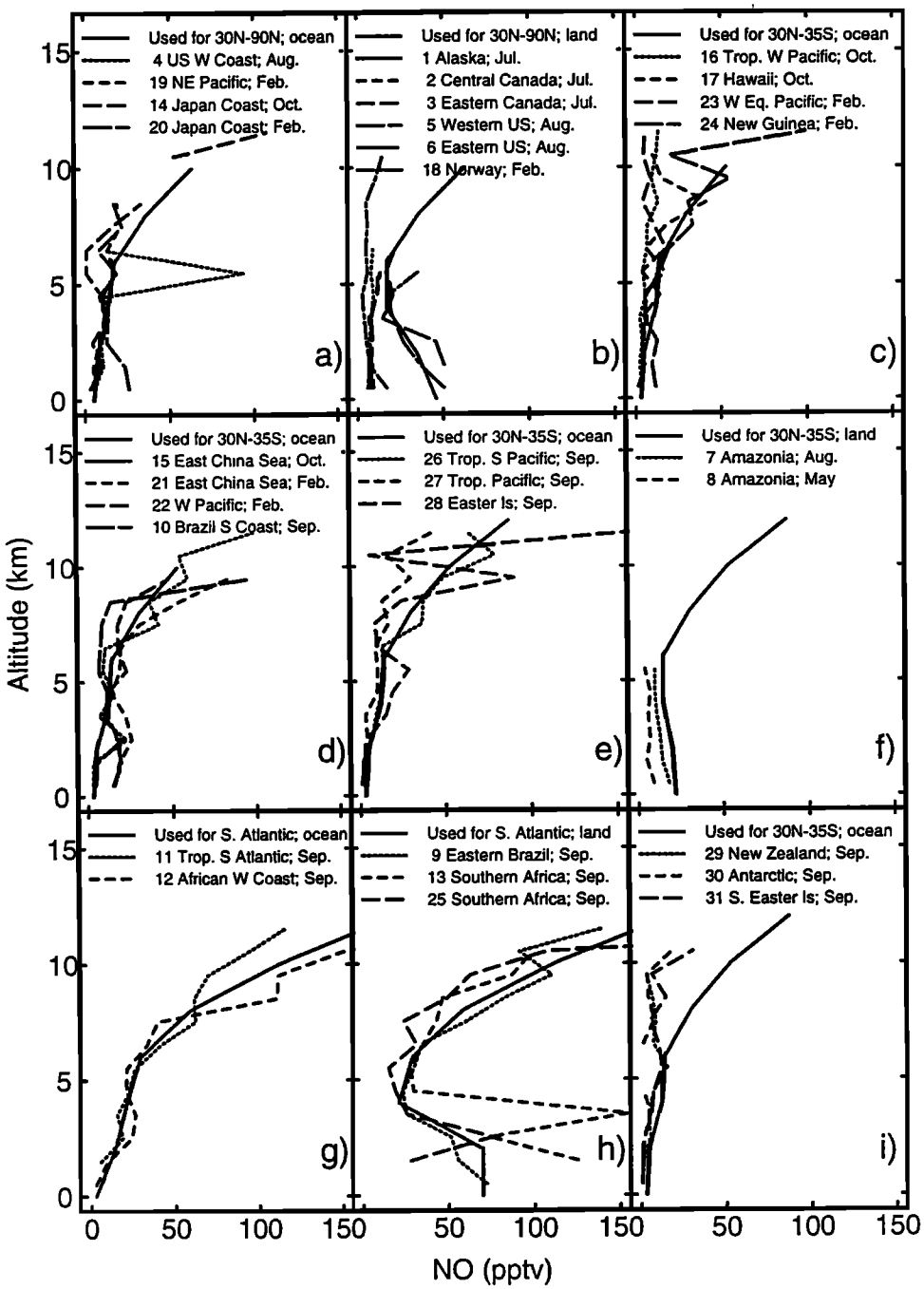

Figure 1. Vertical profiles of NO. The heavy solid lines show the profiles adopted for three regions, land and ocean: 30°N–90°N, 90°S–30°N (based on data from 30°N–35°S), and the South Atlantic region affected by biomass burning for 24°S–0°S, between 60°W and 45°E in August-October. These are compared with observations for 30°N–90°N, (a) ocean and (b) land; for the tropics, 35°S–30°N, (c, d, and e) ocean and (f) land; for the South Atlantic region, (g) ocean and (h) land; (i) for southern midlatitudes (the same profile as adopted for 35°S–30°N, ocean). Profiles compiled from observations for subregions are taken from *Wang et al.* [1998b], where the regions are defined, with the addition of data from PEM-Tropics [*Bradshaw et al.*, 2000; GTE data archives, 1998] for which the data were averaged over the following areas: tropical South Pacific (region 26, 5°N–15°S, 170°E–130°W); subtropical South Pacific (region 27, 10°S–35°S, 170°E–145°W); Easter Island (region 28, 10°S–35°S, 120°W–105°W); New Zealand (region 29, 35°S–55°S, 170°E–170°W); Antarctic (region 30, 55°S–75°S, 170°E–170°W); South Easter Island (region 31, 35°S–55°S, 115°W–105°W). The profiles from the subregions are averages over all NO points obtained with solar zenith angle of less than 70°.

The standard ocean profile of NO adopted for 30°N–35°S is similar to or higher than NO observed in the vicinity of Hawaii, in the western Pacific, and in the southern Pacific in September/October (Figures 1c and 1d), while observations from the western Pacific in winter are somewhat higher than the standard profile (except in the middle troposphere). NO values reported for flights from Japan to Indonesia at 4.5 km (not shown) were about 20 pptv in continental plumes in winter and summer, but only 7 pptv in marine air near the equator [*Kondo et al.*, 1993]. The standard ocean profile for 30°N–35°S is similar to mean profiles for these latitudes derived from measurements made as part of Pacific Exploratory Mission (PEM)-Tropics [*Bradshaw et al.*, 1999] (Figure 1e). The NO profile selected for land in the tropics is based on longitudinal transects from Arctic Boundary Layer Expedition (ABLE) 2A over much of the Amazon [*Torres and Buchan*, 1988], while observations in Figure 1f are for the area around Manaus only. Mean values for NO from TROPOZ II data are 20–60 pptv for 4–8 km between 30°S and 30°N over the Americas, higher than the standard profiles (not shown). The NO profiles selected for tropical regions affected by biomass burning are based on limited data available from TRACE-A (Figure 1g for the Atlantic Ocean, and Figure 1h for the adjoining continents). The land profile for NO for regions of Africa and South America affected by biomass burning in June – October was used over sub-Saharan Africa for the biomass burning season in November – March.

We chose to use the NO profile for 35°S to 30°N for southern midlatitudes prior to the availability of data from PEM-Tropics A and TROPOZ II. The measurements from PEM-Tropics A south of 35°S tend to show lower concentrations of NO than the standard profile, by about a factor of 2 below 5 km, and by as much as a factor of 2–6 at 8 km and above (Figure 1i). However, the TROPOZ II data from the west coast of South America tend to be higher than the selected profile for southern midlatitudes, by up to a factor of 3 (not shown). These differences may reflect seasonality in sources of NO_x, but data are insufficient to resolve this uncertainty.

Below 300 hPa, NO_t is present primarily as NO_x, except in winter at temperate latitudes. Concentrations of NO_x (and NO) are highly variable in surface air over the northern continents. The NO value near the surface selected for the standard profile in Figure 1b corresponds to about 180 pptv of NO_x. Concentrations of NO_x reported for remote locations in the United States and Nova Scotia are ~100–300 pptv, while median values at more polluted rural sites in the eastern U.S. and Canada are 1–2 ppbv in summer, with somewhat higher values in winter; mean values are higher than median values [*Carroll and Thompson*, 1995; *Emmons et al.*, 1997; *Munger et al.*, 1998]. In the boundary layer over industrial regions of Europe and North America we assumed 1 ppbv of NO_t in summer and 2 ppbv in winter.

Concentrations of NO_t adopted for this study are higher than in S90 by factors of 2–5 in the tropics over regions affected by biomass burning and over industrial regions at northern midlatitudes. In addition, concentrations of NO_t below 800 hPa over oceans are higher in the present work, by factors ranging from 1.5 to 2. The changes in the distribution of NO_t resulted in an increase of ~7% in mean OH as compared to S90.

2.4. Carbon Monoxide

For CO we took an approach different from that for O_3 and NO_t. There was no published 3-D climatology for CO as was the case for O_3, and in contrast to NO_t, for CO there was a wealth of surface observations and, in some locations, column observations. We used the CTM as an interpolator to obtain a smooth distribution of CO consistent with observations. For this purpose the inventory of emissions presented by *Wang et al.* [1998a] was adjusted to provide satisfactory agreement with observations of CO from NOAA Climate Monitoring and Diagnostics Laboratory (CMDL) and other surface sites [*Novelli et al.*, 1998; W. Munger, personal communication, 1997; *Scheel et al.*, 1990], and where available, with observations of the CO column [*Dvoryashina et al.*, 1984; *Zander et al.*, 1989; *Rinsland et al.*, 1998] (using the distribution of OH from S90). The agreement between observations and the distribution of CO specified in the present calculation of OH is illustrated in Figures 2a, 2b and 2c for surface, column, and aircraft data, respectively.

Specified values for CO are consistent with GTE aircraft observations over the tropical Pacific and Atlantic, as well as off the west coast of South Africa and east coast of Southern Brazil (Figure 2c). Model levels are also in agreement with observations over Kansas and Maine. Good agreement was also found at southern middle and high latitudes over the Pacific in September, but values over New Zealand are too low above 500 hPa. Over the Hawaiian region, specified values are higher than observations by 20–35% in January but are in agreement in August. Over the West Coast of the United States both in winter and summer (not shown) as well as off the coast of Japan and China specified values are too high.

We also compared the adopted distribution of CO with satellite observations, Measurement of Air Pollution from Satellites (MAPS), which give the major weight to the region between 500 and 250 hPa, for 10 days in April and October (not shown). In April, model levels are consistent with observations, except at southern midlatitudes where the former are too low by as much as 35%. In October, the same discrepancy is evident at southern midlatitudes, and in addition, the biomass burning plumes in the SH are much less pronounced in the model than in MAPS observations, consistent with the underestimation of the column data of *Rinsland et al.* [1998] for October (Figure 2b) at Lauder.

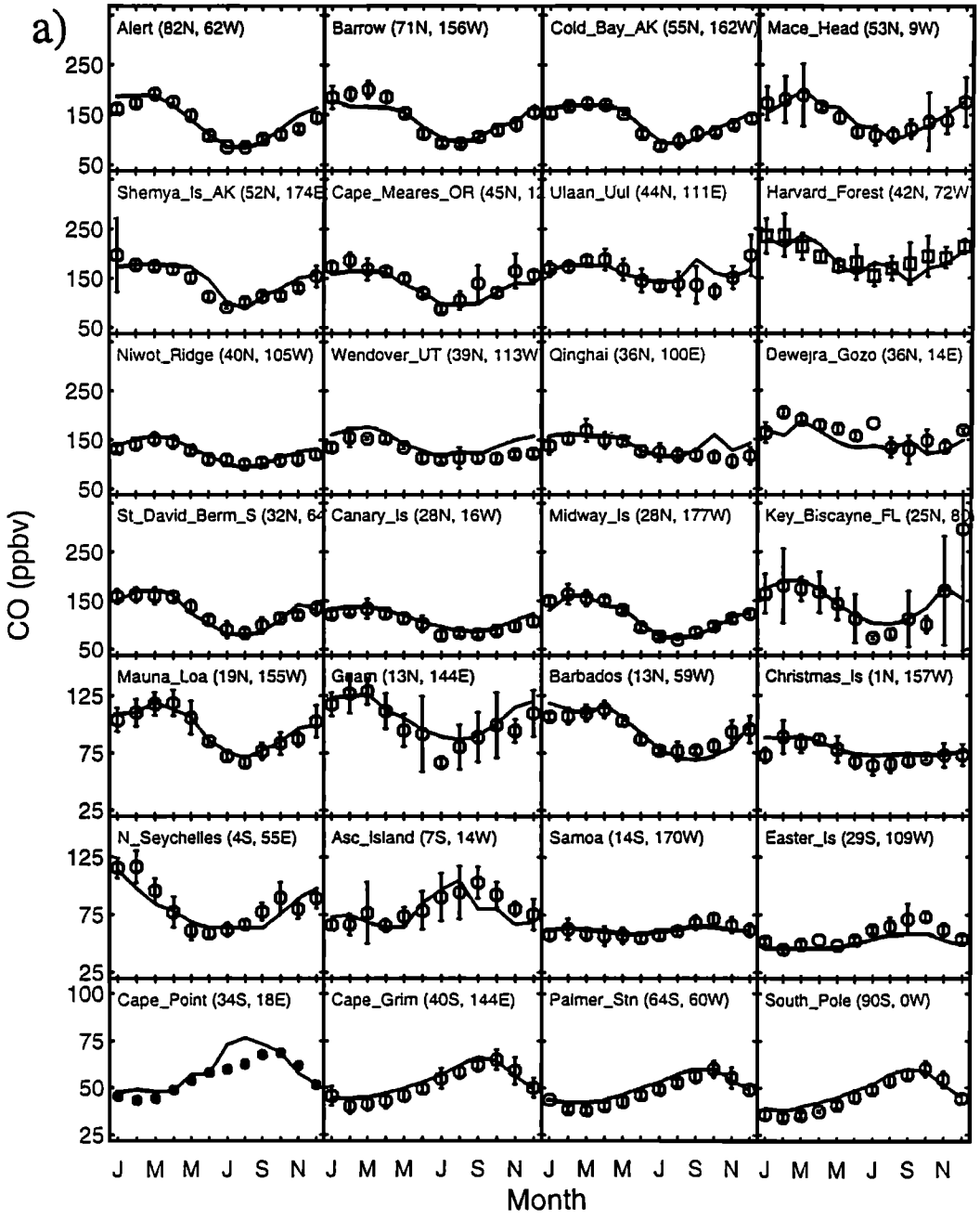

Figure 2. Comparison of model results (lines) used to specify the global distribution of CO with observations at selected sites (a) at the surface, (b) for the column, and (c) using aircraft data from GTE campaigns. For the surface, open circles, solid circles, and squares denote observations of *Novelli et al.* [1998], *Scheel et al.* [1990], and W. Munger (personal communication, 1997, averages over 1990–1994), respectively. For the column, squares, triangles and diamonds refer to observations of *Dvoryashina et al.* [1984], *Zander et al.* [1989], and *Rinsland et al.* [1998], respectively. For the aircraft data, profiles where compiled using GTE data archives for regions defined in caption for Figure 1, with the exception of Hawaii, region 32, 15°N–25°N, 155°W–165°W, from the Stratospheric Tracers of Atmospheric Transport (STRAT) mission; Kansas, region 35, 35°N–40°N, 94°W–101°W, from Subsonic Aircraft Contrail and Cloud Effects Special Study; Maine coast, region 36, 41°N–50°N, 55°W–72°W; and Ireland, region 37, 49°N–54°N, 3°W–13°W from Subsonic Assessment (SASS) Ozone and Nitrogen Oxide Experiment (SONEX). Means are denoted by asterisks, medians are shown as vertical lines inside boxes, 25% and 75% quantiles are represented by boxes, and 10% and 90% quantiles are marked by dots.

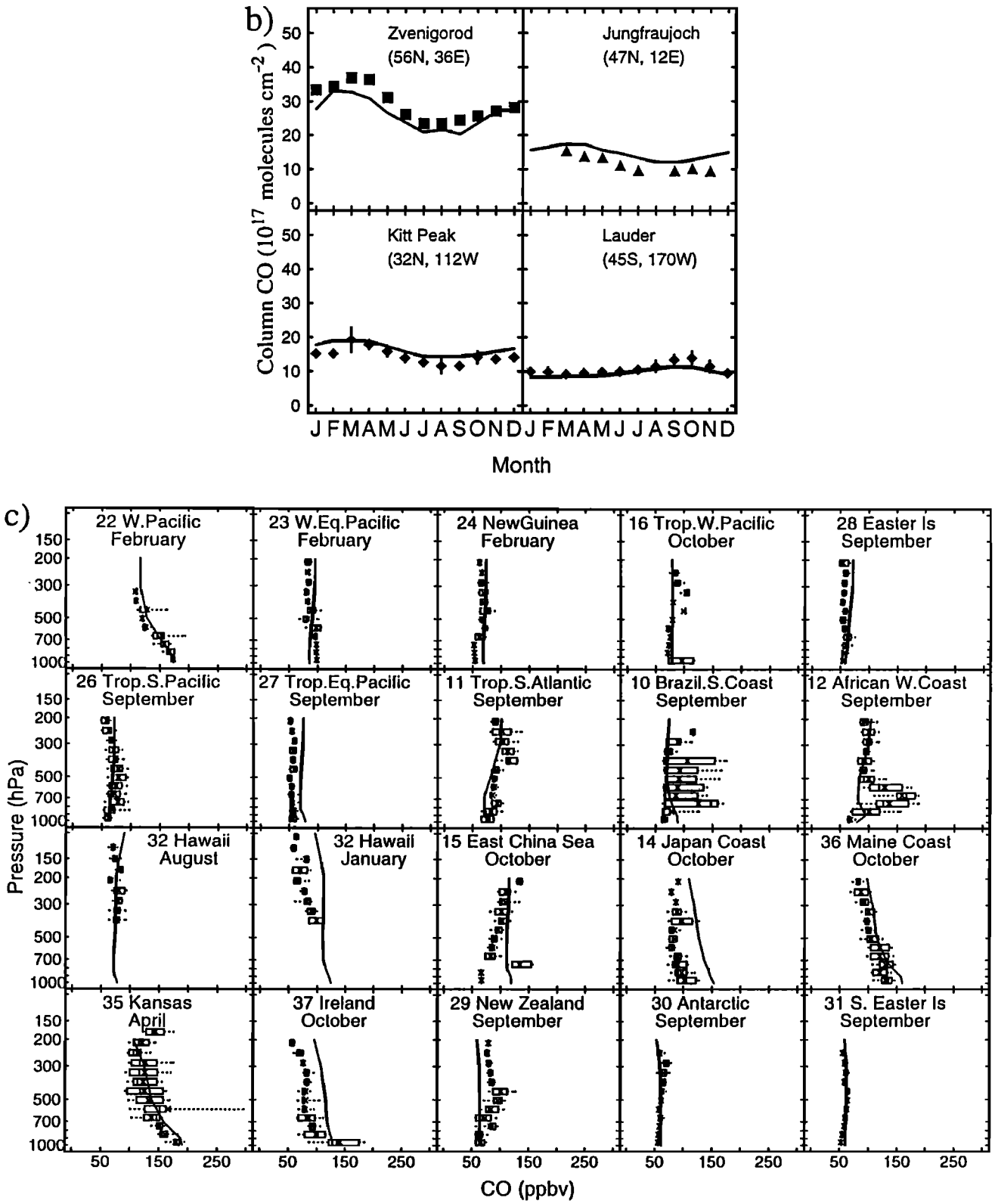

Figure 2. (continued)

Concentrations of CO used in this study are about 20% lower in the SH and in the northern tropics as compared to S90 [cf. *Manning et al.*, 1997], resulting in an increase of ~7% in global mean OH. It is possible, however, that an underestimate of CO at southern midlatitudes suggested by the MAPS data contributed to an overestimate of OH in that region discussed in section 9.

2.5. Hydrocarbons

The methane field was assumed uniform in each semihemisphere with values from south to north of 1645,

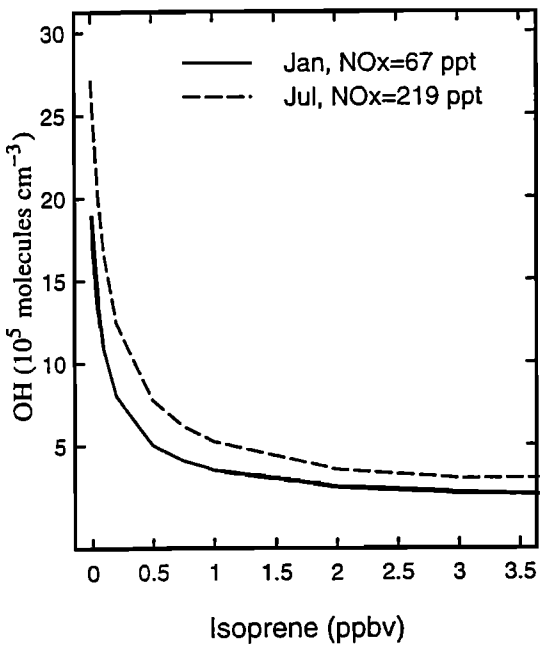

Figure 3. Concentration of OH (10^5 molecules cm^{-3}) at the surface at 15°S versus concentration of isoprene in January, with NO_t at 67 pptv (solid line) and in July, with NO_t at 219 pptv (dashed line). NO_x constitutes more than 99% of NO_t.

1655, 1715, and 1770 ppm, respectively [*Dlugokencky et al.*, 1994, 1995] (for the present resolution, actual divisions are at 32°S, the equator and 32°N).

Isoprene provides a major sink for OH near the surface over land in the tropics and at midlatitudes in summer [e.g., *Greenberg et al.*, 1985; *Zimmerman et al.*, 1988; *Jacob and Wofsy*, 1988]. Concentrations of isoprene, however, are highly variable in space and time, and measurements are few. We specified the distribution of isoprene simulated using the model of *Horowitz and Jacob* [1999]. Emissions of isoprene were reduced for tropical forests and grassland by factors of 2 and 3, respectively, and increased for "snowy mixed" forests (terminology from *Guenther et al.* [1995]) by a factor of 3. In these modifications we were guided by comparisons of model results with observations for vertical profiles of isoprene [*Rasmussen and Khalil*, 1988; *Jacob and Wofsy*, 1988; *Ayers and Gillett*, 1988; *Andronache et al.*, 1994; *Guenther et al.*, 1996; *Helmig et al.*, 1998; GTE data archives, 1998]. For tropical forests, such a decrease in emissions is also supported by direct estimates of *Jacob and Wofsy* [1988, 1990] and *Klinger et al.* [1998]. In addition, emissions for "dry taiga" were reduced by a factor of 3 (A. Guenther, personal communication, 1998).

Over large regions, however, concentrations of isoprene are highly uncertain. Nevertheless, for isoprene above ~250 pptv, OH is depleted by more than a factor of 2, as shown in Figure 3, and therefore uncertainties in concentrations of isoprene above that level do not contribute significantly to those in the tropospheric column of OH. At concentrations of isoprene above 500 pptv, the sensitivity of OH to isoprene is greatly diminished because production of OH is dominated by photolysis of products of isoprene oxidation, such as CH_2O and organic peroxides. As a result, a larger uncertainty in OH is associated with the spatial extent of concentrations of isoprene in excess of 50–100 pptv than with the accuracy of the specified values above 500 pptv. The lifetime of isoprene away from immediate sources is counted typically in hours. Little error is expected to result therefore from uncertainties in the horizontal transport in the CTM. However, vertical transport within the boundary layer may be more rapid than chemical loss, and therefore the vertical extent of significant levels of isoprene is sensitive to errors in the height of the boundary layer and the frequency of convection in the CTM [*Horowitz and Jacob*, 1999]. An additional uncertainty in OH is associated with the spatial extent of significant concentrations of longer-lived intermediate products of isoprene oxidation, for example, methacrolein and methylvinylketone, since our calculation of OH neglects the effect of transport of these compounds by forcing their concentrations to a periodic steady state. Model results for isoprene with the 4° by 5° resolution on σ surfaces were adopted for the 8° by 10° resolution on standard pressure levels using linear interpolation in the logarithm of isoprene because of the highly nonlinear dependence of OH on isoprene. Concentrations of isoprene were specified with the time resolution of a month, with averaging in time conducted also for the logarithm of isoprene. Inclusion of isoprene decreased global tropospheric OH by 3%. For the distribution of isoprene obtained using standard emissions from *Horowitz and Jacob* [1999] rather than reduced emissions, and with interpolation and averaging conducted for concentration (rather than for logarithm of concentration), global tropospheric OH decreased by 9%.

Apart from isoprene and methane, we considered 12 hydrocarbons: alkanes (C_2H_6, C_3H_8, C_4H_{10}, and C_5H_{12}), alkenes (C_2H_4 and C_3H_6), aromatics (C_6H_6, C_7H_8, and C_8H_{10}), and oxygenated species (methanol, ethanol, and acetone). Using observations, we developed concentration profiles for four latitude regions, two seasons, and for land and ocean, and determined which species needed to be included in the calculation of global OH with a series of sensitivity studies.

Measurements of hydrocarbons are most abundant for northern midlatitudes. Values selected for the continental boundary layer were based primarily on the data from surface sites shown in Table 2 and were chosen to represent background conditions; values above the boundary layer in summer were based on data obtained near North Bay, Canada. Median vertical profiles were calculated for each hydrocarbon species for selected geographic regions, using the GTE data merges provided by *Bradshaw et al.* [2000]. The marine profiles were based on data from the Arctic, near Goose Bay, Canada,

Table 2. Data for Alkenes and Alkanes at Northern Midlatitudes

	C_2H_4	C_3H_6	C_2H_6	C_3H_8	C_4H_{10}	C_5H_{12}	C_4+C_5	C_6	Ref.
				Averages for JJA, Surface Stations					
Kejimkujik[a]	160–190	70–90	1080	243	153	170	323	200	1
Lac la Flamme[a]	120–210	50–60	1030	140	60	73	133	150	1
Egbert[a]	170–300	50–70	1130	300	233	217	450	200	1
Saturna[a]	220–260	60	970	310	273	233	406	170	1
Fraserdale[a]	ND	ND	820	78	22	8		ND	2
Rorvik, Sweden	213	34	817	215	381	243	624	ND	3
Harvard Forest[b]	485/179	119/55	1537/959	663/265	419/116	533/153	952/269	107/40	4
				Averages for JJA, Aircraft Data					
ABLE-3A	ND	ND	820	49	8 (n-C4)				5
ABLE-3B[c]	78/51	21/10	853/703	92/79			49/35	LOD/LOD	6
PEM-A[d]	64/89	17/21	1021/1601	153/540	88	33	124/487	7(n-C6)	7
PEM-A[e]	29/30	14/8	632/1019	57/154	20	13	34/101	LOD	7
				Selected for Northern Midlatitudes, JJA					
	160	60	1000	250			300	40	
				Averages for DJF, Surface Stations					
Kejimkujik[a]	300–530	60–170	2230	1350	1040	523	1560	340	1
Lac la Flamme[a]	300	30-60	2370	1310	930	450	1380	280	1
Egbert[a]	460–1230	60–160	3130	2080	1790	840	2630	370	1
Saturna[a]	1000	60–210	2130	1160	1730	790	2520	42	1
Fraserdale[a]	ND	ND	2450	1140	930	490		ND	2
Rorvik, Sweden	995	172	2620	1316	1360	942	2310	ND	3
Harvard Forest[b]	1112/402	181/45	3420/2290	1980/1170	1510/734	849/405	2358/1139	192/95	4
Atlantic			2200	850	600	320	920	100 (nC6+C7)	8
PEM-B[f]	86/90		7/7	2258/2283	877/900	34	553/580	37/40	9
				Selected for Northern Midlatitudes, DJF					
	400	45	2200	1150	1150	100			

For PEM-West A and B, the first number shows the median of all measurements below 1 km for the selected region, and the second number shows the median for $C_2 > 750$ pptv (PEM-A) and for $C_2H_6 > 1000$ pptv (PEM-B). ND, no data. LOD, below detection limit. JJA, June, July, August; DJF, December, January, February. References are 1, *Bottenheim and Shepherd* [1995]; 2, *Jobson et al.* [1994]; 3, *Lindskog and Moldanova*, [1994]; 4, *Goldstein et al.* [1995b]; 5, *Blake et al.* [1992]; 6, *Blake et al.* [1994]; 7, *Blake et al.* [1996b]; 8, *Penkett et al.* [1993]; 9, *Blake et al.* [1997]. Concentrations of hydrocarbons are in pptv.

[a]Canadian stations.

[b]The first and second number correspond to a mean and a 10th percentile, respectively.

[c]The first and second number correspond to values at North and Goose Bay, respectively.

[d]Near the coast, north of 23°N.

[e]East of 143°E, north of 23°N.

[f]North of 21°N.

from the western Atlantic [*Penkett et al.*, 1993], and from the eastern Pacific north of 21°N (PEM-West A); for PEM-West A a filter of $C_2H_6 > 750$ pptv was used to select midlatitude air.

Winter profiles were selected for northern midlatitudes in the same manner as for summer, but the aircraft data were limited to the western Atlantic and the eastern Pacific (PEM-West B), and a few profiles measured in the vicinity of California [*Singh et al.*, 1988]. We used a filter of $C_2H_6 > 1000$ pptv to select midlatitude values from PEM-West B (for latitudes > 21°N) and used these values above 3 km for land and for the entire profile for ocean; this resulted in profiles similar to those reported by *Singh et al.* [1988] and *Rudolph* [1995] for the alkanes. Concentrations of alkenes in the marine boundary layer, which are short lived even in winter, were taken from *Rudolph and Johnen* [1990].

Vertical profiles for the tropics were derived largely from PEM-West A (10°N–22°N) and B (7.5°N–21°N) in the eastern Pacific, TRACE-A in the South Atlantic, Brazil, and Africa, three cruises in the Atlantic [*Singh et al.*, 1988; *Rudolph and Johnen*, 1990; *Koppmann et al.*, 1992], two in the Pacific [*Singh et al.*, 1988; *Donahue and Prinn et al.*, 1993], and continental measurements in Africa and Brazil [e.g., *Zimmerman et al.*, 1988; *Rudolph et al.*, 1992a]. Profiles above the boundary layer in the northern tropics were based almost exclusively on the PEM data, supplemented by limited mea-

surements on TRACE-A transit flights; in the southern tropics, they were based on TRACE-A data for October, and on PEM-West B data near the equator for February. Continental data were lacking for the northern tropics, so the southern data were used to estimate concentrations in the wet and dry season. The continental data are much cruder estimates of typical values as the measurements are for short time periods, usually a few weeks at most. Relatively few vertical profiles were measured over the continents during TRACE-A, and they appear reasonably consistent with the surface data from the dry season reviewed by *Rudolph et al.* [1992a].

Profiles derived for southern midlatitudes were based on measurements from cruises to ~30°S [*Rudolph and Johnen*, 1990; *Koppmann et al.*, 1992] and vertical profiles from TRACE-A that sampled midlatitude air, based on backward trajectory calculations. These data gave lower concentrations of alkanes than surface data from 70°S reported by *Rudolph et al.* [1992b] but were thought to be more representative of middle latitudes.

The concentration profiles for hydrocarbons are most reliable for alkanes, and the reliability decreases for aromatics and oxygenated species, simply because of the quantity of measurements; for short-lived hydrocarbons, such as alkenes, the high spatial and temporal variability results in greater uncertainties. The profiles are better known for June to October than for December to March, because of the timing of the aircraft campaigns, and for northern midlatitudes compared with any other region, because of the availability of surface data, and of several sets of aircraft data. While the vertical profiles selected for the tropics are less defined than those for northern midlatitudes, there appears to be reasonable consistency among the tropical measurements as shown in Table 3 for alkenes.

Surface measurements of benzene and toluene were available for only a few remote surface sites and cruises [*Rasmussen and Khalil*, 1983; *Nutmagul and Cronn*, 1985; *Dann and Wang*, 1995], in addition to measurements from aircraft campaigns [*Penkett et al.*, 1993; *Blake et al.*, 1994, 1996a, b, 1997]. Concentrations of toluene and xylenes were often below detectable levels (2 pptv) in the SH [*Blake et al.*, 1994, 1996a, b]. We found that at present levels reactions involving aromatics have an impact of less than 2% on computed concentrations of OH over most of the globe. Given that inclusion of aromatics adds significantly to computational cost, we chose to exclude them from our calculation [cf. *Houweling et al.*, 1998].

Acetone was measured on the GTE campaigns in eastern Canada, the eastern Pacific (February-March), and the south tropical Atlantic, ethanol on the last two of these, and methanol in the eastern Pacific [*Singh et al.*, 1994, 1995, 1996a]. Acetone concentrations for northern midlatitudes were about the same in summer and winter, ~600 pptv. Methanol concentrations were also about 600 pptv in northern winter, but data for other seasons were lacking. Ethanol concentrations were smaller, 50–80 pptv in the NH and below the limit of detection (20 pptv) in the SH in October.

Omission of isoprene and other NMHCs results in an increase in global tropospheric OH by 3% and 7%, respectively [cf. *Donahue and Prinn et al.*, 1993; *Houwel-*

Table 3. Near Surface Data for Alkenes

Location	Season	C_2H_4	C_3H_6	Reference
	Northern Tropics			
Atlantic cruise	Sep./Oct.	30	ND	1
Pacific aircraft (10°N–22°N)	Oct.	20	8	2
Pacific aircraft (0°–10°N)	Oct.	24	8	2
Atlantic cruise	Mar./Apr.	70	15	3
Pacific cruise (0°–10°N)	Feb./Mar.	60	50	4
Pacific aircraft (7°N–21°N)	Feb./Mar.	7	4	5
Selected for Oct.		30	12	
Selected for Feb.		65	32	
	Southern Tropics			
Atlantic cruise	Sep./Oct.	22	ND	1
Atlantic aircraft	Oct.	13	4	6
Atlantic cruise	Mar./Apr.	25	10	3
Pacific cruise	Feb./Mar.	45	40	4
Pacific aircraft	Feb./Mar.	7	LOD	5
Selected for Oct.		22	10	
Selected for Feb.		35	25	

Aircraft data are shown as median values from ~300 m to 1000 m. References are 1, *Rudolph and Johnen* [1990]; 2, PEM-A, *Blake et al.* [1996b]; 3, *Koppmann et al.* [1992]; 4, *Donahue and Prinn* [1993]; 5, PEM-B, *Blake et al.* [1997]; 6, TRACE-A, D. R. Blake, personal communication (1996). ND, no data; LOD, below detection limit. Concentrations of alkenes are in pptv.

ing et al., 1998]. *Wang et al.* [1998c] found that the global mean OH increased by 20% if emissions of all NMHCs were neglected, with about half of this effect associated with emissions of isoprene. However their results account for higher emissions of isoprene, for transport of longer-lived products of isoprene, and for ensuing changes in O_3, NO_t and CO, whereas in our case the distributions of these species were fixed.

Inclusion of NMHCs, accompanied by a decrease in CO over most of the area south of 30°N, led to a decrease of about 10% in the fraction of OH residing below 700 hPa as compared to S90, because of the increased importance of temperature-dependent loss processes.

2.6. Temperature

Temperature fields were specified using averages of ECMWF monthly means from 1986 to 1989 archived at NCAR [*Trenberth*, 1992]. The replacement of the fields from the general circulation model (GCM) II of the Goddard Institute for Space Studies (GISS) [*Hansen et al.*, 1983], used in S90, had little effect on global mean OH.

2.7. Clouds

The radiation code used in the present work [*Wofsy*, 1978; *Logan et al.*, 1981] treats clouds as sets of N 100% reflective layers placed in the atmosphere one at a time; contributions of these layers to the total reflectivity of the cloud are utilized by first performing N calculations of photolysis frequencies and then computing an average of the results weighted by these contributions.

The ISCCP cloud climatology provides the global distribution of the total optical depth of clouds combined with the height of cloud tops [*Rossow and Schiffer*, 1991]. S90 used the distribution of cloud optical depth from the GISS GCM II [*Hansen et al.*, 1983]. We analyzed ISCCP and GISS GCM II clouds using the radiative code of *Prather* [1974] and *Jacob et al.* [1989] with the Henyey-Greenstein phase function for $g = 0.87$ [*Chandrasekhar*, 1960; *Sobolev*, 1975], represented by 20 quadrature terms, and assuming a black surface at the lower boundary. In the tropics, reflectivities of clouds from GISS GCM II were lower than those from ISCCP by almost a factor of 2. In addition, model clouds (recorded as 5-day means) extended on average to lower altitudes and did not exhibit the observed correlations between the height of cloud tops and cloud albedo evident in the Stage C2 ISCCP data [*Rossow and Schiffer*, 1991]. We replaced GISS GCM II clouds with the ISCCP clouds. Unfortunately, the vertical distribution of optical depth for ISCCP is not available. We chose to distribute the ISCCP cloud optical depth uniformly with height between the cloud top and 900 hPa; cloud layers were assumed to be bounded by the standard pressure levels at which concentrations of OH were computed (Table 1).

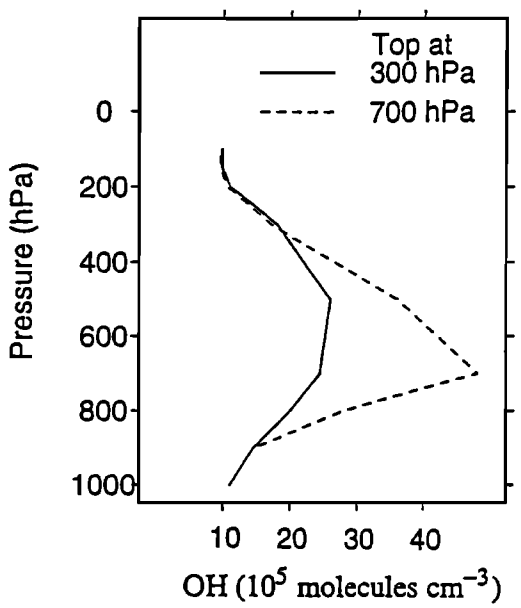

Figure 4. Vertical profiles of OH (10^5 molecules cm^{-3}) averaged over 24 hours at the equator for the cloud with optical depth 5 extending to 700 hPa (dashed line) and to 300 hPa (solid line). The optical depth of the cloud is distributed uniformly with altitude from the cloud top to 900 hPa.

Little error is expected to arise from uncertainties in the vertical distribution of optical depth for clouds with low tops, or for optically thin clouds. The largest error is associated with cases involving a high thin cloud residing above a low thick cloud, masking its actual vertical extent. However, even in these cases, minor errors are expected above and below the cloud deck. For a severe case of misplacement, for example, when a cloud appears to extend to 300 hPa instead of 700 hPa, concentrations of OH are underestimated between the assumed cloud top and 900 hPa, with the largest error occurring just above the actual cloud top (only errors arising from uncertainties in the vertical distribution of optical depth are discussed here, rather than those associated with representing clouds as a set of fully reflective layers). For a cloud with optical depth 5 this error is ~50%, and the resulting error in column OH is ~25% (Figure 4). In addition, the fraction of the column abundance of OH below 700 hPa is underestimated by 6%. As discussed below, on average that fraction for the present distribution is lower by ~21% than in S90, and about half of this difference is associated with the replacement of GISS GCM II clouds by ISCCP clouds. In principle, cases where clouds were extended erroneously to higher altitudes may have contributed to the upward shift in OH. However, only a small fraction of clouds with high tops appear optically thick. Of all the clouds extending above 600 hPa in the tropics, only ~30% have daytime average reflectivities

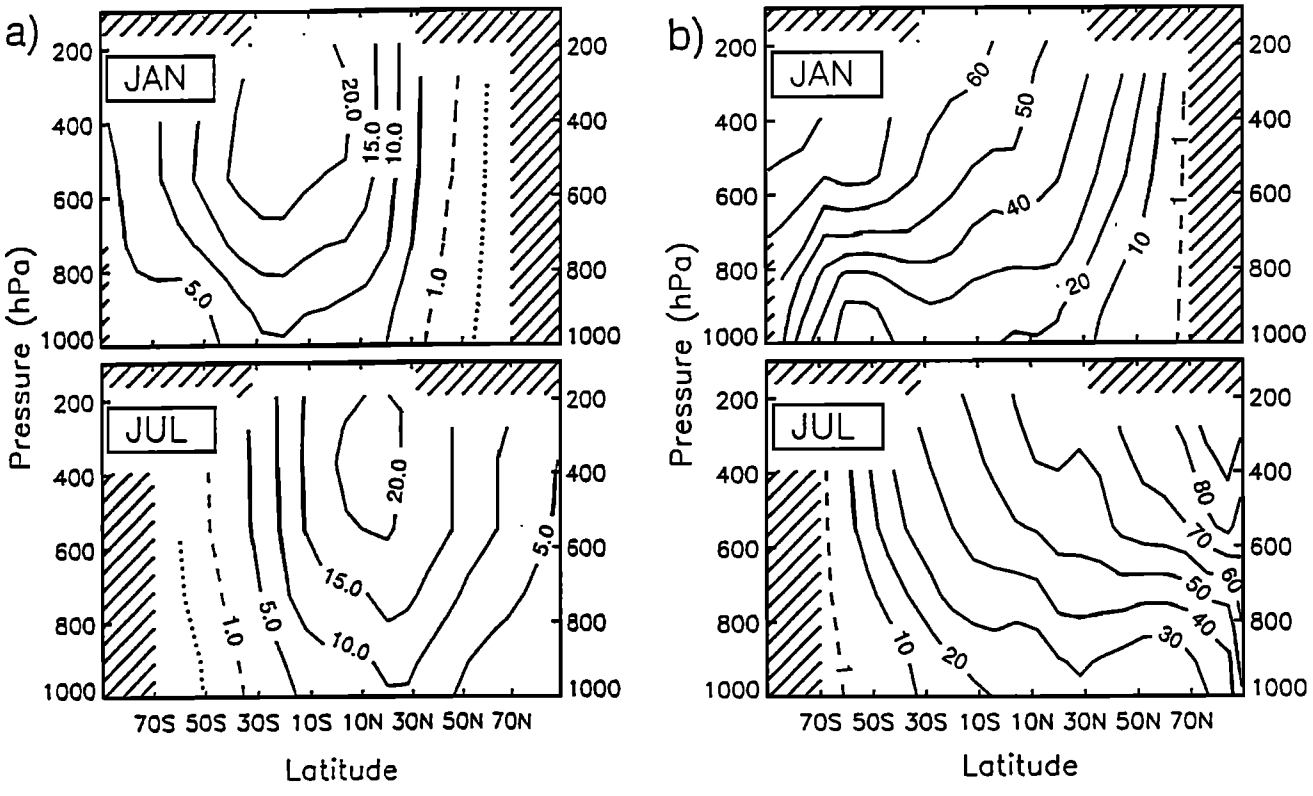

Figure 5. Monthly and zonally averaged J values (including night hours) for January and July for (a) $O_3 \rightarrow O^1D$ (10^{-6} s^{-1}) and (b) NO_2 photolysis (10^{-4} s^{-1}). For $O_3 \rightarrow O^1D$, contours are given for 0.1 (dotted lines), 1 (dashed lines), and for values from 5 to 25 with increments of 5 (solid lines). For NO_2, contours are given for 1 (dashed lines), and for values from 10 to 100, with increments of 10 (solid lines).

higher than 0.2 and only about 10% have reflectivities higher than 0.3; in the extratropics in summer the fraction of thick high clouds is even smaller.

The current distribution of OH was computed using 7-year averages of cloud reflectivities derived from the Stage C2 data. The replacement of GISS GCM II clouds led to a decrease in concentrations of OH below 800 hPa by 5–10% and a similar increase above 700 hPa (except at high latitudes), resulting in an increase in global mean OH by 2%.

3. Photochemical Model

The 3-D distribution of tropospheric OH (averaged over 24 hours) was computed as a function of O_3, CO, NO_t, hydrocarbons, water vapor, temperature, cloud cover, and the density of the overhead ozone column, by forcing the system of kinetic equations to a periodic solution, with a period of 24 hours. The inorganic and methane photochemistry was taken from *DeMore et al.* [1997], modified by *Talukdar et al.* [1998]; the chemical mechanism for NMHC was based on *Atkinson et al.* [1997] using *Talukdar et al.* [1997a, b], except for isoprene chemistry which was based on *Horowitz et al.* [1998].

Photolysis frequencies (J values) were computed using the Harvard six-stream radiative code [*Wofsy*, 1978; *Logan et al.*, 1981]. The distribution of surface albedo (as "gray") was taken from the GISS GCM II [*Hansen et al.*, 1983]. Zonally averaged frequencies of $O_3 \rightarrow O(^1D)$ and NO_2 photolysis for January and July are shown in Figure 5 (monthly means, including night hours). For NO_2, most of the photolysis occurs in the visible, and the 24-hour-average J values are largest in the summer-pole region where the day is the longest. For $O(^1D)$, with most of the photolysis occurring in the ultraviolet, the effect of a longer day is overcome by that of a lower sun and thus the higher absorption by O_3. While more photons are available at higher altitudes, the J values for $O_3 \rightarrow O(^1D)$ decrease with height in the upper troposphere in the tropics as a result of a decrease in the yield of $O(^1D)$ associated with the decrease in temperature.

4. Three-Dimensional Distribution of Tropospheric OH

Zonally averaged concentrations of OH for four seasons are shown in Figure 6; distributions at 700 hPa are presented for January and July in Figure 7. Global,

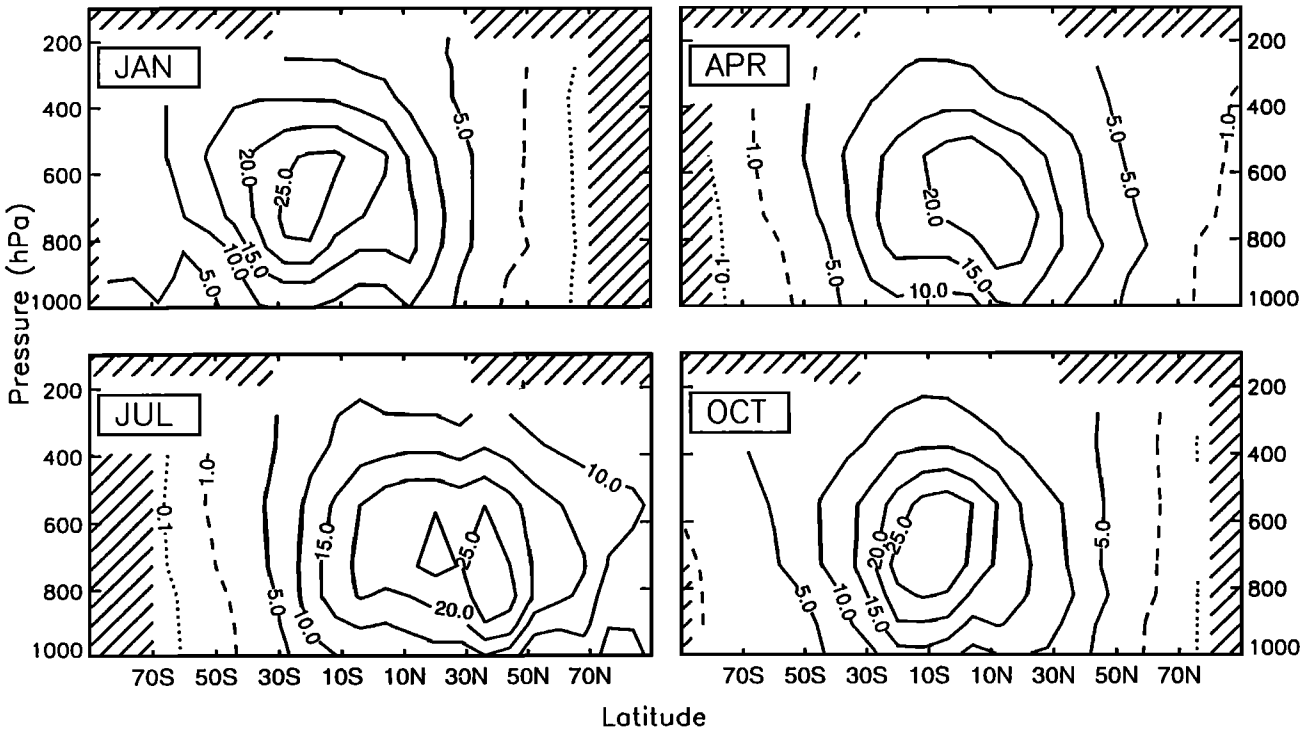

Figure 6. Zonally and monthly averaged concentrations of OH (10^5 molecules cm^{-3}) for January, April, July and October, including night hours. Contours are given for 0.1 (dotted lines), 1 (dashed lines), and for values from 5 to 30, with increments of 5 (solid lines).

hemispheric and semihemispheric averages are given in Table 4, and zonal means are given in Table 5. Consistent with previous studies, highest concentrations of OH arise in the tropics; strong seasonal variations are predicted for midlatitudes reflecting variations in sunlight and water vapor. The global tropospheric mean concentration of OH is 11.6×10^5 molecules cm^{-3}, that is, ~33% higher than in S90 as shown in Table 4 (integrated over the year with respect to mass of air from the surface to 100 hPa between 32°S and 32°N and to 200 hPa outside of this region). Changes in reaction rates, primarily in the $O(^1D)$ quantum yield and in reaction of OH with CH_4 [*DeMore et al.*, 1997; *Talukdar et al.*, 1998] are responsible for a ~19% increase in OH (with about two thirds of that due to the increase in the $O(^1D)$ quantum yield). The remaining difference results from competing effects of increases due to changes in distributions of precursors as described above (~24%), offset by decreases due to inclusion of reactions involving isoprene and other NMHC, of about 3% and 7%, respectively.

As in S90, mean hemispheric concentrations of OH differ little from each other. Mean tropical concentrations (within 32° latitude) are ~5% lower in the north, while ~14% more OH is predicted for the region poleward of 32° in the north than in the south (see Table 4). In contrast to S90, the present distribution of OH reflects the influence of biomass burning in the southern tropics between June and October over Africa, South America, and the Atlantic, and from November to March over sub-Saharan Africa. Accounting for biomass burning resulted in higher concentrations of OH for these regions.

The vertical distribution of OH differs significantly from earlier results as reflected in the shape of the global annual mean profile (Figure 8). In the present distribution, only 33% of tropospheric OH (integrated with respect to mass of air) resides below 700 hPa as compared to 42% in S90. In the lower troposphere, increases in OH caused by changes in reaction rates and in concentrations of precursors (an increase for NO_t and H_2O and a decrease for CO) were offset by decreases resulting from inclusion of NMHC (destroyed more efficiently at higher temperatures) and from higher reflectivities of ISCCP clouds in the tropics than those for clouds used in S90. The latter change in addition enhanced production of OH above the clouds contributing to an increase in OH in the middle and upper troposphere. For gases with slower loss rates at lower temperatures, this upward shift in OH mitigates the effect of the increase in the mean abundance of OH. Thus tropospheric global mean loss frequencies of CH_3CCl_3 and CH_4 increased by ~23% (evaluated using current rate constants for both species) even though the global mean tropospheric abundance of OH increased by ~33%.

Concentrations of OH above 200 hPa in the tropics increased by 60–200%, with more than half of the effect resulting from photolysis of acetone [*Singh et al.*,

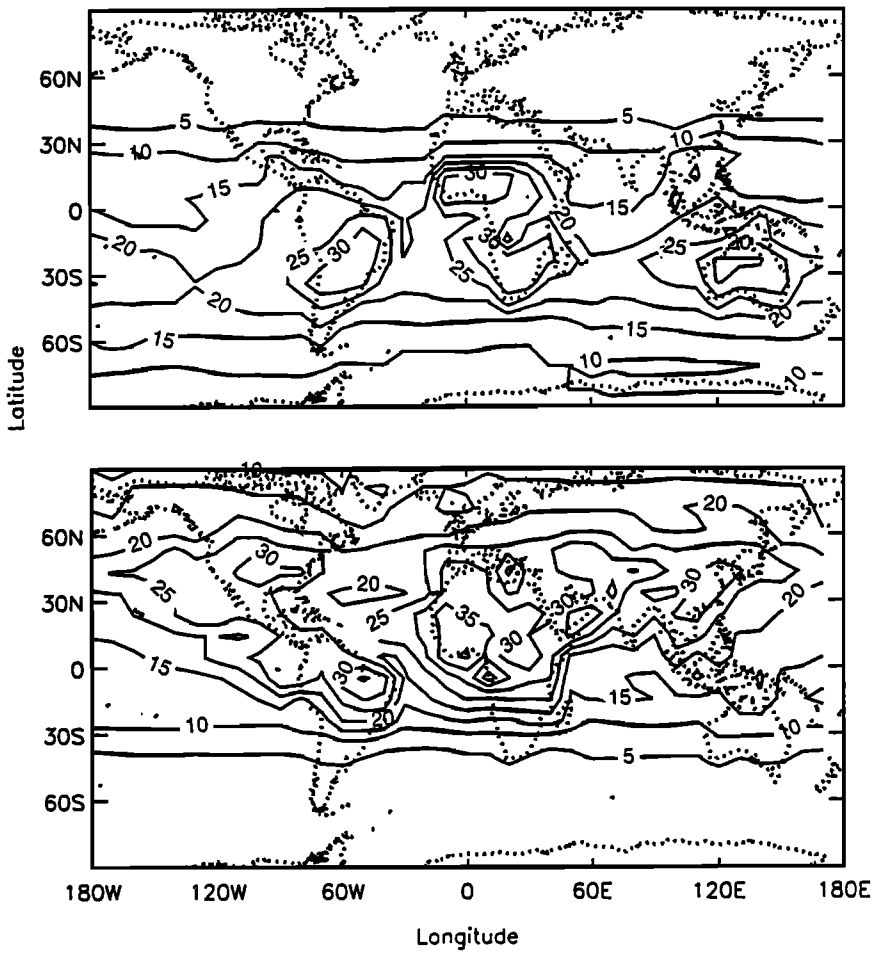

Figure 7. Distribution of OH (10^5 molecules cm^{-3}) at 700 hPa (top) for January and (bottom) for July. Contours are given for values from 5 to 50 with increments of 5.

1995]. We emphasize however that computed concentrations of OH in the upper troposphere may need to be revised significantly because of uncertainties in the distributions of acetone and NO_t. In addition, the assumption of a periodic steady state for H_2O_2, CH_2O, and CH_3OOH may not be appropriate for the upper troposphere due to a significant influx of these species from the boundary layer associated with deep convection [*Prather and Jacob*, 1997; *Jaegle et al.*, 1997].

Global mean OH for the distribution presented here is higher than predicted by the fully coupled CTMs of *Wang et al.* [1998b] and *Hauglustaine et al.* [1998], by 10–15%. The discrepancy is larger in January than in July, particularly in the southern tropics between

Table 4. Mean Concentration of OH

	January		July		Annual	
	This Study	S90	This Study	S90	This Study	S90
90°S–32°S	12.1	9.4	1.8	1.1	6.4	4.7
32°S–0°	17.8	13.7	12.3	8.8	15.4	11.4
0°–32°N	10.6	8.2	17.9	13.1	14.7	10.9
32°N–90°N	1.5	1.1	16.5	13.2	7.3	6.0
Southern Hemisphere	15.3	11.8	8.0	5.8	11.6	8.6
Northern Hemisphere	7.0	5.5	17.3	13.2	11.6	8.9
Globe	11.3	8.8	12.7	9.6	11.6	8.7

Results represent averages integrated with respect to mass of air from the surface to 100 hPa within 32° latitude and to 200 hPa outside that region. Concentrations of OH are in 10^5 molecules cm^{-3}.

Table 5a. Zonally and Monthly Averaged Concentrations of OH for January

	1000 hPa	900 hPa	800 hPa	700 hPa	500 hPa	300 hPa	200 hPa
90°N	—	—	—	—	—	—	—
84°N	—	—	—	—	—	—	—
76°N	—	—	—	—	—	—	—
68°N	0.0	0.0	0.0	0.0	0.0	0.0	0.0
60°N	0.2	0.2	0.2	0.2	0.2	0.2	0.2
52°N	0.4	0.4	0.8	0.6	0.6	0.7	0.8
44°N	0.7	0.9	1.8	1.4	1.6	1.6	1.7
36°N	1.7	2.1	3.6	3.3	3.7	3.5	3.5
28°N	4.3	5.1	6.2	7.1	6.4	4.5	4.6
20°N	7.3	9.2	11.4	12.2	10.0	6.4	5.9
12°N	10.0	13.7	16.3	16.0	14.3	8.5	7.2
4°N	7.0	11.2	15.4	18.5	20.7	11.2	9.2
4°S	7.1	10.9	15.5	20.2	23.0	12.8	9.6
12°S	8.9	13.1	18.4	22.8	26.1	14.2	11.1
20°S	10.2	16.0	24.5	26.6	25.6	14.6	11.2
28°S	10.5	15.8	24.4	26.1	24.3	14.8	11.4
36°S	9.6	13.8	18.4	21.1	21.1	14.7	11.8
44°S	6.2	8.1	11.0	16.2	18.9	14.2	11.4
52°S	4.1	5.1	7.4	12.5	15.5	12.7	10.2
60°S	3.0	3.7	5.2	9.9	12.0	11.0	9.3
68°S	4.5	7.2	7.3	8.6	8.9	9.6	9.0
76°S	4.0	5.0	5.0	6.8	7.3	8.5	8.9
84°S	4.7	5.0	5.0	6.4	6.6	7.9	8.9
90°S	—	—	—	6.5	6.6	7.7	8.6

Concentrations of OH are in 10^5 molecules cm^{-3}.

Table 5b. Zonally and Monthly Averaged Concentrations of OH for April

	1000 hPa	900 hPa	800 hPa	700 hPa	500 hPa	300 hPa	200 hPa
90 °N	0.4	0.6	0.8	1.0	0.8	0.9	1.3
84 °N	0.3	0.5	0.6	0.8	1.0	1.1	1.5
76 °N	0.5	0.7	0.9	1.4	1.4	1.6	2.1
68 °N	3.9	3.5	3.4	3.2	2.2	2.3	2.7
60 °N	3.8	4.1	5.0	4.4	3.5	3.2	3.3
52 °N	4.9	5.3	7.1	6.0	5.1	4.2	4.0
44 °N	7.8	8.7	11.0	8.8	7.7	5.6	5.0
36 °N	9.0	11.9	13.8	12.7	11.3	7.5	6.4
28 °N	12.4	14.8	17.1	18.1	14.8	7.9	6.9
20 °N	15.1	18.9	21.4	23.7	17.8	9.6	8.0
12 °N	14.3	19.4	22.1	23.5	20.4	10.4	8.4
4 °N	7.7	14.1	18.8	22.4	23.5	12.3	10.0
4 °S	7.1	13.4	16.0	20.8	22.3	12.7	10.6
12 °S	7.3	13.6	15.9	19.1	19.8	12.0	10.7
20 °S	8.7	12.8	16.8	18.4	16.7	11.0	9.6
28 °S	7.9	10.4	12.9	14.1	13.6	9.7	8.6
36 °S	5.8	6.8	8.0	9.6	10.5	8.0	6.9
44 °S	2.7	3.1	3.9	5.5	7.5	6.1	5.6
52 °S	1.1	1.4	1.7	2.8	4.3	4.0	3.4
60 °S	0.4	0.5	0.7	1.3	2.1	2.1	1.8
68 °S	0.2	0.3	0.3	0.5	0.7	0.8	0.7
76 °S	0.1	0.1	0.1	0.1	0.2	0.1	0.2
84 °S	0.0	0.0	0.0	0.1	0.1	0.0	0.0
90 °S	—	—	—	—	—	—	—

Concentrations of OH are in 10^5 molecules cm^{-3}.

Table 5c. Zonally and Monthly Averaged Concentrations of OH for July

	1000 hPa	900 hPa	800 hPa	700 hPa	500 hPa	300 hPa	200 hPa
90 °N	5.5	7.4	8.3	10.0	9.7	6.9	8.8
84 °N	3.8	5.2	6.4	8.6	10.9	7.7	9.5
76 °N	3.7	5.1	6.9	9.7	11.5	7.6	8.4
68 °N	7.4	11.6	13.9	15.4	13.2	8.2	7.7
60 °N	6.2	10.6	16.2	17.0	15.3	9.2	8.0
52 °N	6.2	11.8	19.5	19.4	17.5	10.6	8.6
44 °N	12.3	23.1	26.9	25.1	22.1	12.6	10.0
36 °N	14.9	24.7	27.9	28.0	25.0	14.4	11.3
28 °N	12.6	17.9	22.7	24.7	23.3	12.3	8.8
20 °N	13.0	17.6	21.9	26.5	24.8	13.7	10.0
12 °N	10.9	16.4	20.1	24.4	24.8	13.6	10.0
4 °N	10.3	14.6	19.2	22.3	23.2	12.9	10.2
4 °S	10.4	15.4	20.4	21.3	20.1	12.4	10.9
12 °S	9.9	13.8	17.8	17.8	15.9	10.5	9.9
20 °S	7.9	10.9	12.7	13.1	11.3	8.6	7.8
28 °S	4.5	5.6	6.2	7.1	7.1	5.8	5.8
36 °S	2.6	2.8	3.2	4.0	4.6	3.7	3.3
44 °S	0.9	1.0	1.2	1.9	2.6	2.2	1.9
52 °S	0.3	0.3	0.4	0.7	1.1	1.0	0.9
60 °S	0.1	0.1	0.1	0.2	0.3	0.2	0.2
68 °S	0.0	0.0	0.0	0.0	0.0	0.0	0.0
76 °S	—	—	—	—	—	—	—
84 °S	—	—	—	—	—	—	—
90 °S	—	—	—	—	—	—	—

Concentrations of OH are in 10^5 molecules cm $^{-3}$.

Table 5d. Zonally and Monthly Averaged Concentrations of OH for October

	1000 hPa	900 hPa	800 hPa	700 hPa	500 hPa	300 hPa	200 hPa
90 °N	—	—	—	—	—	—	—
84 °N	0.0	0.0	0.0	0.0	0.0	0.0	0.0
76 °N	0.1	0.1	0.1	0.1	0.1	0.1	0.1
68 °N	0.5	0.5	0.5	0.6	0.5	0.4	0.6
60 °N	0.8	0.9	1.2	1.2	1.5	1.3	1.5
52 °N	1.7	1.9	2.9	2.6	3.1	2.8	2.9
44 °N	4.4	4.7	6.5	5.3	5.7	4.9	5.1
36 °N	6.3	8.3	10.1	9.2	9.0	7.3	7.5
28 °N	9.4	12.0	13.5	13.2	11.3	7.0	6.5
20 °N	10.1	13.9	15.3	16.0	14.6	8.8	8.0
12 °N	9.9	15.3	17.4	19.1	20.1	10.6	8.8
4 °N	8.4	13.5	19.1	23.7	25.1	12.4	9.9
4 °S	11.4	18.5	24.5	28.7	28.0	14.3	11.2
12 °S	13.7	19.5	25.5	29.6	26.7	13.9	11.1
20 °S	13.1	19.5	23.8	27.1	22.2	13.6	10.4
28 °S	9.2	13.0	16.0	19.3	17.2	10.6	9.1
36 °S	8.0	9.4	11.0	13.5	13.4	8.9	7.4
44 °S	4.9	5.6	7.0	10.2	10.6	7.2	6.1
52 °S	3.0	3.5	4.5	6.9	7.5	6.0	5.3
60 °S	2.7	2.9	3.2	4.5	5.4	5.6	5.1
68 °S	2.7	3.4	3.3	3.7	3.6	5.3	5.2
76 °S	1.2	1.6	1.0	1.7	1.9	3.4	3.4
84 °S	0.0	0.9	0.9	1.0	1.3	2.3	2.2
90 °S	—	—	—	0.8	1.1	1.7	1.6

Concentrations of OH are in 10^5 molecules cm $^{-3}$.

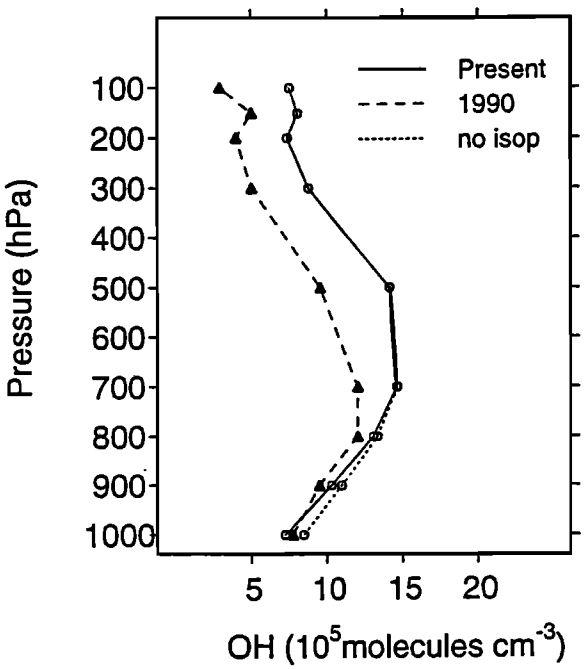

Figure 8. Annually and globally averaged concentrations of OH in 10^5 molecules cm^{-3} for the present distribution (solid line), for OH computed with no isoprene (dotted line), and for OH from S90 (dashed line). Concentrations of OH were integrated with respect to mass of air.

700 and 500 hPa: 25–30% and 30–40% as compared to *Wang et al.* [1998c] and *Hauglustaine et al.* [1998], respectively. Part of the difference between our results for OH and those produced by fully coupled CTMs may be explained by neglect of transport of longer-lived products of isoprene oxidation in our study. However, a significant part of the discrepancy can be attributed to differences in O_3 and NO_x. Zonal means for the distribution of O_3 in the southern tropics in January used in our calculation are higher than predicted in the CTMs by 20-25%, accounting for a difference in OH of 10–15% (see section 5 for a discussion of sensitivity of OH to changes in precursors). Both CTM studies report underestimating O_3 at 500 hPa as compared to ozonesonde data in the southern tropics. Concentrations of NO_x adopted for this study appear to be higher by about a factor of 2 than in the CTMs in that region, accounting for a difference in OH by ~7%. Emissions of isoprene in the tropical forests used by *Wang et al.* [1998b] may be too high. The model of *Horowitz and Jacob* [1999], which differs from that of *Wang et al.* [1998b] mainly by an implementation of the chemical module (on-line solution of kinetic equations versus parameterization) and produces similar results, overestimates concentrations of isoprene over the Amazon region by factors 2–5. As described in section 2, we had to reduce emissions of isoprene in that model significantly (e.g., by a factor of 2 in tropical forests) to achieve reasonable agreement with observations. Global emissions of isoprene were reduced from 580 to 380 TgC yr^{-1}; the latter amount is close to the value for biogenic emissions given by *Hauglustaine et al.* [1998]. As discussed in section 10, observations of ^{14}CO in the tropics do not suggest that our results for OH are too high in that region. However, sparsity of observational data for O_3 and NO_x in the tropics does not allow for either an unambiguous characterization of the distributions in our study or for a definitive evaluation of fully coupled CTMs.

5. Sensitivity of OH to Uncertainties in Specification of Precursors

The tropical troposphere plays a major role in oxidation of CH_4, CO, and other industrial compounds [e.g., *Logan et al.*, 1981]. With the distribution presented here, 74% of tropospheric OH and 78% of CH_4 loss are between 32°S and 32°N, whereas 64% of OH and 79% of CH_4 loss are below 500 hPa. Consequently, the chemistry of OH in the tropics below 500 hPa is the focus of the discussion below. The sensitivity of OH to the specification of precursors is considered only for the current chemical mechanism and present levels of relevant species. The discussion in this section draws heavily on concepts and results from earlier studies [e.g., *Liu*, 1977; *Logan et al.*, 1981; *Ehhalt et al.*, 1991; *Kleinman*, 1994].

Table 6 summarizes changes in the global mean concentration of OH resulting from a scaling (within ±50%) of distributions of various precursors. The muted response to changes in tropospheric concentrations of O_3, H_2O, CO, NO_t, and CH_4 can be understood best in the context of production, loss, and internal transformations of the family of species, HO_x ($OH+HO_2+CH_3O_2+H+CH_3O+O_2CH_2OH$), a subset of a larger family, odd H ($HO_x+2H_2O_2+2CH_3OOH+HNO_4+HNO_2$).

5.1. Sensitivity to Changes in O_3, H_2O, and NO_t

As illustrated in Figure 9, most of HO_x and odd H below 500 hPa is produced in the form of OH:

$$O(^1D) + H_2O \rightarrow OH + OH. \quad (1)$$

Table 6. Relative Change in Global Mean OH due to a Uniform Scaling of Precursors by ±25% and ±50%

	−50%	−25%	25%	50%
H_2O	−24	−11	10	20
O_3	−15	−8	8	17
O_3 and H_2O	−31	−18	20	43
NO_t	−17	−8	8	14
CO	23	10	−8	−14
CH_4	14	6	−5	−10
O_3 column	71	26	−17	−28

Relative change in OH is in percent.

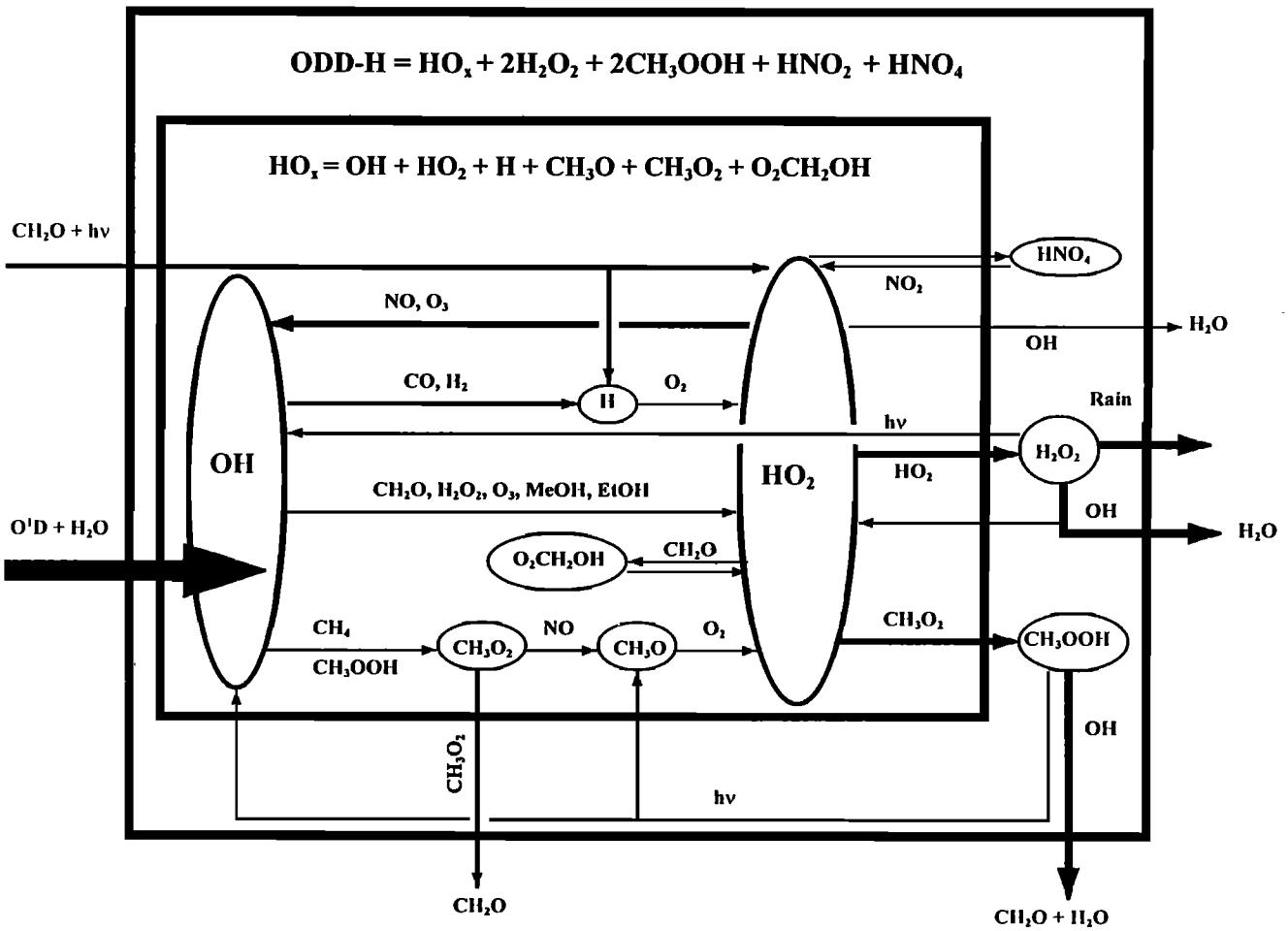

Figure 9. Major chemical transformations affecting HO_x and odd H in the lower and middle troposphere.

Dominant loss processes for OH, such as reactions with CO, CH_4, and NMHC, represent main routes for production of HO_2, the key species for secondary production of OH through reactions

$$HO_2 + NO \rightarrow OH + NO_2, \quad (2)$$

$$HO_2 + O_3 \rightarrow OH + 2O_2. \quad (3)$$

Major loss processes for HO_2 occur through reactions with CH_3O_2 as well as with itself and represent an efficient self-destruction of HO_x (consuming two molecules of HO_x per reaction). An alliance of two factors: (1) the second-order loss of HO_x and (2) the significance of secondary production of OH, is at the root of the weaker-than-proportional dependence of concentrations of OH on the rate of its primary production through (1).

As a result of the second-order loss of HO_x, the role of secondary production of OH is higher at lower levels of HO_x. Secondary production plays a more important role therefore at higher latitudes where there is less $O(^1D)$ and water vapor (Figure 10). In the lower troposphere over tropical oceans (except during biomass burning), (2) and (3) play comparable roles in secondary production of OH, together amounting to less than half of primary production. In polluted regions affected by biomass burning or industrial emissions, (2) is not only more important than (3) but it exceeds primary production of OH. The sensitivity of OH to changes in O_3 and H_2O is vastly different for these two regimes of tropospheric chemistry characterized by the role of secondary production and determined by the abundance of NO_t. In the low-NO_t regime (for NO_t concentrations, see Table 1), a 50% change in concentration of O_3 or H_2O leads to a 25–35% change in OH (Figures 11a and 11b). In contrast, the sensitivity of OH to changes in O_3 or H_2O (and thus in the rate of (1)) is diminished in the high-NO_t regime (Figures 11e and 11f), for example, during the biomass burning season over land below 700 hPa; under these conditions, the rate for secondary production of OH through (2) is higher by more than a factor of 4 than the rate for primary production by (1). Although relative changes in concentrations of O_3 and H_2O affect the rate of (1) roughly in the same way, on average the sensitivity of OH to changes in H_2O is somewhat higher than to those in O_3 (see Table 6). This difference is evident in the

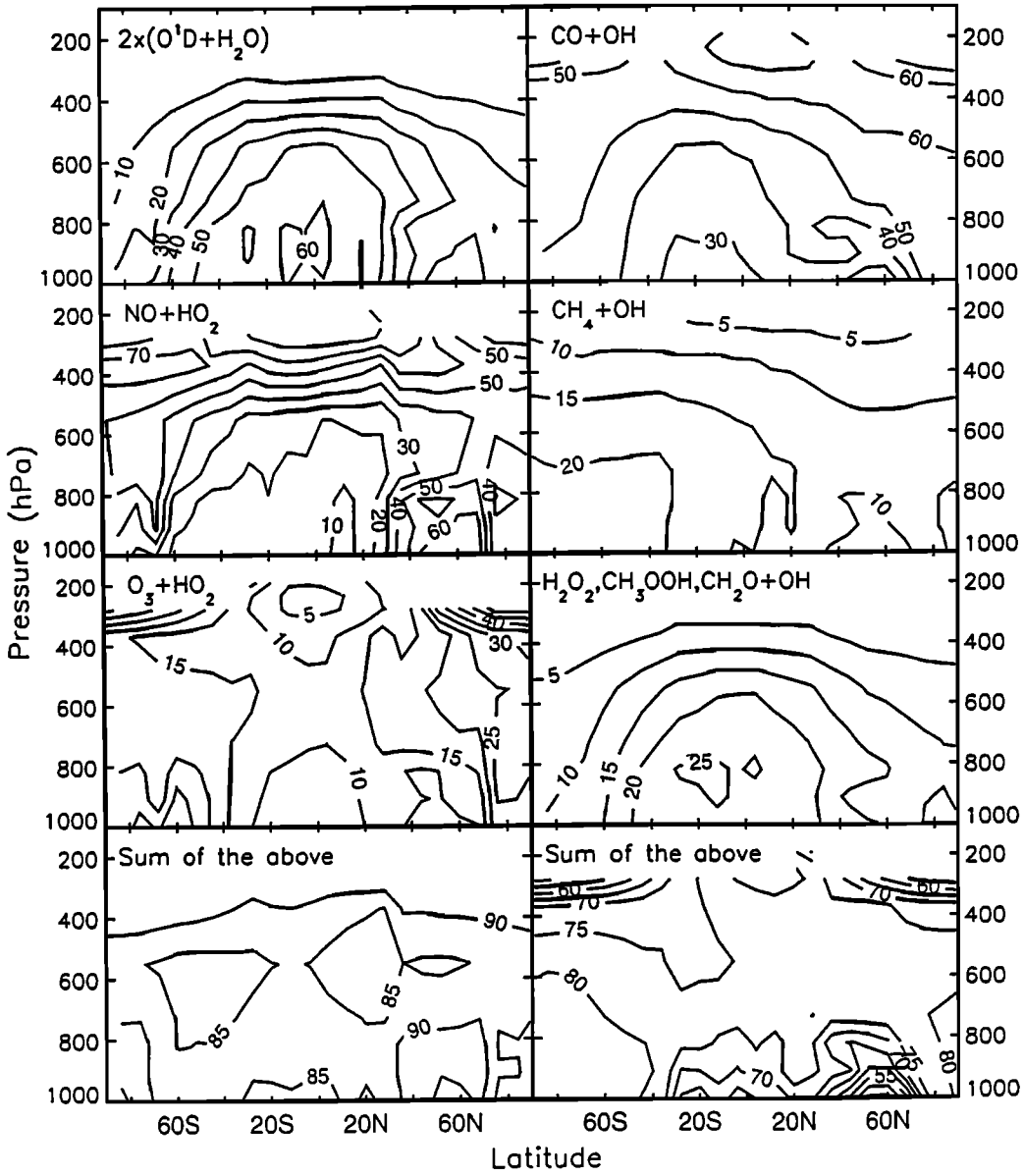

Figure 10. (left) Fraction (percent) of total production of OH occurring through reaction (1), (2), (3), and their sum. (right) Fraction of total loss of OH occurring through reaction with CO, with CH_4, combined in reactions with H_2O_2, CH_3OOH, and CH_2O, and their sum. Fractions are computed for annually averaged rates.

high-NO_t regime (Figures 11e and 11f); it arises from the particular roles that H_2O and O_3 play in determining the rate of (2). Higher concentrations of H_2O lead to lower concentrations of HO_2 by enhancing the rate for an important branch of its self-reaction, whereas O_3 provides the main loss process for NO. In both cases, however, increases in primary production of OH resulting from increases in O_3 or H_2O are mitigated by decreases in the rate of (2). In the upper troposphere where (1) contributes little to production of OH (Figure 10), concentrations of OH are lower at higher levels of O_3 (Figures 11a and 11e); in the region of transition around 300–400 hPa, concentrations of OH are insensitive to changes in O_3.

On average, as shown in Figure 10, primary production of OH through (1) contributes 40–60% to the total production of OH in the tropical troposphere below 500 hPa, with secondary production, through (2) and (3), accounting for a major part of the remainder. The loss processes for HO_x result in production of the reservoir species for HO_x, H_2O_2 and CH_3OOH (Figure 9). Photolysis of H_2O_2 provides most of the remaining production of OH in the lower troposphere (photolysis of CH_3OOH contributes to production of HO_2, via reaction of CH_3O with O_2). As in the case of HO_x, odd H is removed mainly by processes destroying two molecules of odd H per reaction, such as reactions of H_2O_2, CH_3OOH, and HO_2 with OH, and deposition of

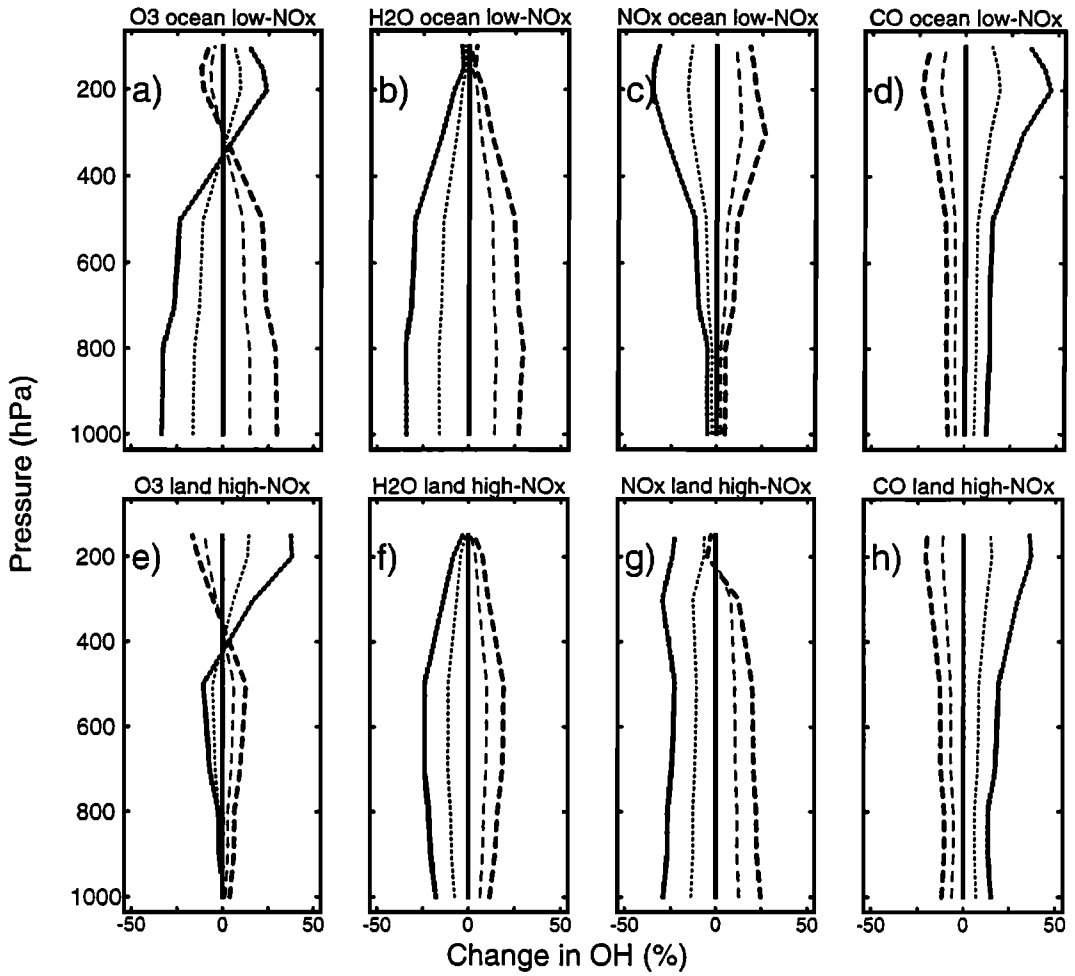

Figure 11. Change in OH (percent) in response to changes by −50%, −25% (dotted lines), +25%, +50% (dashed lines) at 15°S over ocean in January in (a) O_3, (b) H_2O, (c) NO_t, and (d) CO, and over land in July in response to changes in (e) O_3, (f) H_2O, (g) NO_t, and (h) CO. Note that results for July reflect the influence of biomass burning. Thin lines correspond to ±25% perturbations, and thick lines correspond to those of ±50%.

H_2O_2; these decrease further the sensitivity of OH to the rate of (1).

The sensitivity of OH to the rate of (1) is also impeded by a cascade production of species destroying OH, initiated by reactions of OH with CH_4, NMHC, and CO. Reactions with such species, including CH_2O, CH_3OOH, and H_2O_2, contribute more than 20% to the total loss of OH in the tropics below 500 hPa (Figure 10).

Of all the factors affecting OH, the greatest sensitivity is associated with changes in column O_3. A major part of production of $O(^1D)$ in the troposphere occurs around 305 nm [*Jacob*, 1999; *DeMore et al.*, 1997], that is, in the region of the spectrum with a significant absorption by O_3. An O_3 column of 250 Dobson units (DU) has an optical depth in the range 0.88–1.7 between 302.5 and 307.5 nm. In that region, the exponential dependence of extinction on the optical path results in a significant amplification of relative changes in the J value for $O_3 \rightarrow O(^1D)$ photolysis as compared to those in column O_3, particularly for large negative perturbations. (If $1+\delta$ is a scaling factor for the column and τ is the optical path, the relative change in the transmitted flux is $e^{-\tau\delta}-1$). We estimated that the documented reduction of column O_3 over 1979–1994 [*McPeters et al.*, 1996] may have resulted in an increase in global mean OH by 1.5–2% (neglecting the effect of ensuing changes in CO and hydrocarbons) [cf. *Krol et al.*, 1998]; no significant trend in column O_3 was found in the tropics and the reported decrease for midlatitudes averaged 4–6% per decade.

As mentioned in section 3, a dependence of ground albedo on the wavelength [e.g., *Blumthaler and Ambach*, 1988] was not taken into account. As a result, the J values for $O_3 \rightarrow O(^1D)$ photolysis near the surface may be underestimated by ~4% over the ocean and overestimated by 5–15% over the land with errors decreasing with height. The ensuing errors in OH near

the surface are not expected to exceed −2% and +10% over the ocean and land, respectively.

The results of *Liu and Tang* [1992] suggest that the concentrations assumed for water vapor in the lower troposphere should be accurate to ±25% over most of the globe. *Logan* [1999] gives an estimate of ±30% for the overall uncertainty associated with her climatology for O_3. The error in global mean OH resulting from uncertainties in O_3 and H_2O is not expected to exceed ±25% (see Table 6) even if these errors conspire everywhere to change concentrations of OH in one direction. However, since there is no reason for a systematic bias in specified distributions or for a correlation between errors in H_2O and O_3, the actual error in global mean OH is most likely smaller. It is clear that for higher accuracy of computed OH it is more important to minimize uncertainties in H_2O and O_3 in the pristine tropical troposphere than for polluted regions. Unfortunately, it is for the tropical troposphere that our knowledge of O_3 is weakest [*Logan*, 1999]. Larger errors in H_2O above 300 hPa discussed above are not expected to affect significantly local concentrations of OH because (1) contributes less than 20% to production of OH over much of that region (Figure 10).

A relative change in the NO_t distribution (within ±50%) results in a response in global mean OH that is about 3–3.5 times smaller (Table 6). In the high-NO_t regime in the tropics below 800 hPa, as over land in the biomass burning season, a 50% change in NO_t leads to a ~25% change in OH in contrast to a 5% change in OH in pristine regions (Figures 11g and 11c). As discussed in section 2, the climatology of tropospheric NO_t is not well defined and errors may be larger than a factor of 2. However, if concentrations of NO_t for the biomass burning regions below 500 hPa (Table 1b) are scaled by factors of 2 and 3, global mean OH increases by only 2% and 3%, respectively. This lack of sensitivity arises from a relatively small volume of the troposphere affected on average by biomass burning as well as from a lesser dependence of OH on NO_t once NO_t levels exceed ~300 pptv [*Logan et al.*, 1981] (despite the dominant contribution of (2) to production of OH). At these levels of NO_t the rate for (2) is less sensitive to NO_t since (2) becomes the major loss process for HO_2. At still higher levels of NO_t, concentrations of OH decrease as reaction of OH with NO_2 contributes significantly to the removal of OH. Similarly, a decrease in OH with increasing concentrations of NO_t in the upper troposphere over polluted regions, as evident in Figure 11g, results from the increasing importance of reactions with NO_2, HNO_4, and NO as loss processes for OH; the first two reactions, in addition, result in loss of odd H.

In our view, the largest errors in computed mean OH associated with specification of NO_t may arise from uncertainties between 800 and 500 hPa (including the unpolluted regions), where particularly high concentrations of OH are predicted (see Figure 6). A factor of 2 decrease in NO_t at these altitudes results in at least a 10% decrease in OH in the tropics (Figure 11c) and 15% at midlatitudes (not shown). To ascertain further the uncertainties in OH due to those in NO_t, we replaced the distribution of NO_t used to compute standard OH (Table 1) by that simulated using the CTM of *Horowitz and Jacob* [1999] (similar to *Wang et al.* [1998b] as discussed in section 4). The resulting global mean OH (integrated with respect to mass of air) decreased by 6%, the hemispheric mean for the NH changed little, but the hemispheric mean for the SH decreased by 10% (~7% in the tropics and ~22% in the extratropics). Concentrations of NO_t from the CTM simulation, as compared to values in Table 1, are lower in the SH by a factor of 2 over the oceans in the tropics and by a factor of 4–5 at midlatitudes. The available observations of NO do not allow resolution of these differences. A significant underestimate of concentrations of O_3 above 700 hPa in the southern tropics by *Wang et al.* [1998b] may be an indication of insufficient levels of NO_x, in their model. At southern midlatitudes, however, high levels of NO_t assumed in this work may be contributing to a possible overestimation of OH in this region suggested by the analysis of seasonal variations of CH_3CCl_3 and CH_2Cl_2 (section 9.3).

5.2. Sensitivity to Changes in CO

Reaction with CO accounts for 30–50% of the total loss of OH below 500 hPa in the tropics and 40–60% outside the tropics (Figure 10). Reaction with CH_4 contributes 15–20% to the loss of OH south of 20°N in the lower troposphere, with a smaller effect to the north. The remaining loss processes, accounting for 30–50% of removal of OH below 500 hPa, include reactions with the products of methane oxidation, such as CH_3OOH and CH_2O, reactions with other hydrocarbons and their products, with H_2, and with H_2O_2. The importance of loss processes unrelated to CO lessens the sensitivity of OH to changes in CO. A change in CO by ±50% globally modifies global mean OH by −14% and +23% (Table 6). The asymmetry in sensitivity (increase versus decrease) is characteristic of an inverse dependence. The sensitivity of OH to changes in CO increases with height (Figures 11d and 11h) reflecting the increasing importance of CO in removal of OH (Figure 10): rates for reactions of OH with CH_4 and other hydrocarbons, enhanced at higher temperatures, fall off more rapidly with height than the pressure-dependent rate for CO.

5.3. Sensitivity to Changes in Hydrocarbons

If concentrations of NMHC (other than isoprene) are increased by a factor of 4, mean OH decreases by less than 15%. An increase in concentration of acetone by a factor of 4 results in an increase in OH above 200 hPa in the tropics by ~50%, with little effect on the global mean (<1%). Based on simulations using the fully coupled model of *Horowitz and Jacob* [1999], we estimate that uncertainties associated with the specification of

isoprene and with the neglect of transport of the intermediate products of isoprene oxidation are not likely to result in errors in mean OH exceeding 5%. Little uncertainty is associated with the distribution of methane, which is almost uniform and well known. However, the sensitivity of global mean OH to changes in CH_4 is of interest because CH_4 has doubled since preindustrial times and has been increasing until recently [e.g., *Dlugokencky et al.*, 1998]. A ±50% change in concentration of CH_4 throughout the globe results in −10% and +14% change in OH (Table 6).

6. Temperature Appropriate for Rescaling Tropospheric Lifetimes

Atmospheric lifetimes of gases destroyed by OH in reactions with temperature-dependent rate constants, expressed as $k = Ae^{-B/T}$ for temperature T, are often estimated by relating their rate constants to that of a reference species, for example, CH_3CCl_3. *Prather and Spivakovsky* [1990] showed, using the distribution of OH from S90, that this method is accurate to better than 7% over a wide range of B (0–2500 K) if rate constants are evaluated at temperature T = 277 K. However, their result must be revised for the present distribution of OH since a smaller fraction of tropospheric OH resides in the lower troposphere. As shown in Figure 12, which is similar to the key figure from their work, T = 272 K provides a more appropriate choice for the present distribution resulting in a less than 5% error over the whole range of B. Alternatively, errors can be made even smaller if temperatures 271 K and 277 K are used for the lower and higher part of the range, respectively. The error estimate assumes no stratospheric loss and uniform mixing ratios throughout the atmosphere [*Prather and Spivakovsky*, 1990].

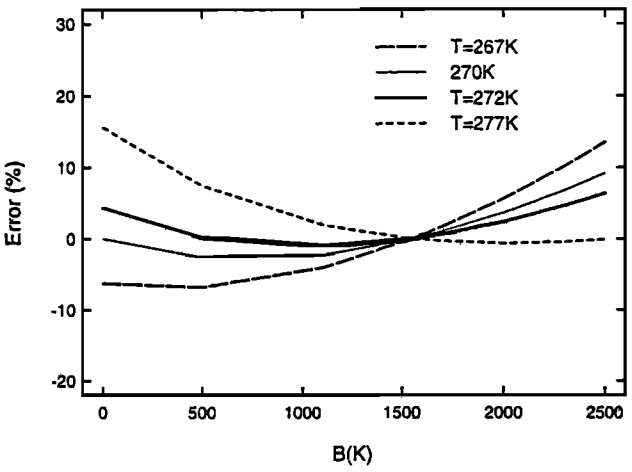

Figure 12. Errors in lifetimes of gases with respect to destruction by tropospheric OH, with the rate constant expressed as $Ae^{-B/T}$ molecules^{-1} cm^3 s^{-1}, by scaling the rate coefficient to that for CH_3CCl_3 [*Prather and Spivakovsky*, 1990] at 277 K (short-dashed line), at 272 K (bold solid line), at 270 K (thin solid line) and at 267 K (long-dashed line). These errors were computed assuming uniform mixing ratio of gases throughout the atmosphere and no OH in the stratosphere. Larger errors may be incurred for tracers with distributions displaying steep gradients (see text, section 6).

We emphasize that this method is appropriate for long-lived species and that additional significant errors can arise for short-lived gases (with lifetimes of several months) because of large spatial gradients characteristic of their distributions. For example, simulations of C_2Cl_4 and CH_2Cl_2 discussed in section 9, revealed that actual lifetimes of these gases are longer by 17% than those obtained by scaling the lifetime of CH_3CCl_3. In this section and throughout this work we define mean lifetime (over a time period, over the whole atmosphere, or over a region) as a ratio of the mean abundance to the mean loss [cf. *Prather*, 1997].

Given the mean atmospheric lifetime of CH_3CCl_3 (with respect to reaction with tropospheric OH), one can obtain an estimate of mean OH averaged with respect to mass of air using the same approach, that is, by seeking to estimate a lifetime of a hypothetical species with the rate constant $Ae^{-B/T}$ at A = 1 cm^3 molecules^{-1}s^{-1} and B = 0 K. It follows from Figure 12 that for the present distribution the error in the mean global OH is negligible if the mean loss frequency of CH_3CCl_3 is evaluated at 270 K (at 272 K the error is ~4%). For example, assuming the mean atmospheric lifetime of CH_3CCl_3 with respect to all losses is 4.6 years (section 8, this work), and with respect to the stratospheric and ocean sink, 34 years [*Volk et al.*, 1997] and 80 years [*Butler et al.*, 1991], respectively, we compute the atmospheric lifetime of CH_3CCl_3 with respect to reaction with tropospheric OH of 5.7 years (1/(1/4.6–1/80–1/34)), which corresponds to the atmospheric mean loss frequency of 5.56×10^{-9}s^{-1}. The rate constant for reaction of CH_3CCl_3 with OH evaluated at 270 K is 5.62×10^{-15} molecules^{-1} cm^3 s^{-1} [*Talukdar et al.*, 1992]. Atmospheric mean OH (integrated with respect to mass of air) would then be equal $5.56 \times 10^{-9}/5.62 \times 10^{-15}$ molecules cm^{-3}, that is, 9.89×10^5 molecules cm^{-3}. This atmospheric mean accounts for OH residing in the troposphere and for zero OH in the stratosphere. It can be adjusted to represent mean OH over only the troposphere by taking into account the fraction of atmospheric mass residing in the troposphere; for example, assuming this fraction is 85% leads to mean OH over the troposphere of $9.89 \times 10^5/0.85 = 11.6 \times 10^5$ molecules cm^{-3}. Although this estimate of mean OH is derived by scaling the lifetime of CH_3CCl_3, the mean is not weighted by the frequency of reaction with CH_3CCl_3.

7. Chemical Tracer Model

Simulations of CH_3CCl_3, HCFC-22, ^{14}CO, C_2H_6, C_2Cl_4, and CH_2Cl_2, discussed below in the context of constraints observations of these gases pose for the com-

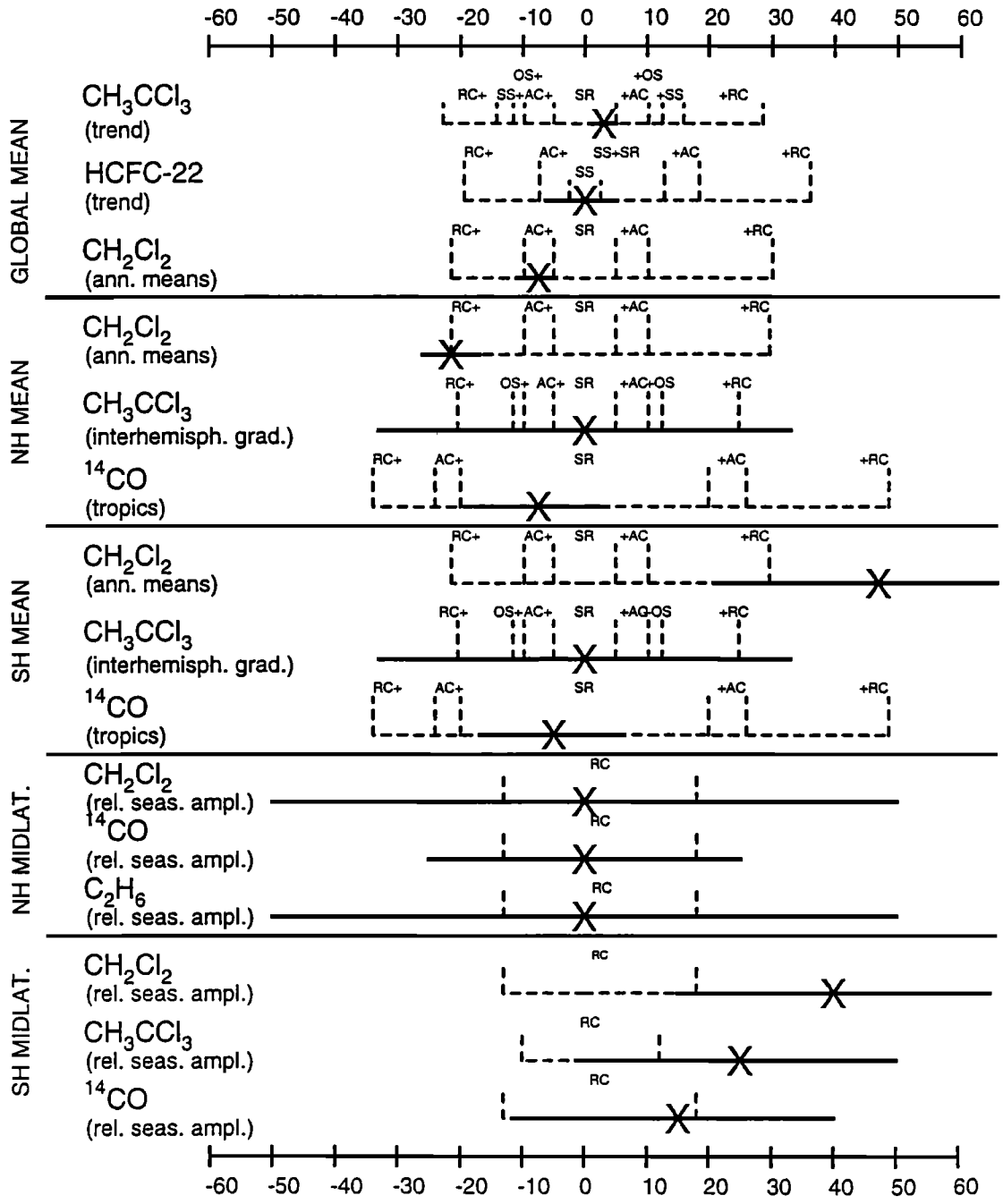

Figure 13. Deviations (percent) of computed OH from empirical OH (see text, section 8). Solid lines show uncertainties in estimating these deviations assuming that OH implied by observations is known exactly, for example, uncertainties associated with possible errors in model transport. Dashed lines denote uncertainties associated with determining empirical OH. They include uncertainties in the magnitude of sources (SR), absolute calibration (AC), strength of other sinks (OS and SS for ocean and stratospheric sinks, respectively), and rate constant for reaction with OH (RC). Estimates of deviations are given for concentrations of OH averaged over the regions specified on the left (weighted by the frequency of reaction with respective tracers).

puted distribution of OH, were performed using the Harvard/GISS/University of California, Irvine CTM [e.g., *Prather et al.*, 1987; *Jacob et al.*, 1987; S90; *Jacob and Prather*, 1990; *Balkanski and Jacob*, 1990; *Balkanski et al.*, 1992, 1993; *Chin et al.*, 1996; *Chin and Jacob*, 1996; *Koch et al.*, 1996; *Wang et al.*, 1998a, b, c]. The CTM uses the wind fields, surface pressures, temperatures and convective mass fluxes recorded every 4 hours for 1 year of the GISS GCM II simulation [*Hansen et al.*, 1983], with a resolution of 5° longitude and 4° latitude; height is resolved in nine layers using σ coordinates, with seven to eight layers in the troposphere. The

present distribution of OH was archived with a coarser horizontal resolution, at standard pressure levels. For the CTM simulations, we used linear interpolation of OH from pressure to σ coordinates. Each 8° by 10° grid box for OH comprises four grid boxes of the CTM; the same value for OH was assigned to these four adjacent boxes.

8. Constraints for Global Mean OH Imposed by the Budgets of CH_3CCl_3 and HCFC-22

In this section, as well as in sections 9 and 10, we will refer to Figure 13 summarizing results of the evaluation of the computed distribution of OH using observations of various tracers. Figure 13 shows deviations of the computed mean OH from "empirical OH" implied by observations of tracers (crosses). Empirical OH is defined for each observational constraint independently assuming the most likely values for the magnitude of sources, absolute calibration, rate constant for reaction with OH, and strength of other sinks. Two kinds of uncertainties are specified. One is defined assuming that empirical OH is known exactly (solid lines); relevant uncertainties in simulated transport rates would belong to this category. The other is associated with determining empirical OH, including uncertainties in the magnitude of sources, in the absolute calibration, rate constant or strength of other sinks (dashed lines). Uncertainties associated with the variability in observations, while reflected in figures for individual constraints, are not included in this summary. Ranges for uncertainties are computed for the worst case scenario, that is, assuming that all errors may affect an estimate in one direction.

8.1. Global Budget of CH_3CCl_3

Results of global simulations of CH_3CCl_3 are compared with observations [*Prinn et al.*, 1995] in Figure 14. The history of emissions of CH_3CCl_3 and their spatial distribution is from *Midgley and McCulloch* [1995] and P. Midgley (personal communication, 1997). The rate constant for reaction with OH is from *Talukdar et al.* [1992]. Simulations were initialized using Atmospheric Lifetime Experiment/Global Atmospheric Gases Experiment (ALE/GAGE) observations [*Prinn et al.*, 1995] for January 1979. We assumed 80 years as a lifetime of CH_3CCl_3 with respect to the ocean sink (i.e., the middle of the range estimated by *Butler et al.* [1991]) and distributed the loss frequency uniformly over the surface of the ocean. The stratospheric loss frequencies (Table 7) were obtained in a manner described by *Prather et al.* [1987] and S90, using the 2-D model of H. R. Schneider et al. (Analysis of residual mean transport in the stratosphere, 1, Model description and comparison with satellite data, submitted to *Journal of Geophysical Research*, 1999.) The atmospheric lifetime of CH_3CCl_3 due solely to the stratospheric loss in the model is 43 years, somewhat longer than 34 ± 7 years estimated by *Volk et al.* [1997]. Solid lines in Figure 14 represent the simulation with the computed distribution of OH (referred to as standard OH below) and with the stratospheric and ocean sink. The mean atmospheric lifetime of CH_3CCl_3 in this simulation is 4.6 years. Dashed lines correspond to simulations with standard OH reduced and increased by 25% (mean atmospheric lifetimes of CH_3CCl_3 are 5.8 and 3.8 years, respectively).

To facilitate the evaluation of the empirical and simulated lifetime of CH_3CCl_3, we compared with observations the time evolution of the global mean of CH_3CCl_3 at the surface (bottom panel in Figure 14); for that purpose, we first approximated station data, for observations and for model results, as a least squares polynomial of 4th degree (results of the evaluation are insensitive to the choice of the degree in the range 2–4). As can be seen in Figure 14, the global rate of growth of CH_3CCl_3 in 1979–1993 is reproduced accurately in the simulation with standard OH, whereas the rate of decline in 1993–1995 is overestimated. We assume here that larger uncertainties may be associated with the magnitude of emissions during the latter transitional period and evaluate the accuracy of the simulation using data for 1979–1993. We conclude that the simulation with standard OH (mean atmospheric lifetime of 4.6 years) gives the empirical lifetime of CH_3CCl_3. If the comparison with observations is conducted using concentrations of CH_3CCl_3 in the NH only (not shown), the computed lifetime appears to be longer by 1% than that implied by observations; the data for the SH imply a smaller error of the opposite sign. (The slightly different rate of growth in the two hemispheres does not signify a hemispheric asymmetry in OH but rather a delay with which changes in emissions affect the SH. Small discrepancies with observations in reproducing the rate of change in each hemisphere are expected since the rate of emissions was represented as a step function constant within a year.) An additional 1% uncertainty in the simulated mean lifetime of CH_3CCl_3 may be associated with the excessive rate of the stratosphere-troposphere exchange in the model (discussed below).

If we adopt as true the estimate of *Volk et al.* [1997] (which was based on observational data, however limited), the stratospheric loss amounts to ~14% (4.6/34) of the total loss of CH_3CCl_3 as compared to ~11% (4.6/43) in the model; therefore the loss with respect to stratospheric sinks is underestimated by 3%. In total, mean standard OH appears too high by $3 \pm 2\%$ (as denoted in Figure 13 by a cross placed in the middle of this range).

Assuming estimates for uncertainties in emissions from *Midgley and McCulloch* [1995] (less than ±5%), and those for the absolute calibration from *Prinn et al.* [1995] (less than ±5%), we conclude that the estimate of the mean lifetime of CH_3CCl_3 implied by observations (4.6 years), with respect to all loss processes, is accurate to better than ±10%. This uncertainty may be

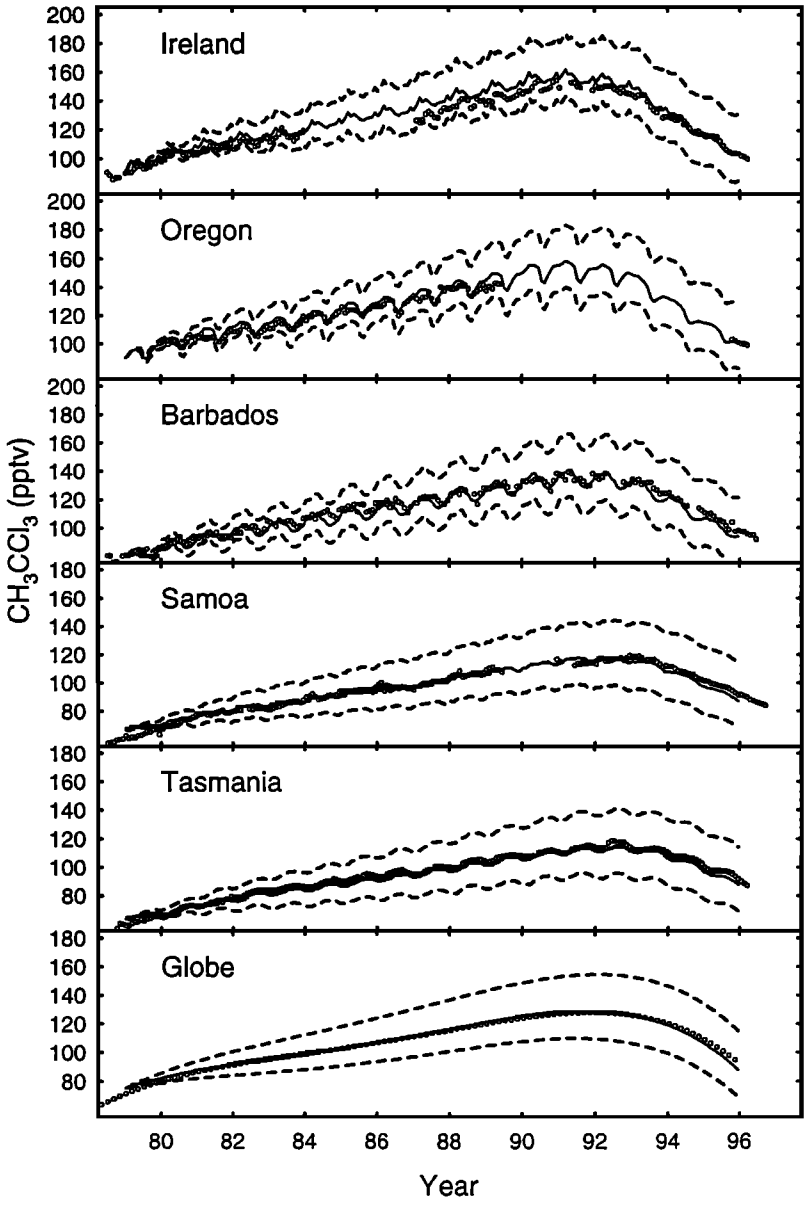

Figure 14. Observed long-term trend in CH_3CCl_3 [*Prinn et al.*, 1995] (circles) simulated using standard OH (solid lines), and with standard OH reduced and increased by 25% (dashed lines) in Ireland (52–53°N, 10°W), Oregon (45°N, 124°W), Barbados (13°N, 59°W), Samoa (14°S, 171°W), and Tasmania (41°S, 145°E). The lowest panel (marked Globe) shows a mean of least squares polynomials of 4th degree fitted to observations and model results (Ireland+Barbados+Samoa+Tasmania)/4. Data for Oregon were excluded because of a shorter record than for other stations. However, the conclusions from the comparison do not change if a shorter period, 1980–1989, is used for all stations, and northern midlatitudes are represented as a mean of the data for Ireland and Oregon (not shown).

reduced significantly in the next several years, as emissions of CH_3CCl_3 are phased out in compliance with the Montreal Protocol [*Ravishankara and Albritton*, 1995], as discussed in section 11.

The second tier of uncertainties in estimating the average abundance of OH in the troposphere using the long-term trend in CH_3CCl_3 arises from determining the role of loss processes other than reaction with OH. The range of 59–128 years for the atmospheric lifetime of CH_3CCl_3 with respect to the ocean sink corresponds to an uncertainty of ±2% in global mean OH. The estimate of *Volk et al.* [1997], 34 ± 7 years, for the atmospheric lifetime with respect to the stratospheric loss, results in an uncertainty for global mean OH in the range ±3%, giving together with the ocean sink an uncertainty of ±5%.

Table 7. Stratospheric Loss Frequencies

	0°	15°N	30°N	45°N	60°N	75°N
			CH_3CCl_3, 10–70 hPa			
January	0.939	0.517	0.133	0.017	0.001	0.000
April	1.174	1.104	0.631	0.261	0.073	0.013
July	0.928	1.180	1.022	0.761	0.517	0.304
October	1.145	0.970	0.531	0.183	0.039	0.009
			CH_3CCl_3, 70–150 hPa			
January	0.067	0.033	0.010	0.004	0.001	0.000
April	0.093	0.096	0.047	0.017	0.008	0.005
July	0.067	0.097	0.082	0.057	0.039	0.020
October	0.093	0.076	0.039	0.017	0.009	0.004
			HCFC-22, 0–70 hPa			
January	0.087	0.073	0.052	0.027	0.004	0.000
April	0.095	0.097	0.090	0.072	0.051	0.031
July	0.089	0.103	0.113	0.113	0.113	0.133
October	0.095	0.092	0.082	0.062	0.039	0.018
			HCFC-22, 70–150 hPa			
January	0.004	0.004	0.003	0.002	0.000	0.000
April	0.004	0.005	0.006	0.006	0.004	0.003
July	0.004	0.005	0.008	0.010	0.011	0.008
October	0.005	0.005	0.007	0.006	0.004	0.002
			^{14}CO, 10–70 hPa			
January	4.308	3.695	2.790	1.528	0.231	0.000
April	4.415	4.792	4.665	3.807	2.806	1.611
July	4.311	5.053	5.403	5.441	5.373	5.779
October	4.534	4.516	4.123	3.326	2.263	1.047
			^{14}CO, 70–150 hPa			
January	1.470	1.263	1.065	0.533	0.088	0.000
April	1.587	1.663	1.897	1.322	0.913	0.625
July	1.500	1.920	2.609	2.231	1.868	1.203
October	1.591	1.713	2.068	1.434	0.919	0.402

Loss frequencies are in yr^{-1}.

The third source of uncertainty in the estimate of global tropospheric OH arises from uncertainty in the rate constant for reaction with CH_3CCl_3, estimated in the range from −10% to +11% [*Talukdar et al.*, 1992]. As shown in Figure 13, the combined uncertainty in the estimate for empirical tropospheric OH (weighted by the frequency of reaction with CH_3CCl_3) is in the range −23% to +28%. Errors, however, are not expected to exceed ±15%, since potential corrections (in absolute calibration, emissions, the rate constant, and non-OH sinks) are not expected to affect results in one direction.

8.2. Global Budget of HCFC-22

Results of global simulations of HCFC-22 for 1992–1996 are compared with observations [*Montzka et al.*, 1993, 1996; *CMDL*, 1998; *Miller et al.*, 1998] in Figure 15. The history of emissions is from *Midgley and McCulloch* [1997] for 1992–1994, and from Alternative Fluorocarbons Environmental Acceptability Study [1998] for 1995–1996. The unreported emissions, believed not to exceed 10% (P. Midgley, personal communication, 1998), were not included. Simulations were initialized using observations [*Montzka et al.*, 1993] for January 1992. Stratospheric loss frequencies (Table 7) were computed in the same manner as for CH_3CCl_3. Most of the stratospheric loss of HCFC-22, mainly through reaction with OH, occurs above 10 hPa, outside the domain of the CTM. The average loss frequency for 70–0 hPa was applied to the layer of the model from 70 to 10 hPa. The mean atmospheric lifetime of HCFC-22 in the simulation with standard OH and stratospheric loss (solid lines) is 11.4 years [cf. *Kanakidou et al.*, 1995; *Miller et al.*, 1998]. Dotted lines represent simulations with standard OH modified by ±25% (giving lifetimes of 15.0 and 9.3 years). A comparison with observations (bottom panel in Figure 15) was conducted in a manner described above for CH_3CCl_3. The evolution of the simulated global mean concentration of HCFC-22 at the surface agrees closely with the observed. If the comparison is conducted using sites only in one hemisphere (not shown), the global mean lifetime of HCFC-22 in the simulation with standard OH appears to be too long or too short by ~5%, based on the NH and SH, respectively.

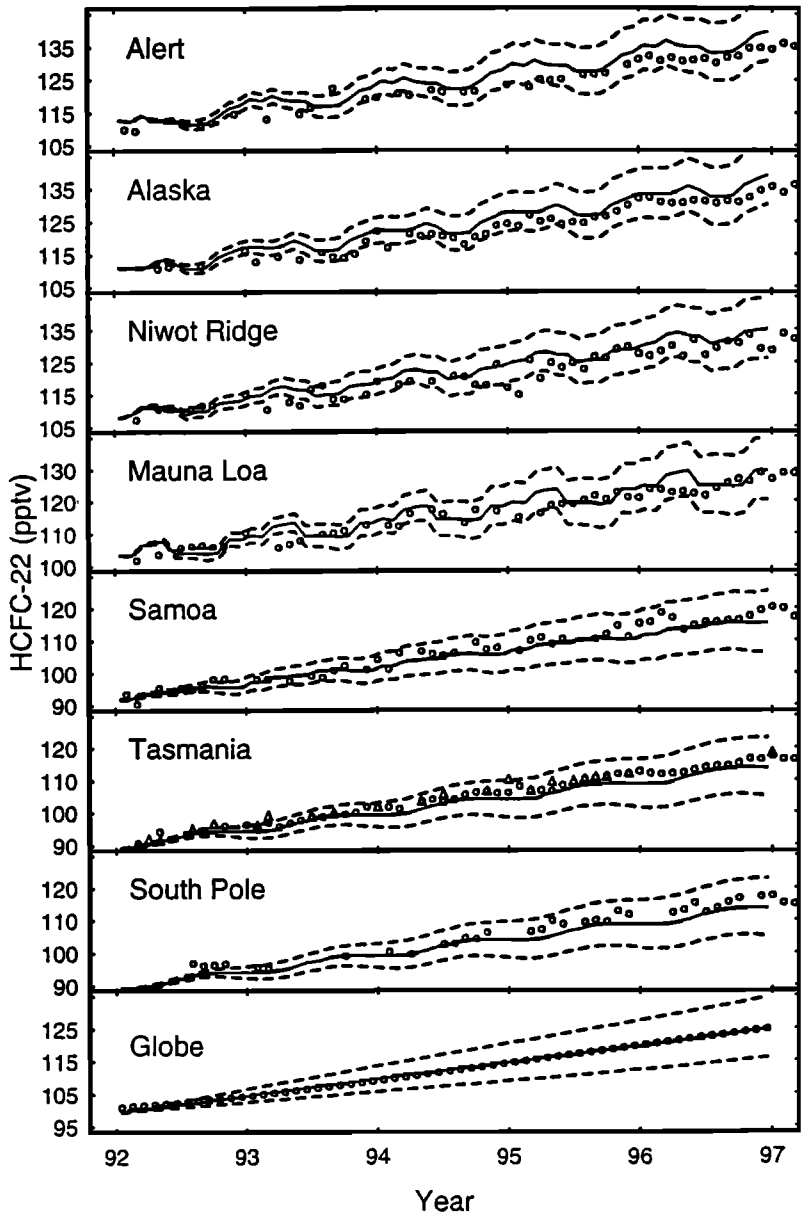

Figure 15. Observed long-term trend in HCFC-22 (circles [*Montzka et al.*, 1993, 1996; *CMDL*, 1998] and triangles [*Miller et al.*, 1998]) simulated using standard OH (solid lines), and with standard OH reduced and increased by 25% (dashed lines) at Alert (82°N, 63°W), Alaska (71°N, 137°W), Niwot Ridge, Colorado (40°N, 106°W), Mauna Loa (20°N, 156°W), Samoa (14°S, 171°W), Tasmania (41°S, 145°E), and South Pole (90°S, 102°E). The lowest panel (marked Globe) shows a mean of least squares polynomials of 4th degree fitted to observations and model results ((Alert+Alaska+Niwot Ridge+Mauna Loa)/4+(Samoa+Tasmania+South Pole)/3)/2.

The relation of global mean OH presented here to empirical OH implied by observations of HCFC-22 depends on the accuracy of the stratospheric loss in our model, resulting in an atmospheric lifetime of 229 years, that is, accounting for ~5% of the total loss of HCFC-22. *Kanakidou et al.* [1995] reported an atmospheric lifetime of 214 years due to stratospheric loss of HCFC-22, and four out of six stratospheric models (NASA MM-II) give estimates in the range 197–223 years (the range for all six models is 135–309 years). In the absence of a standard, we assume here for simplicity that the stratospheric loss in our model is accurate (with an uncertainty ±50%).

Since the simulation with standard OH and with a correct stratospheric loss accurately reproduces the trend in HCFC-22, to ±5%, we conclude that global mean OH presented here (weighted by the frequency of reaction with HCFC-22) is accurate to ±5% as compared to empirical OH. The combined uncertainty in empirical OH, including that for the absolute calibra-

tion, ±5% [*Montzka et al.*, 1993], for the magnitude of emissions, +10% (P. Midgley, personal communication, 1998), for the rate constant, from −13% to +15% [*DeMore et al.*, 1997], and for the stratospheric loss, ±2.5%, is in the range −20% to 36%. Although significant uncertainties are associated with determining empirical global mean OH using observed long-term trends of CH_3CCl_3 and HCFC-22 (dashed lines in Figure 13), consistent results for two independent constraints afford a degree of confidence in these estimates.

9. Constraints on the Hemispheric and Semihemispheric Scale

9.1. Annual Mean Levels of CH_2Cl_2 and C_2Cl_4 As a Constraint for Regional Concentrations of OH

Estimates of mean concentrations of OH on scales smaller than global are required to interpret measurements and quantify sources of species such as CO, with a lifetime of about a month in the tropics and in summer at temperate latitudes. There is a distinct interhemispheric asymmetry in distributions of precursors for tropospheric OH. Species involved in both production and loss of OH are present at significantly higher concentrations at northern than at southern midlatitudes [e.g., *Logan et al.*, 1981]. The disparity extends to lower latitudes. Concentrations of CO, the species providing the major sink for OH, are in general higher in the northern than in the southern tropics because of the proximity of industrial regions of Europe and North America. However, concentrations of O_3, the major source species for OH, appear to be lower in the northern tropics than in the south [*Fishman et al.*, 1990], as discussed above. Mean concentrations of OH for the tropics are slightly higher in the south, whereas more OH is predicted for midlatitudes in the north (Table 4).

Two industrial compounds, C_2Cl_4 and CH_2Cl_2, with relatively short lifetimes with respect to reaction with OH (about 2 and 3.5 months in the tropics, respectively), have been added recently to the list of species with documented releases and observational constraints. Observations of both gases [*CMDL*, 1998] are compared with simulations in Figures 16 and 17. Only industrial sources and the OH sink are included in these simulations (unless noted). Estimates of emissions are from *McCulloch and Midgley* [1996] for 1989–1992 and

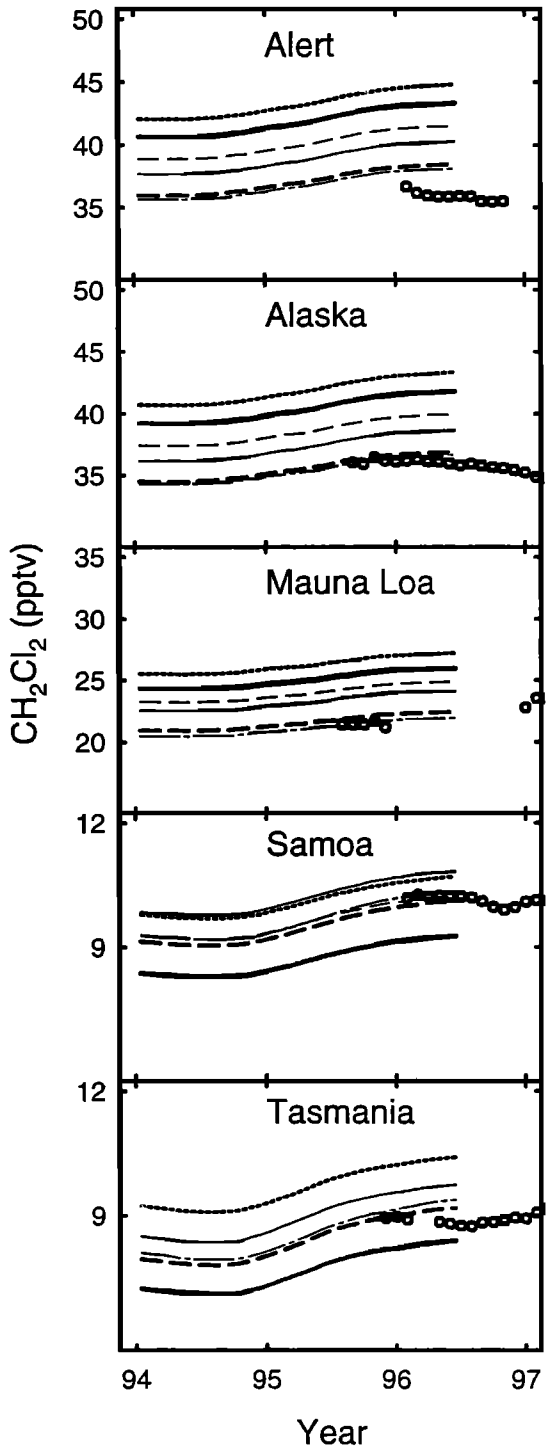

Figure 16. Observed (circles) and simulated concentrations of CH_2Cl_2 using (1) standard OH and standard rate of interhemispheric mixing, $D = 180$ km (bold solid lines); (2) standard OH and increased interhemispheric mixing, $D = 250$ km (thin solid lines); (3) standard OH and $D = 220$ km (thin dashed lines); (4) standard OH increased in the NH by 35% and decreased in the southern tropics by 60%, and $D = 180$ km (dot-dashed lines); (5) standard OH increased in the NH by 20% and decreased in the southern tropics by 25%, and $D = 220$ km (thick dashed lines); (6) standard OH, $D = 180$ km, with a source of 40 Gg of CH_2Cl_2 distributed uniformly over the ocean surface (dotted lines). Note that results of simulations 4 and 5 are close throughout the globe and that in the SH they are also close to simulation 3. Comparisons are presented as 12-month running means (omitted if monthly values are available for fewer than 10 months encompassing 6 previous and 5 following months). Observations are from *CMDL* [1998] (see Figure 15 for coordinates of the sites).

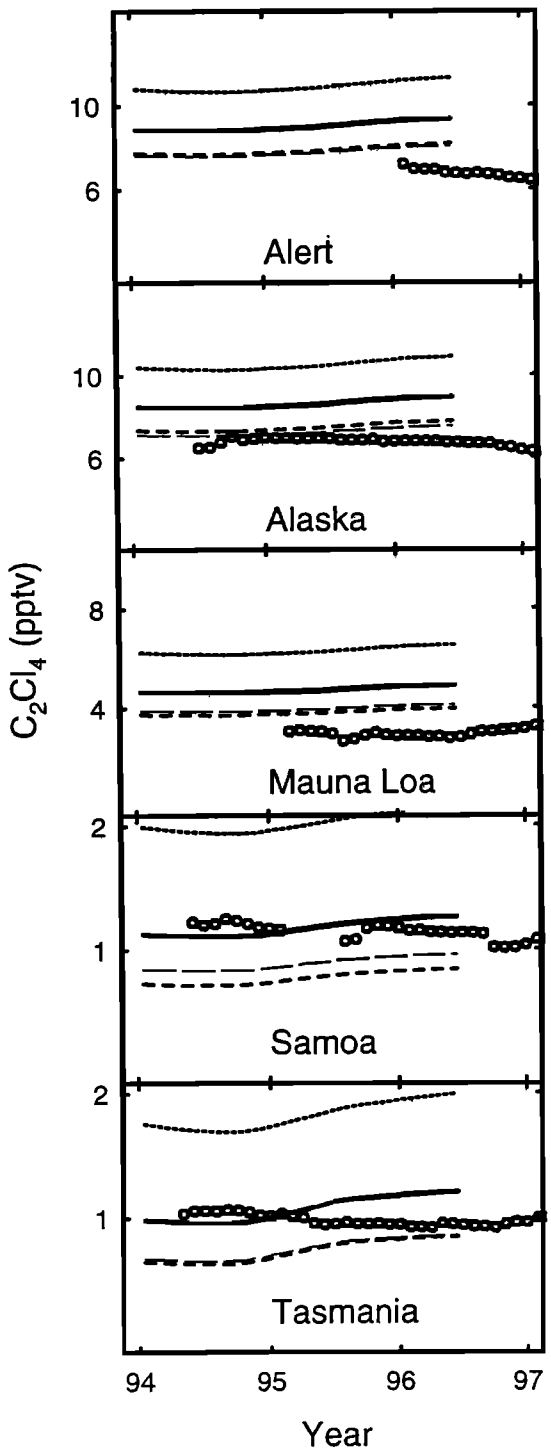

Figure 17. Observed (circles) and simulated concentrations of C_2Cl_4 using standard rate of interhemispheric mixing, D = 180 km, and standard OH (bold solid lines); standard OH, D = 180 km, but the rate constant for reaction with OH increased and reduced by 30% (short-dashed and dotted lines, respectively); standard OH, D = 180 km, recommended rate constant [*DeMore et al.* , 1997], and a 24-hour average concentration of Cl of 1.25×10^4 molecules cm^{-3} in the lowest 500 m over the oceans (long-dashed lines). Comparisons are presented as 12-month running means (omitted if monthly values are available for fewer than 10 months encompassing 6 previous and 5 following months). See Figure 15 for coordinates of the sites.

P. Midgley (personal communication, 1998) for 1993–1996. For C_2Cl_4, the rate constant for reaction with OH is from *DeMore et al.* [1997], whereas for CH_2Cl_2 we used $1.92 \times 10^{-12}e^{-897/T}$ cm^3 molecules^{-1} s^{-1} representing a fit to four recent measurements, all within 15% of each other (W. B. DeMore, personal communication, 1998). Simulations were initialized for 1988 using the distribution observed by *Koppmann et al.* [1993]. We focus first on overall levels of these compounds as a possible constraint for mean hemispheric and semihemispheric concentrations of OH; seasonal variations, considered in section 9.3, were removed here by using 12-month running means.

For CH_2Cl_2, model results for standard OH are 15–20% higher than observations in the NH and ~10% lower than observations in the SH; for C_2Cl_4, model results are higher than observations in the NH by 30–50%, and on average are close to observed in the SH (Figures 16 and 17, bold solid lines). A comparison of the discrepancies for C_2Cl_4 and CH_2Cl_2 (or alternatively, a comparison with observations of the ratio of C_2Cl_4 to CH_2Cl_2, which is insensitive to OH [*Singh et al.*, 1996b]) suggests that a significant loss process for C_2Cl_4 is missing in the simulation. *Singh et al.* [1996b] and *Rudolph et al.* [1996] used the high reactivity of C_2Cl_4 with Cl to define an upper limit for the abundance of Cl in the troposphere. A simulation of C_2Cl_4 allowing for 24-hour average concentrations of Cl of 1.25×10^4 molecules cm^{-3} in the lowest 500 m over the oceans (consistent with estimates of these authors) displays discrepancies with observations similar to those for CH_2Cl_2: concentrations are too high by 10–25% in the NH and too low in the SH (see Figures 16 and 17). Alternatively, a 30% increase in the rate constant for reaction of C_2Cl_4 with OH (at the upper limit of the present uncertainty [*DeMore et al.*, 1997]) leads to similar results (short-dashed lines in Figure 17).

For tracers such as CH_2Cl_2 and C_2Cl_4, that is, relatively short lived and emitted mainly at northern midlatitudes, a uniform scaling of the loss frequency globally (e.g., by scaling the rate constant) disproportionally affects concentrations in the SH. As expected for a tracer with a nearly steady state behavior, scaling the loss frequency globally by −25% and +50% leads to a change in the global abundance by about ±33%. Concentrations at northern midlatitudes display a lower than average sensitivity, with a response of about ±20%, because they are determined to a large degree by a balance between the rate of emissions and the rate of transport to the tropics. In contrast, at southern midlatitudes such modifications of the loss frequency globally lead to changes in calculated concentrations by about ±60%, reflecting the cumulative effect of modified losses of tracer en route from northern midlatitudes. The uncertainty of ±30% in the rate constant for reaction of C_2Cl_4 with OH leads to the uncertainty in simulated annual mean concentrations of C_2Cl_4 at northern midlatitudes from −13% to +22%; however, at southern

midlatitudes, the same uncertainty is −35% to +70% as depicted by the distance between dotted and short-dashed lines in Figure 17. Of the two tracers, CH_2Cl_2 and C_2Cl_4, the former appears better suited to constrain OH, given the large uncertainties in the rate constant for reaction of C_2Cl_4 with OH and in the magnitude of the Cl sink for C_2Cl_4.

Large modifications of OH would be needed to eliminate the discrepancies between model results for CH_2Cl_2 and observations (Figure 16). If we were to attribute the ~20% excess of CH_2Cl_2 simulated for the NH solely to errors in OH, most of it would be eliminated by an increase in OH in the NH by ~35%, that is, OH in the NH may be lower than empirical OH by ~26% ($1/1.35 - 1 = 0.26$). However, this would decrease the flux of CH_2Cl_2 into the SH and thus exacerbate the deficit of CH_2Cl_2 simulated for the SH. A decrease in OH by 60% in the southern tropics would be needed to achieve agreement with observations, resulting in a decrease by ~42% in the hemispheric mean for OH in the SH, that is, OH in the SH may be higher than empirical OH by 72% ($1/0.58 - 1 = 0.72$). Given our current knowledge of distributions of precursors for OH and of the limited sensitivity of concentrations of OH to their specification, it is hard to contemplate errors of that magnitude. As will be clear from Figure 13, independent observational constraints render such large errors unlikely.

At the same time, other imperfections of the model may be contributing significantly to discrepancies between simulated and observed levels of CH_2Cl_2. Concentrations of tracers such as C_2Cl_4 and CH_2Cl_2, particularly in the SH, are more sensitive to the rate of interhemispheric mixing than those for the long lived species, CFCs and ^{85}Kr, used to test the accuracy of this rate in the model [*Prather et al.*, 1987; *Jacob et al.*, 1987]. The current CTM includes a parameterization of horizontal mixing with a diffusion coefficient proportional to the intensity of local convection and to the square of the length parameter D, introduced by *Prather et al.* [1987] to account for processes unresolved in the parent GCM. In the standard CTM we use a value for D of 180 km. Figure 18 illustrates small differences, as compared to observational constraints, in results for ^{85}Kr with mixing lengths of 180 and 250 km. Observations of CFCs at the ALE/GAGE sites suggest ~220 km as an upper limit for D (Figure 19). For $D = 220$ km, an increase in OH in the NH by 20% combined with a decrease in the southern tropics by 25% (i.e., a decrease in the SH by 18%) brings simulated levels of CH_2Cl_2 close to observed in both hemispheres, signifying discrepancies between standard OH and empirical OH of −17% for the NH ($1/1.2 - 1 = 0.17$) and +22% for the SH ($1/0.82 - 1 = 0.22$).

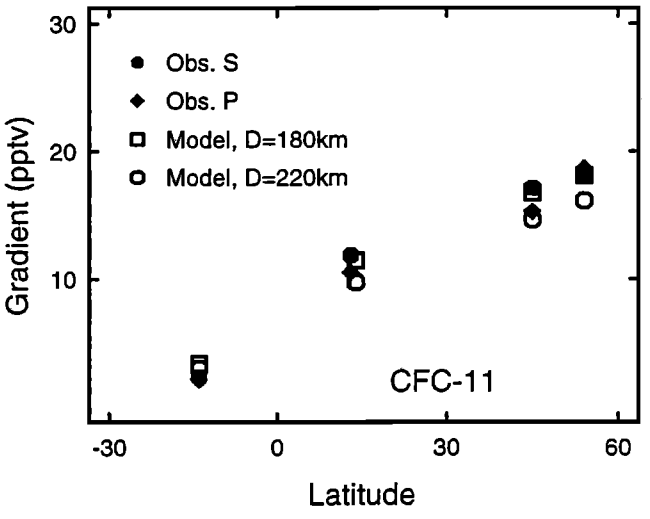

Figure 19. Latitudinal gradient of CFC-11 as represented by differences between monthly values at ALE/GAGE stations and those at Tasmania (see Figure 14 for coordinates of the sites), averaged over 1980–1983. Observations [*Cunnold et al.*, 1994] are denoted by solid symbols: circles for silicone column (S) and diamonds for Porasil column (P). Simulations are shown by open squares and circles for $D = 180$ km and $D = 220$ km (see text, section 9.1), respectively. For both model and observations, the monthly values for each site were obtained using a second-order polynomial providing the least squares fit to monthly means for the running 30-day medians, to filter out the influence of local pollution and to minimize the impact of missing data. The distribution and history of emissions were taken from *McCulloch et al.* [1994] and *Fisher et al.* [1994].

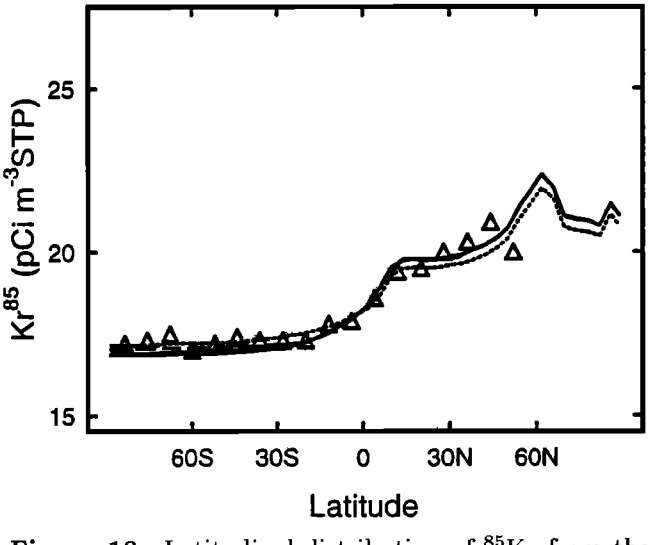

Figure 18. Latitudinal distribution of ^{85}Kr from the Atlantic cruise in March 1983 [*Weiss et al.*, 1983] (triangles). The solid line shows results for the standard model ($D = 180$ km), the dotted line shows results for the simulation with increased interhemispheric mixing ($D = 250$ km) and the dashed line corresponds to the simulation with $D = 180$ and additional diffusion in the southern extratropics (see section 10 and caption for Figure 25).

Results for CH_2Cl_2 (expressed as annual means) suggest that for mixing lengths consistent with observations of ^{85}Kr and CFCs (i.e., for D in the range of 180–220 km), in the NH mean OH is lower than empirical OH by 17–26%, and in the SH mean OH is higher than empirical OH by 22–72%, with larger errors corresponding to lower diffusion rates (crosses in Figure 13 correspond to the middle of these ranges). In reality the sensitivity of the distribution of CH_2Cl_2 to the representation of north-south transport may even be greater than shown in Figure 16, if larger errors in the rate of mixing arise in the season when the interhemispheric gradient of CH_2Cl_2 is at its peak (northern winter – spring) than for other seasons. We emphasize that the estimate of the deviation from empirical OH for the SH depends strongly on that adopted for the NH.

Industrial sources of CH_2Cl_2 are sufficient to balance the budget of CH_2Cl_2 for the present distribution of OH, using the newly measured rate constant. Thus results for the standard OH and D = 250 km are higher than observations throughout the globe by 5–10% (Figure 16, thin solid lines), while the global abundance of CH_2Cl_2 in this simulation is lower than that for standard OH and D = 180 km by only 1%. Nonindustrial sources of CH_2Cl_2, from the ocean and from biomass burning, have been suggested in earlier studies [*Singh et al.*, 1996b; *Rudolph et al.*, 1996]. If, however, these sources prove to represent a significant fraction of the industrial source, it may be difficult to reconcile constraints for the global abundance of OH imposed by long-term trends in CH_3CCl_3 and HCFC-22 with those given by the levels of CH_2Cl_2 (see Figure 13 under "global mean"). An addition of 40 Gg yr^{-1} of CH_2Cl_2 distributed uniformly over the ocean surface (which amounts to only 13% of the mean industrial source for 1994–1996) would result in concentrations of CH_2Cl_2 higher than observed in both hemispheres using standard OH and standard mixing (dotted lines in Figure 16).

The estimate for global mean OH is sensitive to the spatial distribution of OH in relation to that of CH_2Cl_2. Thus results for standard OH and D = 250 km suggest that global mean OH (weighted by the frequency of reaction with CH_2Cl_2) is lower than empirical OH by 5–10%. The simulation of CH_2Cl_2 with OH increased in the NH by 35% and decreased in the SH by 42% (D = 180 km), corresponding to a decrease of ~4% in global mean OH (weighted by the mass of air), results in a global abundance of CH_2Cl_2 decreased by 8% (because the loss frequency of CH_2Cl_2 increased in the region immediately affected by emissions).

The combined uncertainty in empirical global mean OH implied by observed levels of CH_2Cl_2, including those for the absolute calibration, ±5%, for the magnitude of industrial emissions, ±5% [*McCulloch and Midgley*, 1996] and for the rate constant, ±15% (W. B. DeMore, personal communication, 1998), is in the range −21% to +30%. We also neglected loss of CH_2Cl_2 in the stratosphere which is not expected to amount to more than a few percent because of a relatively short lifetime of CH_2Cl_2 in the troposphere.

9.2. Observations of CH_3CCl_3 As a Constraint for the Ratio of Hemispheric Means for OH

The present distribution of OH results in nearly equal hemispheric means (Table 4). Corrections to the computed distribution of OH resulting in ratios larger than 2 would be inconsistent with our understanding of uncertainties in the calculated values (for the present chemical mechanism), and those in the range 1.5–2 would be unlikely.

Observations of tracers with lifetimes significantly longer than the interhemispheric exchange time, such as CH_3CCl_3, may help constrain the ratio of mean hemispheric concentrations of OH. For example, in a steady state with a constant rate of emissions located in the NH, the net flux to the SH could range from zero to the full emissions, if the loss were confined to one hemisphere, northern or southern, respectively; in the case of symmetric loss frequencies, the flux would be approximately equal to half of emissions. The interhemispheric gradient would adjust accordingly to ensure the transmission of a proper flux.

The interhemispheric gradient of CH_3CCl_3 is sensitive to the rate of interhemispheric mixing in the model, for example, if interhemispheric transport is too vigorous, an erroneous interhemispheric bias, with higher loss frequencies in the SH, could be deduced from a comparison of simulated and observed gradients of CH_3CCl_3. Figures 18 and 19 discussed in section 9.1 presented tests of the rate of interhemispheric mixing in the CTM using observations of ^{85}Kr [*Weiss et al.*, 1983] and CFC-11 [*Cunnold et al.*, 1994].

The location of the Intertropical Convergence Zone (ITCZ) in the model, as an actual boundary between the hemispheres, may also affect the interhemispheric gradient of CH_3CCl_3: (1) by influencing the effective mean concentration of OH in each hemisphere (since the near-equatorial region in question is characterized by particularly high concentrations of OH), and (2) by defining the effective dilution volume for the NH. The simulation of ^{85}Kr reproduces the observed latitudinal distribution in boreal winter, spring and autumn (as shown in Figure 18 for March) giving no indication of a significant misplacement of the ITCZ over the Atlantic. However, a comparison of observed and simulated peak intensities of the Hadley circulation [*Rind and Lerner*, 1996] suggests that on average the ITCZ in the GCM II may have been shifted north by one grid box in latitude, that is, by 4°. This would result in an exaggeration of the interhemispheric gradient of CH_3CCl_3 which could conceal an overestimate of the north-to-south ratio for OH. (The shift in the location of the ITCZ to the north may be partly responsible for the overestimate of the interhemispheric gradient of CH_2Cl_2 discussed in sec-

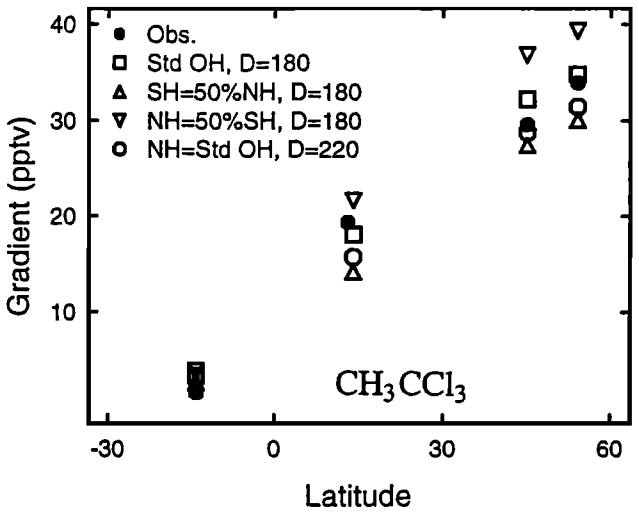

Figure 20. Latitudinal gradient of CH_3CCl_3 as represented by differences between monthly values at ALE/GAGE stations and those at Tasmania (see Figure 14 for coordinates of the sites), averaged over 1980–1983. Observations [*Prinn et al.*, 1995] are denoted by solid circles. Simulations are shown by open symbols: squares for $D = 180$ km and standard OH; triangles for $D = 180$ km and for an interhemispheric ratio in OH of 50%, north to south (pointed down) and south to north (pointed up); and circles for $D = 220$ km and standard OH. For both model and observations, the monthly values for each site were obtained using a second-order polynomial providing the least squares fit to monthly means for the running 30-day medians, to filter out the influence of local pollution and to minimize the impact of missing data.

tion 9.1.) For the present distribution of OH, a 4° latitude shift of the ITCZ (for the full range in longitude) results in less than a 10% difference in the effective ratio of interhemispheric means for the loss frequency of CH_3CCl_3. We estimated, using a simple two-box model, that this would result in a less than 5% error in the interhemispheric gradient of CH_3CCl_3.

The interhemispheric gradient of CH_3CCl_3 is compared with observations [*Prinn et al.*, 1995] in Figure 20 for simulations with standard mixing ($D = 180$ km) using (1) standard OH, and (2) and (3) using distributions of OH obtained by scaling standard OH in each hemisphere to give the north-south ratios of hemispheric means for OH of 2 and 0.5, but the same mean atmospheric lifetime of CH_3CCl_3 for all three simulations. Also shown is the simulation with $D = 220$ km for standard OH. We chose to average the latitudinal distribution over 1980–1983 because during this time, emissions were relatively stable, within 3% of the mean. (Modifications of the interhemispheric gradient associated with the El Niño from mid-1982 to mid-1983 [*Prinn et al.*, 1992] are not expected to affect significantly the mean gradient over 1980–1983.)

For $D = 180$ km (standard model), the present distribution of OH (with nearly equal hemispheric means) provides a better agreement with observations than those with a factor of 2 difference between the hemispheric means. For a given global mean OH, constraining the ratio of hemispheric means to a factor of 2 is equivalent to constraining hemispheric mean concentrations of OH to better than ±33%. When the rate of interhemispheric mixing is increased to the upper limit consistent with observations of CFCs ($D = 220$ km), the simulated gradient for standard OH is too low, and an increase in the north-to-south ratio in OH would exacerbate the discrepancy with observations of CH_3CCl_3.

The two constraints using (1) the interhemispheric gradient of CH_3CCl_3 and (2) annual means of CH_2Cl_2 suggest distinctly different empirical hemispheric means for OH. As follows from section 9.1, observations of CH_2Cl_2 imply corrections resulting in the ratio (north to south) of hemispheric means for empirical OH ranging from 1.5 to 2.3 (an increase of standard OH in the NH by 20% accompanied by a decrease in the SH by 18%, suggested by the simulation with $D = 220$ km, defines the lower limit for the ratio; an increase of standard OH in the NH by 35% combined with a decrease in the SH by 42% using $D = 180$ km defines the upper limit). An increase in magnitude of emissions and a decrease in the absolute calibration for CH_3CCl_3, within the range of their uncertainties, would bring these constraints closer to each other (but would increase empirical OH constrained by the long-term trend of CH_3CCl_3). For example, a 5% increase in emissions combined with a 5% decrease in calibration, would lead to a 5% increase in the simulated interhemispheric gradient of CH_3CCl_3 and a 5% decrease in the observed gradient. The standard simulation would then result in a more than 4 pptv overestimate at Cape Meares (45°N, 124°W) and Adrigole (52°N, 10°W) and about 1 pptv overestimate at Barbados (13°N, 59°W), with an implication that (1) the ratio of hemispheric means, north to south, is too low for standard OH and (2) that global mean OH (weighted by the frequency of reaction with CH_3CCl_3) is too low by about 7%. As discussed in section 10, observations of ^{14}CO suggest that standard OH may be too low in the tropics in winter, in contrast, however, to the result obtained for the southern tropics using annual means of CH_2Cl_2 (see Figure 13).

Part of the apparent discrepancy between the empirical partitioning of global OH among the hemispheres suggested by the analysis of observations of CH_3CCl_3 and CH_2Cl_2 could be associated with a different weighting (resulting from higher gradients and a weaker temperature dependence of the rate constant for CH_2Cl_2 than for CH_3CCl_3). The difference in the locations of observational sites in the NH for the two compounds may also play a certain role. Thus, in the tropics, observations of CH_2Cl_2 at Mauna Loa (20°N, 156°W) represent predominantly the air over the Pacific in contrast to those for CH_3CCl_3 at Barbados (13°N, 59°W) sampling the Atlantic air; in the extratropics, observations of CH_2Cl_2 are indicative of high latitudes, whereas those

for CH_3CCl_3 represent midlatitudes. Errors in simulation of transport and of the location of the ITCZ may affect these regions in a different way. Additional uncertainties are associated with determination of the simulated "background levels" of CH_3CCl_3, CH_2Cl_2 as well as CFCs at the NH sites in the proximity of the source regions. For example, the simulation of CH_3CCl_3 with standard OH (and $D = 180$ km) underestimates concentrations at Barbados but overestimates them at Cape Meares (Figure 20). Results for CFC-12 (not shown) display similar errors at Barbados and Cape Meares, but not for CFC-11 (Figure 19). We attribute these discrepancies to errors in representation of short-range transport of tracers from source regions, to uncertainties in the distribution of emissions within large countries and to difficulties of relating grid box results to observations at a particular site in a region of steep gradients. Additional observational sites, particularly in the NH, would have been beneficial for this analysis. Within the next several years, when emissions of CH_3CCl_3 will nearly cease as envisaged in the Montreal Protocol, observations of CH_3CCl_3 may provide a unique opportunity to improve the constraint on the ratio of hemispheric means for OH as discussed in section 11.

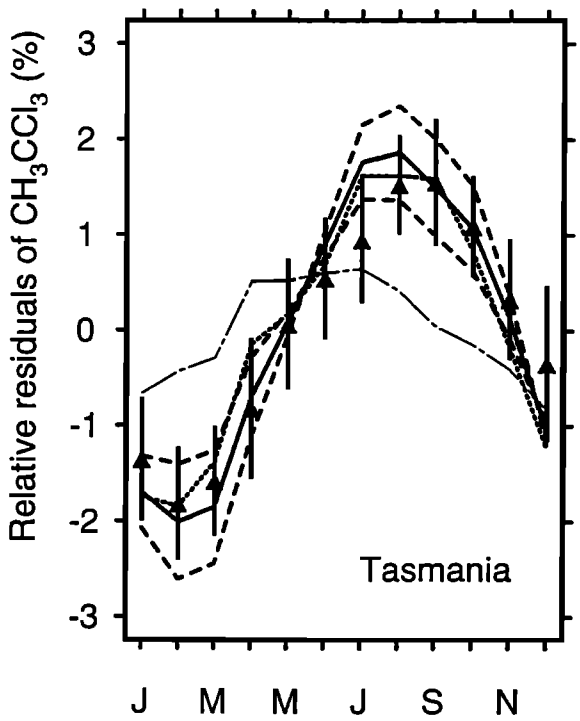

Figure 21. Annual cycle of CH_3CCl_3 at Tasmania (41°S, 145°E) averaged over 1980–1991 (percent). Relative residuals from the long-term trend were computed in a manner described in S90. Triangles denote observations [*Prinn et al.*, 1995], with error bars corresponding to 1 standard deviation from the mean. The solid line corresponds to the simulation with standard OH. Dashed lines show simulations with concentrations of OH reduced and increased by 50% south of 28°S; the dot-dashed line shows the simulation with aseasonal OH: concentrations of OH were averaged over the year in each grid box. The dotted line shows the simulation with standard OH and additional diffusion in the southern extratropics discussed in section 10 (see caption for Figure 25).

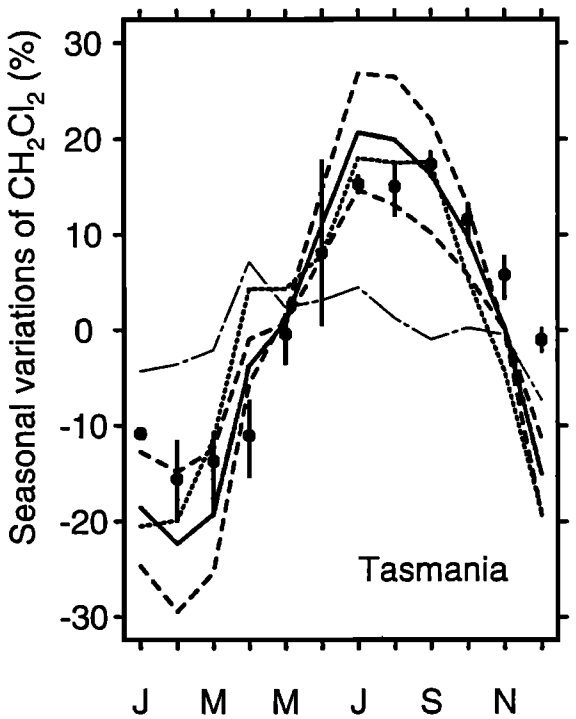

Figure 22. Observed [*CMDL*, 1998] and simulated relative seasonal variations of CH_2Cl_2 at Tasmania (41°S, 145°E) (percent). Symbols show averages of monthly means (relative to the yearly average), over 1994–1997. Error bars depict the full range of monthly mean values over this period. The simulation with standard OH corresponds to the solid line, and those with concentrations of OH reduced and increased by 50% south of 28°S are shown as dashed lines. The dot-dashed line shows the simulation with aseasonal OH: concentrations of OH were averaged over the year in each grid box. The dotted line shows the simulation with standard OH and additional diffusion in the southern extratropics discussed in section 10 (see caption for Figure 25).

9.3. Seasonal Variations of Tracers As a Constraint for OH at Temperate Latitudes

A relative amplitude of the annual cycle of CH_3CCl_3 at Tasmania (41°S) provides a measure of the tropospheric concentration of OH integrated over southern extratropics (weighted by the frequency of reaction with CH_3CCl_3) (S90). Figure 21 compares relative amplitudes of simulated and observed seasonal variations of CH_3CCl_3 averaged over 1980–1991 at Tasmania. Dashed lines present results with the standard OH reduced and increased by 50% south of 28°S. The comparison suggests that standard OH in that region may be higher than implied by observations by 15–25%.

An uncertainty of about ±25% is associated with the magnitude of the dynamical component of seasonal variations at Tasmania for long-lived tracers emitted mainly at northern midlatitudes (dot-dashed line in Figure 21). The present record for CFCs at Tasmania spans over 17 years and includes three sets of observations [*Cunnold et al.*, 1994], none of which exhibits a statistically significant annual cycle (at the confidence level of 95%). The CTM simulation of CFCs (not shown) predicts small seasonal variations at Tasmania, with amplitudes less than 0.3%, that is, comparable to the instrumental noise in observations. The present model uses meteorological fields from 1 year of the GCM simulation, therefore model results characterize seasonal variations in transport over the course of 1 year rather than a recurring annual cycle.

Similarly to results for CH_3CCl_3, a comparison of the simulated and observed amplitude of relative seasonal variations for CH_2Cl_2 at Tasmania (Figure 22) suggests an overestimation of OH in that region, but of somewhat larger magnitude, by 30–50% (see Figure 13); as for CH_3CCl_3, we estimated that for CH_2Cl_2 about ±25% uncertainty is associated with the magnitude of the dynamical component.

At northern midlatitudes, observations of a variety of industrial pollutants with relatively short lifetimes can potentially be used to evaluate computed concentrations of OH in that region. However, uncertainties in the magnitude and distribution of sources present a major difficulty. In addition, the proximity of source regions to sampling locations contributes greatly to the variability in observations and complicates interpretation of measurements using models with a horizontal resolution typically of hundreds of kilometers across a grid box. *Goldstein et al.* [1995a] circumvented some of these difficulties by defining "background concentrations" at Harvard Forest (42.5°N, 72.2°W) afforded by continuous, high-frequency observations. Using the relative amplitude of seasonal variations, they demonstrated that the seasonal behavior of ethane, acetylene, propane, butane, pentane, and hexane, with lifetimes in summer ranging from 40 to 1.5 days, can be explained in the context of a simple one-box model, assuming a constant rate of emissions for each gas. Their work suggests that seasonal variations in OH in fact determine the seasonality of background levels of these compounds at the site, as predicted by simulations using the CTM. Mean tropospheric concentrations of OH presented here are higher by about 20% north of 32°N than those used by *Goldstein et al.* [1995a] (see Table 4); however, the currently recommended rate constant for reaction of C_2H_6 with OH is lower by about 15% [*DeMore et al.*, 1997]; in addition, less OH resides in the lower troposphere in the present distribution as discussed in section 4. Consequently, our simulation of seasonal variations of C_2H_6 at Harvard Forrest (Figure 23) leads to results similar to those of *Goldstein et al.* [1995a]: average concentrations of OH at northern midlatitudes are constrained to

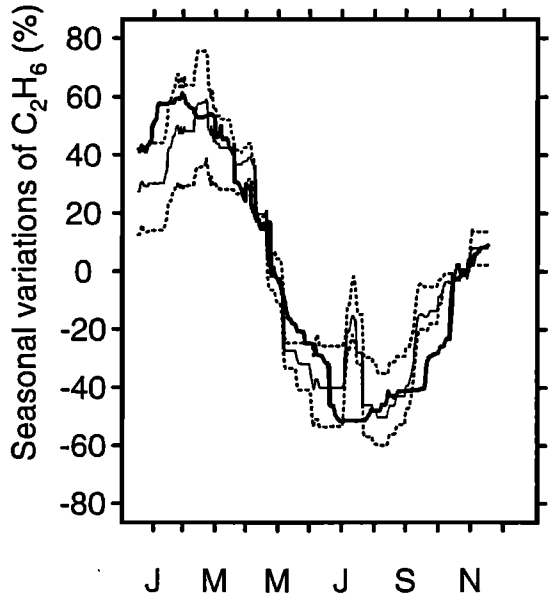

Figure 23. Comparison of observed (bold solid line) and simulated relative seasonal variations of C_2H_6 at Harvard Forest, Massachusetts (43°N, 72°W) [*Goldstein et al.*, 1995a]. The simulation with standard OH is shown as a thin solid line, and those with standard OH reduced and increased by 50% north of 28°N as dotted lines. Observations and simulations are presented as 30-day running 10% quantiles relative to their yearly mean.

±50%, with the simulation for standard OH falling near the middle of the range consistent with observations.

For CH_2Cl_2, the relative amplitude of seasonal variations in northern extratropics is also consistent with observations for the simulation with standard OH (Figure 24). We assigned a ±50% uncertainty to the estimate of mean OH in the northern extratropics using observations of CH_2Cl_2 (see Figure 13). For C_2Cl_4, results suggest that the loss frequency using standard OH is too low (not shown). A comparison of simulations using standard OH for C_2Cl_4 and CH_2Cl_2 implies that a sink of about 25–50% with the seasonality similar to that for OH is missing in the simulation of C_2Cl_4 (the magnitude of this missing sink appears somewhat smaller in northern than in southern extratropics).

Unlike other constraints, those afforded by the relative amplitude of seasonal variations are insensitive to uncertainties in the absolute calibration and magnitude of the industrial emissions; they are sensitive, however, to errors in representing the seasonality of emissions and transport.

10. Utility and Limitations of ^{14}CO As a Test for OH

Since the pioneering work of *Weinstock and Niki* [1972], ^{14}CO has been considered as one of the few gases that can provide a measure of the tropospheric abundance of OH, because the magnitude and distribution

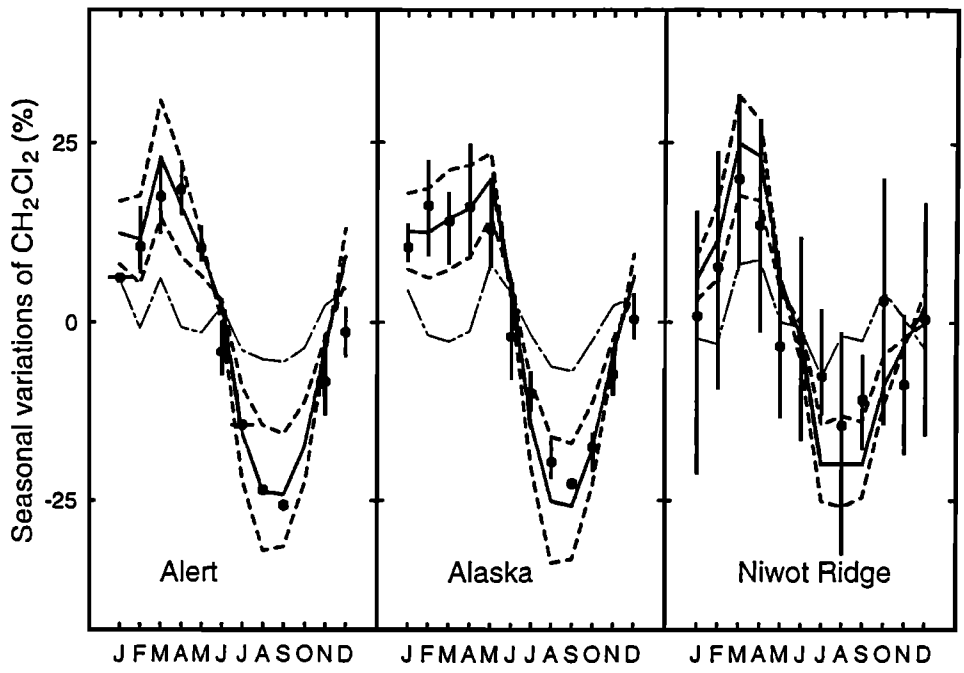

Figure 24. Observed [*CMDL*, 1998] and simulated relative seasonal variations of CH_2Cl_2 in northern extratropics (percent). Symbols show averages of monthly means, relative to the yearly mean, over 1994–1996. Error bars depict the full range of monthly mean values over this period. The simulation with standard OH is shown as bold solid lines, and those with concentrations of OH modified by ±50% north of 28°N are shown as dashed lines. Dot-dashed lines correspond to a simulation with aseasonal OH: concentrations of OH were averaged over the year in each grid box. See Figure 15 for coordinates of the sites.

of its source, mainly of cosmic origin, were believed to be known, and reaction with OH constituted the major sink. By virtue of its relatively short lifetime (1–1.5 months in the tropics and midlatitude summer), observations of ^{14}CO were expected to provide estimates of OH on a hemispheric and semihemispheric scale [e.g., *Volz et al.*, 1981; *Brenninkmeijer et al.*, 1992].

However, the interpretation of observations of ^{14}CO proved to be difficult because it involves simulation of complicated dynamical processes which cannot be readily tested. About 50% of the cosmic production of ^{14}CO outside the tropics occurs above 150 hPa. Therefore the effective tropospheric source of ^{14}CO (of cosmic origin) in models may differ by as much as a factor of 2 in the extratropics, depending on the flux from the stratosphere which in turn is determined by the relative magnitudes of the stratospheric loss frequency and the rate of transport to the troposphere. Results may appear insensitive to the rate of troposphere-stratosphere exchange if loss frequencies in the stratosphere are too low [cf. *Mak et al.*, 1992]. Recent successes in measuring and modeling concentrations of OH in the lower stratosphere [*Wennberg et al.*, 1994] may reduce significantly uncertainties in the rate of chemical destruction of ^{14}CO in the stratosphere. However, adequate testing of the rate of transport from the stratosphere remains problematic; observations of excess $^{14}CO_2$ after nuclear bomb tests [*Johnston*, 1989] customarily used for that purpose, although helpful for identifying gross errors, do not allow for discrimination between (1) erroneous rates for the troposphere-stratosphere exchange and (2) inaccurate representation of transport within the stratosphere, north to south and to higher altitudes [*Shia et al.*, 1989; *Jackman et al.*, 1991; *Prather and Remsberg*, 1993].

Another factor affecting simulated concentrations of ^{14}CO in the troposphere, particularly outside the tropics, is the height of the tropopause in the model, especially at high latitudes. Mean rates for production of cosmic ^{14}CO outside the tropics between 250 and 200 hPa and between 200 and 150 hPa amount to about 35% and 45%, respectively, of production between the surface and 250 hPa. If the model tropopause is too high, a region of the stratosphere with fast production is erroneously attributed to the troposphere, and ^{14}CO produced in this region is allowed to escape destruction by stratospheric OH, resulting in an overestimate of the tropospheric source of ^{14}CO. Most of the models used thus far to interpret observations of ^{14}CO, including the present model, were developed with an emphasis on tropospheric processes and lacked both adequate resolution in the vicinity of the tropopause, and appropriate physics [cf. *Spivakovsky and Balkanski*, 1994; *Mak et al.*, 1994].

Equally important is the representation of intrahemispheric transport in the troposphere (on a seasonal time scale) because most of ^{14}CO originates at high and middle latitudes, and the highest loss frequencies occur in the tropics. More vigorous mixing between midlatitudes and the tropics would decrease the intrahemispheric gradient and expose higher levels of ^{14}CO to loss in the tropics, resulting in a lower abundance of ^{14}CO for the entire hemisphere. In the NH, observations of CFCs and ^{85}Kr provide some constraint on the rate of intrahemispheric mixing, but in the SH they indicate that latitudinal gradients are small (Figure 18) and thus provide only a lower limit for this rate.

Because of the difficulties discussed above, absolute levels of ^{14}CO at midlatitudes cannot provide a definitive measure of OH. They may help nevertheless identify model defects, and in conjunction with other tracers they can provide useful constraints as illustrated below.

The distribution of cosmic emissions and their dependence on the sunspot number in our simulations of ^{14}CO were taken from *Lingenfelter* [1963] and *O'Brien* [1979], respectively, assuming that 95% of ^{14}C is emitted as ^{14}CO [*Volz et al.*, 1981]. Noncosmic emissions of ^{14}CO (biomass burning and oxidation of CH_4, isoprene and other NMHC) were computed using emissions of CO from *Wang et al.* [1998a] (with the corrections for emissions of isoprene discussed in section 2) and $^{14}CO/^{12}CO$ ratios in individual sources from *Volz et al.* [1981]. The rate constant (for reaction of CO with OH) was taken from *DeMore et al.* [1997]; based on recent laboratory results, the uncertainty in the value for the rate constant derived from the expression given by *DeMore et al.* [1997] is less than 15% at 273 K at tropospheric pressures (A. R. Ravishankara, personal communication, 1999). As shown in Figure 25a, the standard model significantly overestimates the relative amplitude of seasonal variations of ^{14}CO at southern midlatitudes, determined in the model primarily by seasonality in OH. This may suggest [S90; *Goldstein et al.*, 1995a] that computed concentrations of OH are too high in that region. However, the model also overestimates the annually averaged concentration (as can be seen in Figure 25b showing the same data and simulations as in Figure 25a, but on an absolute scale), with the implication that OH levels may be too low. The apparent contradiction indicates an inadequate representation of the effective net flux of ^{14}CO reaching the lower troposphere at southern midlatitudes, either in its magnitude, or seasonality, or both.

In particular, a poor representation of the stratosphere may explain a large part of the discrepancy. The stratosphere in this model is resolved in two layers in the extratropics, from 150 to 70 hPa, and from 70 to 10 hPa. The tropopause in the model is located at about 150 hPa outside the tropics all year around, which is too high except in summer [e.g., *Holton et al.*, 1995]. A simulation of the evolution of the global distribution of $^{14}CO_2$ after the nuclear bomb tests [*Johnston*, 1989]

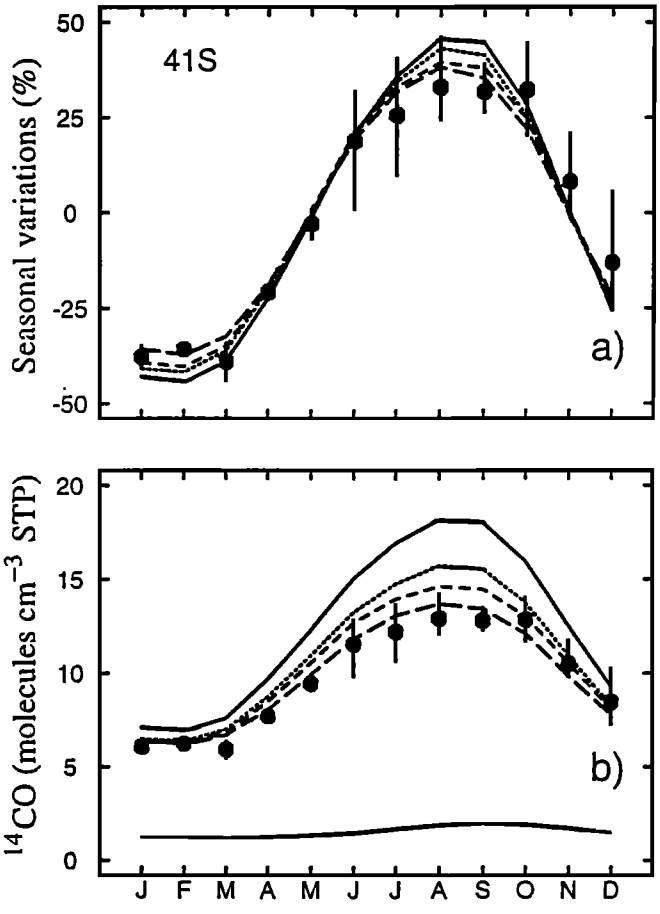

Figure 25. Annual cycle of ^{14}CO at Baring Head, New Zealand, averaged over 1989–1991: (a) residuals with respect to the annual mean in percent and (b) concentrations on absolute scale, in molecules cm^{-3} (STP). Solid lines correspond to the simulation with the standard dynamics. Dotted lines show the simulation with the rate of stratosphere-troposphere exchange decreased by a factor of 2. Short-dashed lines correspond to the simulation which in addition to reduced air flux from the stratosphere, included relocation of emissions that the model erroneously attributes to the troposphere (see text). Long-dashed lines show the simulation including two previous corrections, and an additional diffusion below 400 hPa of 1.5×10^{10} cm^2 s^{-1} south of 28°S combined with vertical diffusion of 8×10^5 cm^2 s^{-1} south of 60°S. The thin solid line in Figure 25b shows results for the simulation with no cosmic source. The standard distribution of OH was used in all simulations. Observations (symbols) are from *Brenninkmeijer* [1993]. Error bars represent the full range of monthly mean values over 1989–1991.

suggests that the rate of transport from the stratosphere in the model may be too high by as much as a factor of 2 (Figure 26). This rate may be particularly excessive in the SH, where it is slightly higher than in the north, in contradiction to the analysis of *Rosenlof and Holton* [1993], *Yang and Tung* [1996], and *Eluszkiewicz et al.* [1996], indicating a more vigorous troposphere-stratosphere exchange in the north. (Observations of

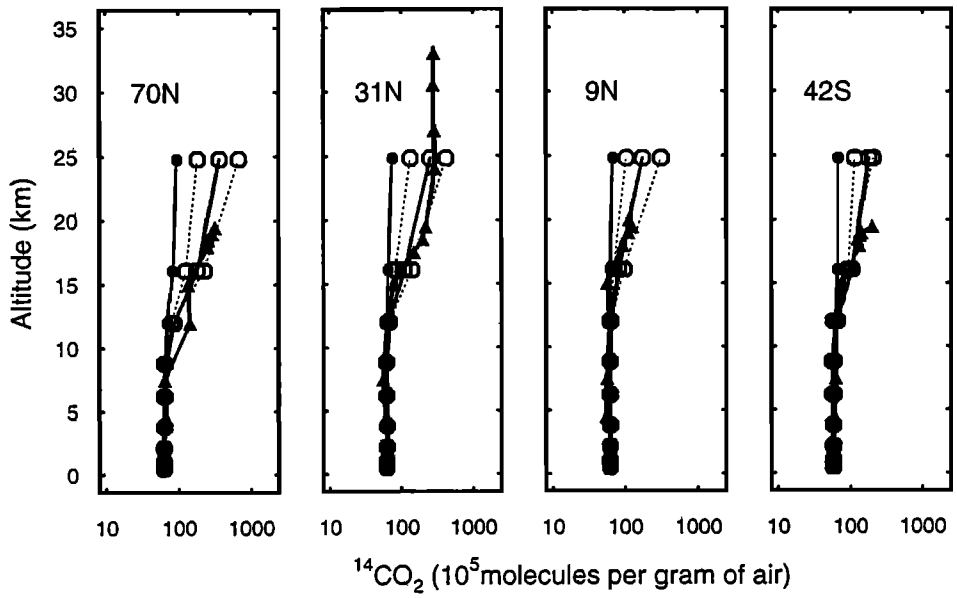

Figure 26. Global distribution of excess $^{14}CO_2$ (10^5 molecules per gram of air) observed in July 1966 (solid lines with triangles). Simulations were initialized in October 1963 using observations from *Johnston* [1989] along with the lower-boundary conditions. Solid lines with solid circles show the simulation with the standard model. Dotted lines with open circles correspond to simulations with the air flux through the 150 hPa surface reduced by 25% and 75%. Solid lines with open circles show the simulation with the air flux reduced by 50%.

bomb $^{14}CO_2$ are available only at 42°S in the SH and do not extend above 22 km.)

To estimate the magnitude of the error in our simulation of ^{14}CO due to inadequate representation of the stratosphere, we (1) reduced the air flux across the 150 hPa surface by a factor of 2 based on results for bomb $^{14}CO_2$, and (2) moved the portion of stratospheric emissions that the model erroneously attributes to the troposphere to the model layer above 150 hPa; the seasonal tropopause heights used to estimate the magnitude of the misplaced emissions were taken from *McCormick et al.* [1993].

As can be seen in Figures 25, 27, and 28, in austral winter in particular, simulations with the reduced flux from the stratosphere still exaggerate not only the absolute concentrations of ^{14}CO but also vertical and horizontal gradients in the SH. Our analysis of GCM II temperature fields revealed highly exaggerated horizontal gradients and uncharacteristically low temperatures poleward of 60°S below 400 hPa in winter; for example, at 600 hPa, the temperature gradient between 60°S and 80°S is about 20°C higher than observed: 28°C versus 8°C [*Peixoto and Oort*, 1992]. In addition, the jet stream in the SH is about twice as strong as observed, whereas the transient eddy energy is lower by more than a factor of 2 than observed, with a maximum displaced toward the equator by more than 20°. These discrepancies may indicate that mixing between southern high latitudes and the tropics in the GISS GCM II is too slow [cf. *Rind and Lerner et al.*, 1996]. Unfortunately, this is one of the aspects of transport that is not readily testable. The latitudinal distribution of ^{85}Kr changes little if an additional arbitrary horizontal diffusion of 1.5×10^{10} cm^2 s^{-1} is introduced south of 28°S below 400 hPa, combined with vertical diffusion of 8×10^5 cm^2 s^{-1} south of 60°S (dashed line in Figure 18). This modification of model transport sufficiently decreases the absolute level of ^{14}CO in the SH, as well as its gradients (Figures 25, 27, and 28). Importantly, relative amplitudes of seasonal variations of CH_3CCl_3 and CH_2Cl_2 at southern midlatitudes were not significantly affected by this enhancement of intrahemispheric mixing (dotted lines in Figures 21 and 22) because latitudinal gradients of these gases in the SH are small. The sensitivity of extratropical levels of ^{14}CO to the yet untestable aspects of model transport limits the utility of observed absolute concentrations of ^{14}CO as a measure of OH in that region. They provide, however, a stringent test for an overall performance of the model in simulating combined effects of chemistry and transport.

The annual cycle of ^{14}CO at northern midlatitudes is compared with observations in Figure 29, relative to the annual mean (Figure 29a) and on the absolute scale (Figure 29b). The relative amplitude for the simulation with standard OH is consistent with observations, while the absolute concentrations are low even for the standard simulation (solid lines), that is, with the flux from the stratosphere that most likely is too high. Therefore, results for ^{14}CO at northern midlatitudes suggest that

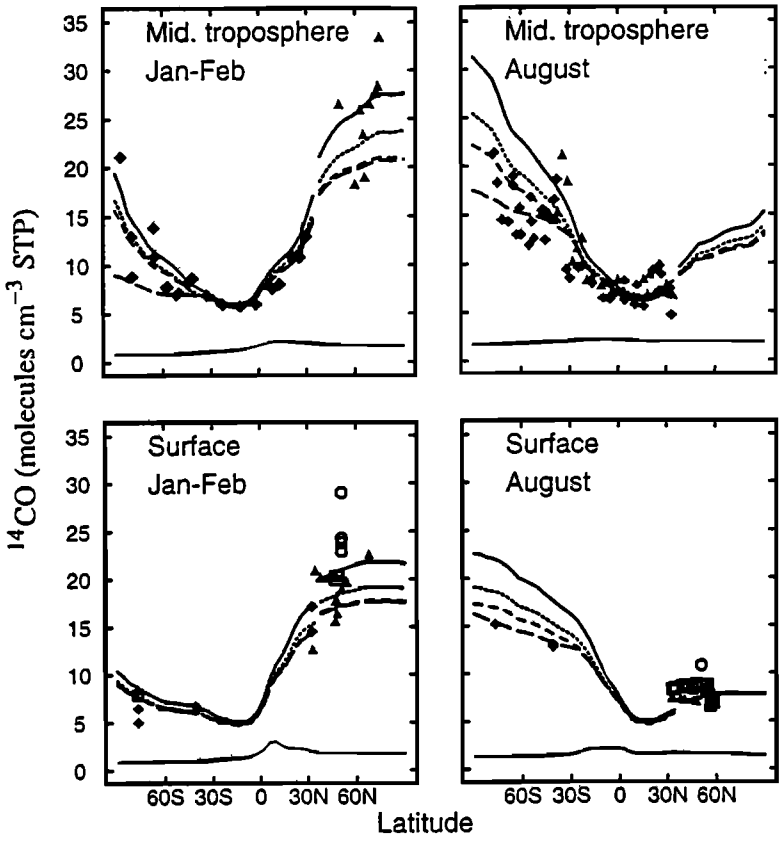

Figure 27. Concentration of ^{14}CO (molecules cm^{-3} STP) (top) at 6–7 km altitude and (bottom) at the surface (left) in January-February and (right) in August. Observations for 1990–1991 (diamonds) are from *Mak et al.* [1992], and for 1992 (squares) and 1993 (triangles) are from *Mak et al.* [1994]. Note that the cosmic source was approximately constant in 1990–1991, increasing by 8% in 1992 and additional 5% in 1993. See Figure 25 for the description of simulations and designation of line types. To facilitate a comparison with observations, model results south of 32°N are shown for 1990–1991, and north of 32°N for 1993. We also included observations in 1977–1978 from *Volz et al.* [1981] (open circles); the cosmic source for 1977–1978 was comparable to that in 1992–1993.

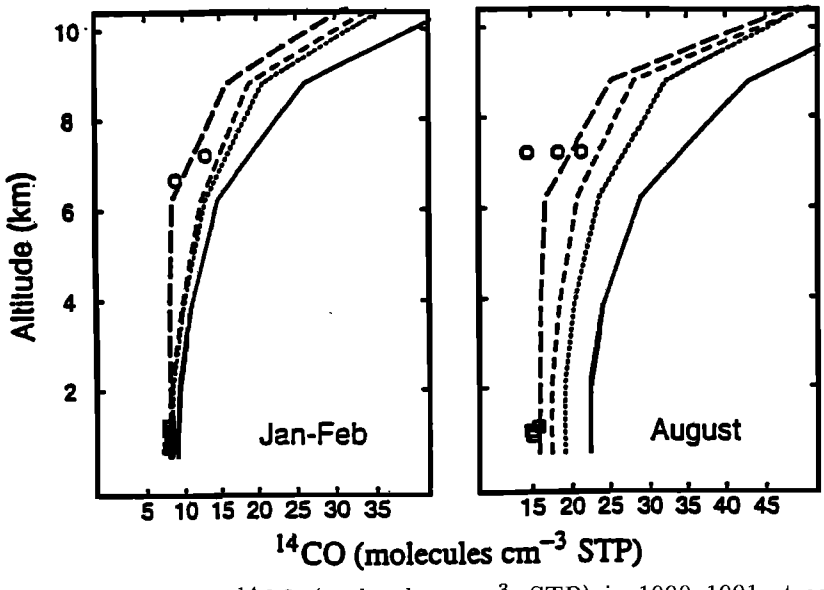

Figure 28. Vertical profiles of ^{14}CO (molecules cm^{-3}, STP) in 1990–1991 at southern mid-latitudes (left) in January-February and (right) in August. See Figure 25 for the description of simulations and designation of line types. Observations (symbols) at the surface are from *Brenninkmeijer* [1993] and aloft from *Mak et al.* [1992].

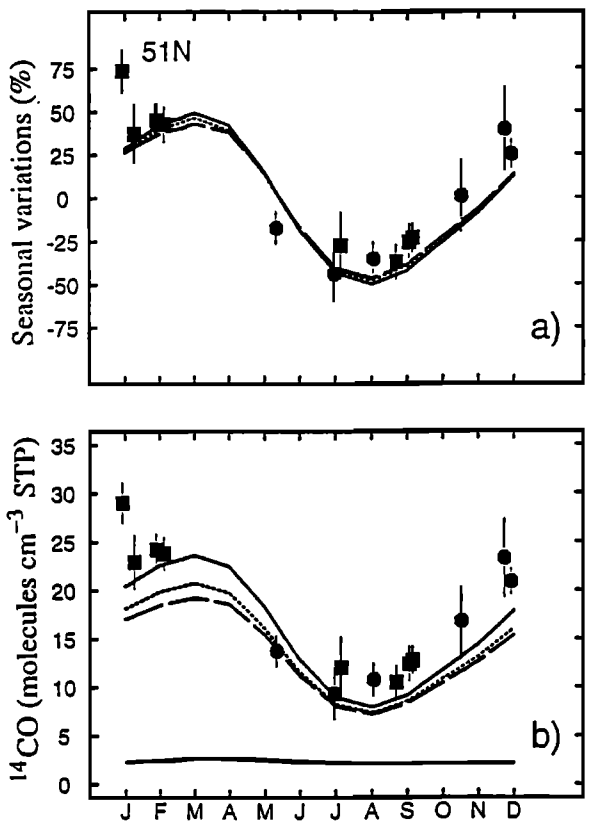

Figure 29. Seasonal variations of ^{14}CO in 1977–1978 at northern midlatitudes: (a) residuals with respect to the annual mean in percent and (b) on absolute scale in molecules cm^{-3} (STP). See Figure 25 for the description of simulations and designation of line types. Observations are from *Volz et al.* [1981].

a significant underestimation of concentrations of OH in the northern extratropics is unlikely.

In the tropics, concentrations of ^{14}CO are less sensitive to modifications of the flux from the stratosphere, or to the rate of intrahemispheric mixing in the troposphere (Figure 27), since about two thirds of ^{14}CO in the tropical troposphere is produced in situ (with about a half of that amount coming from biomass burning and oxidation of hydrocarbons), and since the lifetime of ^{14}CO in that region (about a month) is short as compared to average rates of mixing between tropics and midlatitudes. Using observations of ^{14}CO in the tropics, *Mak et al.* [1992] first suggested that concentrations of OH from S90 were too low. Results for the present distribution of OH are consistent with observations of ^{14}CO [*Mak et al.*, 1992, 1994] in the southern tropics in January-February and in the northern tropics in August (Figure 27). However, in winter in the tropics of both hemispheres, simulated concentrations of ^{14}CO are too high, with an implication that concentrations of OH are too low in that season by 15–20% in the north and by 10–15% in the south. While in the northern tropics results for annual means of CH_2Cl_2 also suggested that concentrations of OH may be too low, in the southern tropics the opposite conclusion was implied by observations of CH_2Cl_2 (see Figure 13). Because of the significance of the noncosmic sources of ^{14}CO in the tropics, a simulation including all CO isotopes in the OH-CO coupled model would be particularly beneficial for testing both sources of CO and the computation of OH.

11. Last Offerings of a Departing Friend

The Montreal Protocol required that consumption of CH_3CCl_3, was to cease by January 1996 in all but developing countries (consumption is defined as production + imports - exports). Emissions are expected to diminish sharply as reserves in the developed world are exhausted (P. Midgley, personal communication, 1997). The developing countries are allowed to consume up to 100 Gg yr^{-1} until 2010. However, in 1993 and 1994–1996, total emissions in developing countries were only about 51 and 30 Gg yr^{-1}, respectively, and total emissions in the following years are not expected to exceed 30 Gg yr^{-1} significantly [*Midgley and McCulloch*, 1995; P. Midgley, personal communication, 1997], that is, less than 6% of the mean rate of emissions in 1980–1983. Were the emissions of CH_3CCl_3 to cease entirely, the rate of relative decrease of the atmospheric abundance of CH_3CCl_3 would unambiguously define the lifetime of CH_3CCl_3, free of the uncertainties in the absolute calibration of measurements and the magnitude of emissions associated with the estimate using the trend in CH_3CCl_3 over the two previous decades [*Ravishankara and Albritton*, 1995]. Even if emissions were to linger near ~30 Gg yr^{-1}, the sensitivity to these uncertainties will diminish during the next several years because atmospheric levels of CH_3CCl_3 will be a factor of 8–4 higher than the steady state at 30 Gg yr^{-1} (about 6 pptv).

As another benefit of diminished emissions, we expect that observations of CH_3CCl_3 over the next several years will allow us to tighten constraints for the loss frequency of CH_3CCl_3 on scales smaller than global. In previous decades, seasonal variations of CH_3CCl_3 at the surface at northern midlatitudes were determined largely by the seasonality of convection and other processes responsible for dispersal of CH_3CCl_3 away from the source regions. Under the new conditions, an annual cycle of CH_3CCl_3 at northern midlatitudes is expected to bear mainly the signature of seasonal variations in the loss frequency, without significant interference from short-term variability ("pollution events"). As can be seen in Figures 30 and 31 for simulations discussed below, with no emissions or with small lingering emissions, zonally averaged results (lines) differ little from results at ALE/GAGE and NOAA sites (circles), in sharp contrast to the manifest zonal asymmetry simulated for the distribution of CH_3CCl_3 in the 1980s (S90). Improvement of accuracy in constraining OH is expected for southern midlatitudes as well. In previous decades, the

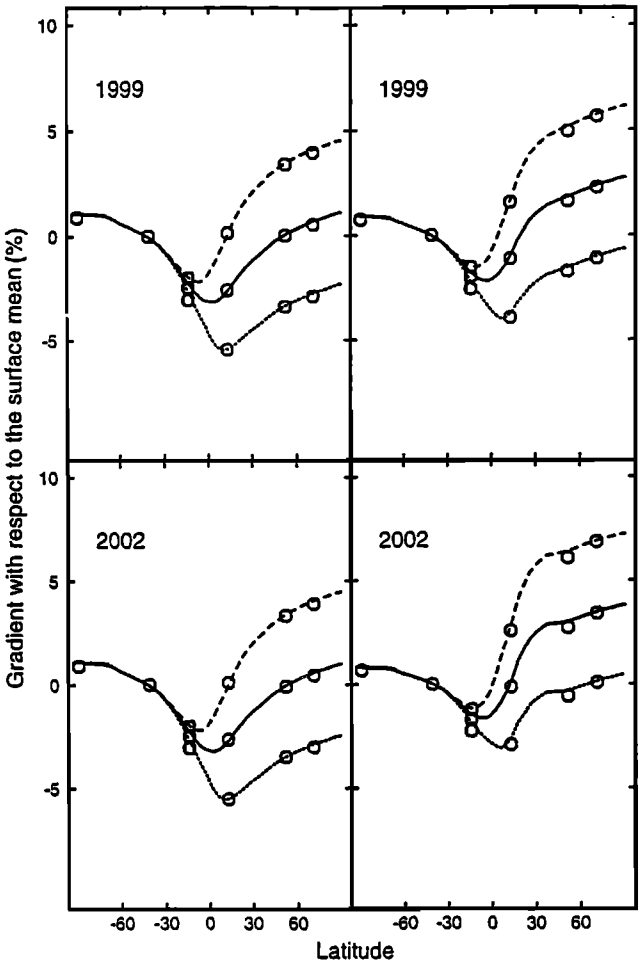

Figure 30. Annually averaged latitudinal distribution of CH_3CCl_3 in excess of concentrations at Tasmania, relative to the global mean at the surface, (top) in 1999 and (bottom) in 2002 with emissions, beginning in January 1998, of (left) 0 and (right) 30 Gg yr^{-1}. Zonal means for simulations with standard OH are shown as solid lines, and those with an interhemispheric ratio for OH of 1.5, north to south, and south to north, as dotted and dashed lines, respectively. Concentrations of OH were scaled to give the same lifetime of CH_3CCl_3 in all simulations. Results for selected NOAA and ALE/GAGE stations (at South Pole, Tasmania, Samoa, Barbados, Alaska, Ireland) are shown as open circles.

distribution of CH_3CCl_3 was characterized by a positive north-south gradient, including that between the southern tropics and extratropics, maintained by the NH emissions. With emissions at present levels and lower, it is expected that a negative gradient between the tropics and southern midlatitudes will become a permanent feature of the distribution of CH_3CCl_3 (Figures 30 and 31, solid lines) [cf. *Fung et al.*, 1991]. A comparison of observed seasonal variations of CH_3CCl_3 at southern midlatitudes for the two periods, characterized by the opposite signs of the gradient, may help determine the role of the dynamical component and thus tighten constraints for OH in that region.

The interhemispheric gradient of CH_3CCl_3 has decreased dramatically in the last few years [e.g., *Prinn et al.*, 1995; *Montzka et al.*, 1996; T. Thompson, personal communication, 1998] reflecting the drop in emissions (P. Midgley, personal communication, 1997). If emissions ceased, a significant interhemispheric asymmetry in the loss frequency of CH_3CCl_3 should manifest itself in an interhemispheric gradient which, when averaged over a year, would differ significantly from zero, as shown in Figure 30 (left panels). Here a simulation with the standard OH (solid line) is compared to those with north/south ratios of hemispheric means of 1.5 and 1/1.5, but with the same global mean concentration of

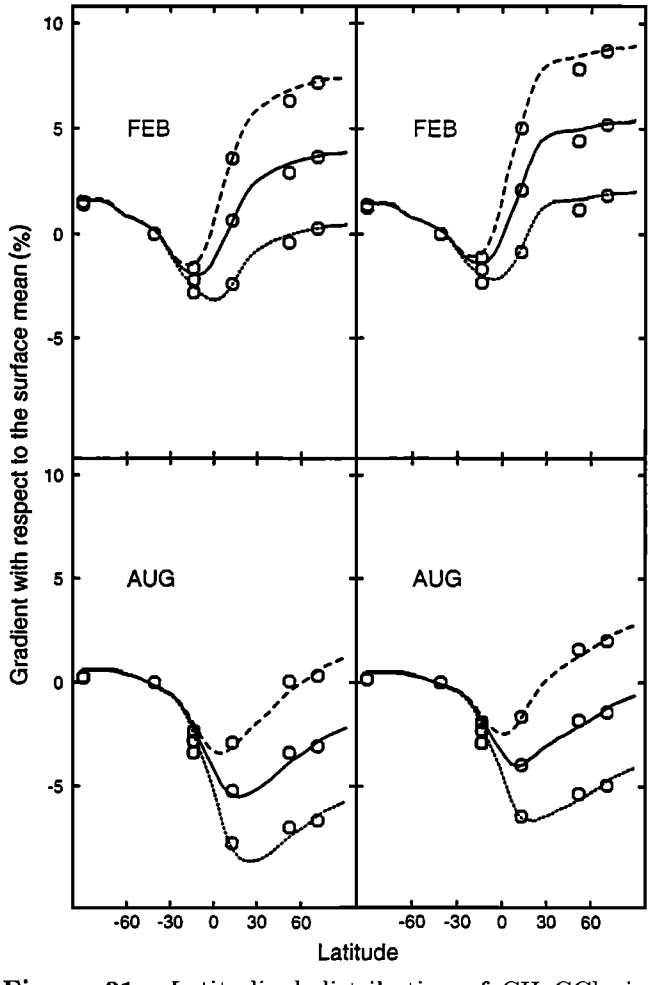

Figure 31. Latitudinal distribution of CH_3CCl_3 in excess of concentrations at Tasmania, relative to the global mean at the surface, (top) in February 1999 and (bottom) in August 1999 with emissions, beginning in January 1998, of (left) 0 and (right) 30 Gg yr^{-1}. Zonal means for simulations with the standard OH are shown as solid lines, and those with an interhemispheric ratio in OH of 1.5, north to south, and south to north, as dotted and dashed lines, respectively. Concentrations of OH were scaled to give the same lifetime of CH_3CCl_3 in all simulations. Results for selected NOAA and ALE/GAGE stations (at South Pole, Tasmania, Samoa, Barbados, Alaska, Ireland) are shown as open circles.

OH. Results at the surface are shown as a difference with those at 42°S, relative to the global average of surface concentrations. Simulations were initialized from observations at the end of 1996 (T. Thompson, personal communication, 1997). At that time the global mean concentration of CH_3CCl_3 at the surface was about 90 pptv, with a gradient between northern and southern high latitudes of about 9 pptv. Results are shown for 1999 and 2002; as expected, on the relative scale, they are virtually the same for different years in the absence of emissions (left panels). A factor of 1.5 bias in the mean hemispheric loss frequencies of CH_3CCl_3 leads to a gradient between midlatitudes of the two hemispheres of ±4% (averaged annually) in contrast to a nearly zero for standard OH. For comparison, the current precision of ALE/GAGE observations is better than 0.5% [*Prinn et al.*, 1995]. With standard OH, the north-south gradient fluctuates from about +3.5% in February to −3.5% in August (Figure 31, left panels). In contrast, it remains positive throughout the year for the simulation with OH depleted in the NH (ranging from about 7% in northern winter to nearly zero in summer) and remains negative throughout the year for the opposite case.

Right panels in Figures 30 and 31 show results for a constant rate of emissions of 30 Gg yr^{-1} (chosen arbitrarily) from 1998 on and distributed over developing countries only, in accordance with *Midgley and McCulloch* [1995]. This distribution results in about 10% of world emissions in the SH (as compared to only 3% in 1992 and 6% in 1993). In contrast to simulations with zero emissions (in which the interhemispheric gradient was maintained solely by the difference in loss frequencies in the two hemispheres), results for different years vary on the relative scale because the part of the gradient determined by emissions remains constant while atmospheric levels of CH_3CCl_3 decline. If emissions are monitored, observations of the latitudinal distribution of CH_3CCl_3, conducted with carefully maintained precision, should allow us to constrain the interhemispheric ratio of its loss frequency to a factor of 1.5 or better, while the global burden remains high (compared to the steady state corresponding to the level of lingering emissions). This would be equivalent to constraining hemispheric mean loss frequencies of CH_3CCl_3 to ±20%, assuming that the global mean is known. If it will not be possible to monitor emissions, then observations of the latitudinal distribution of CH_3CCl_3 over the next several years will provide a lower limit for the north-to-south ratio in OH, since most of the remaining emissions are expected to occur in the NH (P. Midgley, personal communication, 1997). If concentrations of CH_3CCl_3 turn out to be significantly lower on average in the NH than in the SH, it would signify unambiguously higher levels of OH in the NH than in the SH.

12. Summary and Conclusions

The climatological distribution of tropospheric OH presented here results in a global annual average of 1.16×10^6 molecules cm^{-3} (integrated with respect to mass of air from the surface to 100 hPa within ±32° latitude and to 200 hPa outside that region). For the present distribution, exclusion of isoprene would increase global mean OH by 3%. Exclusion of other NMHC would increase global mean OH by 7%. Measurements affording better definition of NO_x from 800 to 500 hPa, and those for O_3 in unpolluted regions, particularly in the tropics, would be most effective in improving the accuracy of computed OH.

While global mean OH increased by 33% compared to S90, mean loss frequencies of tracers such as CH_3CCl_3 and CH_4 increased by only 23% because of redistribution of OH within the tropospheric column: the fraction of OH residing below 700 hPa in the present distribution is lower than in S90 by ~21% (33% versus 42%). This upward shift in OH occurred in part because of the new distribution of clouds, in part because of inclusion of NMHC combined with a decrease in CO over most of the globe. As a result of the decrease in the fraction of the abundance of OH residing in the lower troposphere, the value 277 K used for scaling lifetimes of HCFCs and other long-lived gases to a known lifetime [*Prather and Spivakovsky*, 1990] is revised to 272 K.

On average, there is little interhemispheric bias in the computed distribution of OH. Mean tropical concentrations (within ±32°) are 5% lower in the north, while 14% more OH is predicted for the region poleward of 32° in the north than in the south.

The present distribution of OH results in a global annual mean lifetime for CH_3CCl_3 of 4.6 years [cf. *Prinn et al.*, 1995], including a stratospheric sink with an atmospheric lifetime of 43 years and an ocean sink with an atmospheric lifetime of 80 years. The global mean concentration of OH (weighted by the frequency of reaction with CH_3CCl_3) is 3±2% higher than implied by the observed long-term trend in CH_3CCl_3, using the most likely values for non-OH sinks, absolute calibration, emissions, and rate constant. The uncertainty in mean OH implied by observations is estimated to be in the range from −23% to +28% assuming that errors in all relevant values may affect an estimate in the same direction.

For HCFC-22, the present distribution of OH results in a global annual mean of 11.4 years, including the stratospheric sink with an atmospheric lifetime of 229 years. The evolution of the global abundance of HCFC-22 implies that the computed annual global mean concentration of OH (weighted by the frequency of reaction with HCFC-22) is accurate to ±5%, with an uncertainty in the value implied by observations estimated between −20% and +36%. Only emissions reported by the industry were used for HCFC-22. Results using long-term trends of CH_3CCl_3 and HCFC-22 are consistent within a few percent.

Observed annually averaged levels of CH_2Cl_2 imply that computed global mean OH (weighted by the frequency of reaction with CH_2Cl_2) is too low by 5–10%, whereas an uncertainty associated with defining the

value for empirical OH is estimated to be in the range from −21% to +30%. This estimate may not be correct for a different spatial distribution of OH. Industrial sources of CH_2Cl_2 are sufficient to balance the budget of CH_2Cl_2 using the recently measured rate constant and the present distribution of OH. Uncertainties in the strength of the Cl sink for C_2Cl_4 and in the rate constant for reaction with OH restrict at present the utility of observations of C_2Cl_4 as a test of OH.

The sensitivity of tracer concentrations to rates of transport is an intrinsic difficulty in efforts to constrain regional levels of OH. The use of independent constraints based on observations of tracers with different lifetimes and distinct distributions of sources is essential for meaningful estimates of the accuracy of computed OH on scales smaller than global. On the hemispheric scale the rate of interhemispheric mixing in the CTM affects greatly the levels of empirical OH inferred from observations of CH_2Cl_2. If this rate is taken at the upper limit consistent with observations of CFCs and ^{85}Kr, observed annual means of CH_2Cl_2 suggest that computed OH has to be increased by 20% in the NH and decreased by 25% in the southern tropics. If, however, the rate of interhemispheric mixing is taken at its lower limit, these observations indicate that OH has to be increased by 35% in the NH and decreased by 60% in the southern tropics. Such corrections would imply a considerable interhemispheric bias in OH with north-to-south ratios of hemispheric means for OH of 1.5 and 2.3, for the upper and lower limit of the rate of interhemispheric mixing, respectively. Observations of the interhemispheric gradient of CH_3CCl_3 in the 1980s suggest north-to-south ratios less than 1.5 for the upper limit and little interhemispheric bias in OH for the lower limit.

The large corrections for concentrations of OH in either hemisphere suggested by annually averaged concentrations of CH_2Cl_2 are not supported by other constraints. In the northern extratropics, tests using the relative amplitude of seasonal variations of CH_2Cl_2, C_2H_6 and ^{14}CO do not suggest significant errors in the average levels of OH in that region. Absolute levels of ^{14}CO predicted for that region are too low even though the flux of ^{14}CO from the stratosphere in the model is too high, with the implication that concentrations of OH at northern midlatitudes are not underestimated (in contrast to the estimate inferred from observed annual means of CH_2Cl_2). Observations of ^{14}CO in the northern tropics in summer support the accuracy of computed OH in that region; in winter, however, concentrations of OH in the northern tropics appear too low by 15–20%. Weighing all the available evidence, some increase may be in order for computed OH in winter at low northern latitudes which may result in a small increase in the annual mean concentration of OH for the whole NH (5–10%). A greater underestimate of OH in the NH is unlikely since, in order to satisfy global constraints such as lifetimes of CH_3CCl_3 and HCFC-22, it would have to be compensated by a comparable overestimate for the SH. However, observations of ^{14}CO in the southern tropics call for an increase in OH in that region in winter by 10–15%, and indicate no error in summer. A decrease in OH by 15–25% in the SH may be indicated in the extratropics by the tests using the relative amplitude of seasonal variations of CH_2Cl_2, CH_3CCl_3 and ^{14}CO, but such a decrease would have little effect on the mean concentration of OH for the SH.

We used the interhemispheric gradient of CH_3CCl_3 as a constraint for the ratio of mean hemispheric concentrations of OH. We emphasize, however, that the interhemispheric gradient of CH_3CCl_3 is insensitive to increases as well as to moderate decreases (within 25%) in the lifetime of CH_3CCl_3 if the latitudinal distribution of the loss frequency remains unchanged [*Plumb and McConalogue*, 1988; S90; *Spivakovsky*, 1991].

Interpretation of observations of ^{14}CO presents an additional level of difficulty as compared to tracers such as CH_2Cl_2 because it requires an accurate simulation of the rate of transport from the stratosphere, of the stratospheric loss, and of the position of the tropopause. In addition, steep gradients of ^{14}CO between tropics and midlatitudes, enhanced by a shorter lifetime and high-latitude sources, make results at midlatitudes particularly sensitive to the rate of intrahemispheric mixing, which in the SH is not readily testable. Therefore, unless these other aspects of the model, unrelated to OH, are proved accurate, absolute levels of ^{14}CO outside the tropics cannot be regarded as an unambiguous measure of the abundance of OH but rather as an important test of an overall performance of CTMs. Observations of seasonal variations of CH_3CCl_3, CH_2Cl_2, ^{14}CO and C_2H_6 offer no evidence for higher levels of OH in the southern than in the northern extratropics suggested by the early interpretation of data for ^{14}CO [cf. *Brenninkmeijer et al.*, 1999].

Unless a significant change in the mechanism is recommended, it is difficult to contemplate errors in excess of ±15% in global and hemispheric climatological averages for the abundance of OH, given our present knowledge of the distributions of precursors and the limited sensitivity of computed concentrations of OH to changes in their specification. It is difficult, however, to test the computed values to that level of accuracy, especially on scales smaller than the global.

In the next few years, while the global burden of CH_3CCl_3 remains high but emissions are reduced, observations of CH_3CCl_3 will present a unique opportunity to constrain global and regional abundances of OH. The relative rate of change in the global burden of CH_3CCl_3 will be less sensitive to errors in the absolute calibration and magnitude of emissions. The latitudinal distribution of CH_3CCl_3 will be defined primarily by the distribution of the loss frequency rather than that of emissions. A factor of 1.5 excess in the loss frequency in one hemisphere (as compared to the other) would result in about a 4% gradient for annual mean concentrations between midlatitudes of the two hemispheres (with respect to the global mean at the surface). In contrast

to the 1980s, interference from pollution events is not expected to confound the analysis of the latitudinal gradient of CH_3CCl_3 in the next several years because the global burden of CH_3CCl_3 in 1999-2002 will be 8 to 4 times higher than that in balance with the rate of emissions, whereas in the 1980s, the imbalance was of the opposite sign. Our analysis suggests that if emissions are monitored, observations of the latitudinal distribution of CH_3CCl_3 could allow us to constrain the interhemispheric ratio of loss frequencies to better than a factor of 1.5. Such an estimate would limit the range of hemispheric loss frequencies to ±20% (as compared to a distribution with no interhemispheric bias) assuming that the global mean is known. As in the past, most of the remaining emissions are expected to occur in the NH. If significant uncertainties in the magnitude of emissions cannot be eliminated, the interhemispheric gradient of CH_3CCl_3 should provide a lower limit for the ratio, north to south, of the mean hemispheric loss frequencies.

Estimates of the abundance of OH in the extratropics will be also improved under the new conditions. In the north, both the interference of short-term variability and the seasonality of convection are expected to have little impact on the annual cycle of CH_3CCl_3 as long as the global burden remains high compared to the steady state level associated with the rate of emissions. In the south, a negative north-south gradient between the tropics and midlatitudes is expected to become a steady feature of the distribution of CH_3CCl_3 as opposed to the positive gradient characteristic of previous decades. A comparison between annual cycles of CH_3CCl_3 for the two periods, with opposite signs of the gradient, will help constrain the magnitude of the dynamical component of seasonal variations at southern midlatitudes. The depth of the tropical dip in concentrations of CH_3CCl_3 will present a test for the combined effects of intrahemispheric mixing and the disparity between tropical and extratropical levels of OH.

In this work we did not consider changes in OH from year to year or on a longer timescale. Out of necessity, observations of precursors for OH used to compile the climatology as well as observations of tracers used to evaluate computed OH, span different periods between 1978 and 1996. Thus temperature and water vapor were for 1986–1989, cloud reflectivities for 1984–1990, ozone columns for 1978–1992; for CO the time span varied from station to station, and for NO and hydrocarbons mostly "snapshots" were available. Similarly, concentrations of CH_3CCl_3 span over 1978–1996, while for HCFC-22 observations for 1992–1996 where used, with even shorter periods for CH_2Cl_2 (1995–1996), C_2H_6 (1992–1994), and ^{14}CO (1977–1978 for midlatitudes, 1990–1993 for the tropics and 1989–1991 for southern midlatitudes). During the two decades, trends in various precursors for OH were observed, for example, an increase in CH_4 [*Dlugokencky et al.*, 1998], an increase in CO in the early 1980s [*Zander et al.*, 1989; *Brunke et al.*, 1990] followed by a decrease in CO in the 1990s [e.g., *Novelli et al.*, 1998], small increases in NO_x [*Logan*, 1994], and a decrease in column ozone [*McPeters et al.*, 1996]. *Krol et al.* [1998] simulated an increase in mean tropospheric OH up to 6% over 1978–1993 in response to these changes. They deduced a similar increase (7%) using observations of CH_3CCl_3, however, with a large uncertainty allowing for an increase of 16.5% as well as a decrease of 1.5% over 1978–1993. *Prinn et al.* [1995], using the same observations of CH_3CCl_3, deduced 0±0.2% change in OH over 1978–1994. *Wang and Jacob* [1998] estimated that tropospheric OH increased by less than 10% since preindustrial times, despite the vast changes in the chemical composition of the atmosphere. At the root of the stability of mean tropospheric OH is the nature of the chemistry of OH, buffered by various feedbacks as discussed above [cf. *Krol et al.*, 1998]. In addition, human activity tends to increase simultaneously concentrations of species contributing to both production and destruction of OH.

Acknowledgments. We are grateful to the late John Bradshaw and to Scott Smyth of the Georgia Institute of Technology who provided merged data files and gridded data for NO measurements from the GTE and AASE programs prior to 1995. Data for PEM-Tropics were obtained from the GTE data archive (http://www-gte.larc.nasa.gov). We thank Paul Novelli, Bill Munger, Don Blake, Thayne Thompson, Paul Fraser, and Martin Manning for sharing with us unpublished data. We are indebted to Pauline Midgley for providing promptly essential information on emissions. We acknowledge important discussions with Daniel Jacob, Hans Schneider, Hanwant Singh, Ross Salawitch, Ravi Ravishankara, Kevin E. Trenberth, Brian Farrell, David Keith, Michael Trainer, Lyatt Jaegle, Bryan Duncan, Isabelle Bey, and Martin Schultz. Two anonymous reviewers provided thorough and thoughtful comments which helped to improve the paper significantly. We benefited from expert help in data analysis provided by Amy Munson and Inna Megretskaia. We thank Renate D'Arcangelo and Cecilia Demore McCormack for editorial assistance. This work was supported by the National Science Foundation (ATM-9320778) and by the National Aeronautics and Space Administration (NAGW-2632 and NAG1-1909).

References

Alternative Fluorocarbons Environmental Acceptability Study, *Production, Sales and Atmospheric Release of Fluorocarbons through 1996*, AFEAS Sci. and Policy Services, Inc., Washington, D. C., 1998.

Andronache, C., W.L. Chameides, M.O. Rodgers, J. Martinez, P. Zimmerman, and J. Greenberg, Vertical distribution of isoprene in the lower boundary layer of the rural and urban southern United States, *J. Geophys. Res., 99*, 16,989–16,999, 1994.

Atkinson, R., D.L. Baulch, R.A. Cox, R.F. Hampson Jr., J.A. Kerr, M.J. Rossi, and J. Troe, Evaluated kinetic, photochemical and heterogeneous data for atmospheric chemistry, supplement 5: IUPAC subcommittee on gas kinetic data, evaluation for atmospheric chemistry, *J. Phys. Chem Ref. Data, 26*, 521–1011, 1997.

Ayers, G.P., and R.W. Gillett, Isoprene emissions from vegetation and hydrocarbon emissions from bush fires in tropical Australia, *J. Atmos. Chem., 7*, 177–190, 1988.

Balkanski, Y.J., and D.J. Jacob, Transport of continental air to the Subantarctic Indian Ocean, *Tellus, 42*, 62–75, 1990.

Balkanski, Y.J., D.J. Jacob, R. Arimoto, and M.A. Kritz, Long-range transport of radon-222 over the North Pacific Ocean: Implications for continental influence, *J. Atmos. Chem., 14*, 353–374, 1992.

Balkanski, Y.J., D.J. Jacob, G.M. Gardner, W.M. Graustein, and K.K. Turekian, Transport and residence times of continental aerosols inferred from a global 3-dimensional simulation of ^{210}Pb, *J. Geophys. Res., 98*, 20,573–20,586, 1993.

Blake, D.R., D.F. Hurst, T.W. Smith, W.J. Whipple, T-.Y. Chen, N.J. Blake, and F.S. Rowland, Summertime measurements of selected nonmethane hydrocarbons in the Arctic and Subarctic during the 1988 Arctic Boundary Layer Expedition (ABLE 3A), *J. Geophys. Res., 97*, 16,559–16,588, 1992.

Blake, D.R., T.W. Smith, T.-Y. Chen, W.J. Whipple, and F.S. Rowland, Effects of biomass burning on summertime nonmethane hydrocarbon concentrations in the Canadian wetlands, *J. Geophys. Res., 99*, 1699–1719, 1994.

Blake, D.R., N.J. Blake, T.W. Smith, O.W. Wingenter, and F.S. Rowland, Nonmethane hydrocarbon and halocarbon distributions during Atlantic Stratocumulus Transition Experiment Marine Aerosol and Gas Exchange, June 1992, *J. Geophys. Res., 101*, 4501–4514, 1996a.

Blake, D.R., T-.Y. Chen, T.W. Smith, C.J.L. Wang, O.W. Wingenter, N.J. Blake, F.S. Rowland, and E.W. Mayer, Three-dimensional distribution of nonmenthane hydrocarbons and halocarbons over the Northwestern Pacific during the 1991 Pacific Exploratory Mission (PEM-WEST A), *J. Geophys. Res., 101*, 1763–1778, 1996b.

Blake, N.J., D.R. Blake, T.-Y. Chen, J.E. Collins, G.W. Sachse, B.E. Anderson, and F.S. Rowland, Distribution and seasonality of selected hydrocarbons and halocarbons over the western Pacific basin during PEM-WEST A and PEM-WEST B, *J. Geophys. Res., 102*, 28,315–28,331, 1997.

Blumthaler, M., and W. Ambach, Solar UVB-albedo of various surfaces, *Photochem. Photobiol., 48*, 85–88, 1988.

Bottenheim, J.W., and M.F. Shepherd, C_2-C_6 hydrocarbon measurements at 4 rural locations across Canada, *Atmos. Environ., 29*, 647–664, 1995.

Bradshaw, J., S.B. Smyth, S.C. Liu, R. Newell, D.D. Davis, and S.T. Sandholm, Observed distributions of nitrogen oxides in the remote free troposphere from the NASA Global Tropospheric Experiment programs, *Rev. Geophys. 38*, 61–116, 2000.

Bradshaw, J., et al., Photofragmentation two-photon laser-induced fluorescence detection of NO_2 and NO: Comparison of measurements with model results based on airborne observations during PEM–Tropics A, *Geophys. Res. Lett., 26*, 471–474, 1999.

Brenninkmeijer, C.A.M., Measurement of the abundance of ^{14}CO in the atmosphere and the $^{13}C/^{12}C$ and $^{18}O/^{16}O$ ratio of atmospheric CO, with applications in New Zealand and Antarctica, *J. Geophys. Res., 98*, 10,595–10,614, 1993.

Brenninkmeijer, C.A.M., M.R. Manning, D.C. Lowe, G. Wallace, R.J. Sparks, and A. Volz-Thomas, Interhemispheric asymmetry in OH abundance inferred from measurements of atmospheric ^{14}CO, *Nature, 356*, 50–52, 1992.

Brenninkmeijer, C.A.M., T. Rockmann, M. Braunlich, P. Jockel, and P. Bergamaschi, Review of progress in isotope studies of atmospheric carbon monoxide, *Chemosphere, 1*, 32–55, 1999.

Brune, W.H., et al., Airborne in situ OH and HO_2 observations in the cloud-free troposphere and lower stratosphere during SUCCESS, *Geophys. Res. Lett., 25*, 1701–1704, 1998.

Brunke, E.-G., H.E. Scheel, and W. Seiler, Trends of tropospheric CO, N_2O and CH_4 as observed at Cape Point, South Africa, *Tellus, Ser. A, 24*, 585–595, 1990

Butler, J.H., J.W. Elkins, T.M. Thompson, B.D. Hall, T.H. Swanson, and V. Koropalov, Oceanic consumption of CH_3CCl_3: Implications for tropospheric OH, *J. Geophys. Res., 96*, 22,347–22,355, 1991.

Carroll, M.A., and A.M. Thompson, NO_x in the non-urban troposphere, in *Problems and Progress in Atmospheric Chemistry, Adv. Phys. Chem.*, vol. 3, edited by J. Barker, pp. 198–255, World Sci., River Edge, N.J., 1995.

Chameides, W.L., and A. Tan, The two-dimensional diagnostic model for tropospheric OH: An uncertainty analysis, *J. Geophys. Res., 86*, 5209–5223, 1981.

Chandrasekhar, S., *Radiative Transfer*, Dover, Mineola, N.Y, 1960.

Chin, M., and D.J. Jacob, Anthropogenic and natural contributions to atmospheric sulfate: A global model analysis, *J. Geophys. Res., 101*, 18,691–18,700, 1996.

Chin, M., D.J. Jacob, G.M. Gardner, M. Foreman-Fowler, P.A. Spiro, and D.L. Savoie, A global three-dimensional model of tropospheric sulfate, *J. Geophys. Res., 101*, 18,667–18,690, 1996.

Climate Monitoring and Diagnostics Laboratory (CMDL), Summary report 1996–1997, *NOAA Environ. Res. Lab., 24*, 1998.

Crutzen, P.J., and J. Fishman, Average concentrations of OH in the troposphere and the budgets of CH_4, CO, H_2, and CH_3CCl_3, *Geophys. Res. Lett., 4*, 321–324, 1977.

Crutzen, P.J., and L.T. Gidel, A two-dimensional photochemical model of the atmosphere, 2, The tropospheric budgets of the anthropogenic chlorocarbons CO, CH_4, CH_3Cl and the effect of various NO_x sources on tropospheric ozone, *J. Geophys. Res., 88*, 6641–6661, 1983.

Crutzen, P.J., and P.H. Zimmermann, The changing photochemistry of the troposphere, *Tellus, Ser. A, 43*, 136–151, 1991.

Cunnold, D., P. Fraser, R. Weiss, R. Prinn, P. Simmonds, F. Alyea, and A. Crawford, Global trends and annual releases of CCl_3F and CCl_2F_2 estimated from ALE/GAGE and other measurements from July 1978 to June 1991, *J. Geophys. Res., 99*, 1107–1126, 1994.

Dann, T.F., and D.K. Wang, Ambient air benzene concentrations in Canada (1989–1993): Seasonal and day of week variations, trends and sources influences, *J. Air Waste Manage. Assoc., 45*, 695–702, 1995.

DeMore, W.B., S.P. Sander, D.M. Golden, R.F. Hampson, M.J. Kurylo, C.J. Howard, A.R. Ravishankara, C.E. Kolb, and M.J. Molina, Chemical kinetics and photochemical data for use in stratospheric modeling, Evaluation No. 9, *JPL Publ. 94-1*, Jet Propul. Lab., Pasadena, Calif., 1994.

DeMore, W.B., S.P. Sander, D.M. Golden, R.F. Hampson, M.J. Kurylo, C.J. Howard, A.R. Ravishankara, C.E. Kolb, and M.J. Molina, Chemical kinetics and photochemical data for use in stratospheric modeling, *JPL Publ. 97-4*, Pasadena, Calif., 1997.

Dlugokencky, E.J., L.P. Steele, P.M. Lang, and K.A. Masarie, The growth rate and distribution of atmospheric methane, *J. Geophys. Res., 99*, 17,021–17,043, 1994.

Dlugokencky, E.J., L.P. Steele, P.M. Lang, and K. A. Masarie, Atmospheric methane at Mauna Loa and Barrow observatories: Presentation and analysis of in situ measurements, *J. Geophys. Res., 100*, 23,103–23,113, 1995.

Dlugokencky, E.J., K.A. Masarie, P.M. Lang, and P.P. Tans, Continuing decline in the growth rate of the atmospheric methane burden, *Nature, 393*, 447–450, 1998.

Donahue, N.M., and R.G. Prinn, In situ nonmethane hydro-

carbon measurements on SAGA-3, *J. Geophys. Res., 98*, 16,915–16,932, 1993.

Drummond, J.W., D.H. Ehhalt, and A. Volz, Measurements of nitric oxide between 0–12 km altitude and 67°N to 60°S latitude obtained during STRATOZ III, *J. Geophys. Res., 93*, 15,831–15,849, 1988.

Dvoryashina, Y.V., V.I. Dianov-Klokov, and L.N. Yurganov, Variations of the content of carbon monoxide in the atmosphere in the period 1970–1982, *Izv. Acad. Sci. USSR, Atmos. Oceanic Phys.*, Engl. Transl., *20*, 27–33, 1984.

Ehhalt, D.H., and J. Drummond, NO_x sources and the tropospheric distribution of NO_x during STRATOZ III, in *Proceedings of the NATO Advanced Research Workshop on Regional and Global Ozone and Its Environmental Consequences, NATO ASI Ser. C*, vol. 227, edited by I.S.A. Isaksen, pp. 217–237, D. Reidel, Norwell, Mass., 1988.

Ehhalt, D.H., H.P. Dorn, and D. Poppe, The chemistry of the hydroxyl radical in the troposphere, *Proc. R. Soc. Edinburgh, 97B*, 17–34, 1991.

Eisele, F.L., G.H. Mount, D. Tanner, A. Jefferson, R. Shetter, J.W. Harder, and E.J. Williams, Understanding the production and interconversion of the hydroxyl radical during the tropospheric OH photochemistry experiment, *J. Geophys. Res., 102*, 6457–6465, 1997.

Eluszkiewicz, J., D. Crisp, R. Zurek, L. Elson, L. Froidevaux, J. Waters, R.G. Grainger, A. Lambert, R. Harwood, and G. Peckham, Residual circulation in the stratosphere and lower mesosphere as diagnosed from Microwave Limb Sounder data, *J. Atmos. Sci., 53*, 217–240, 1996.

Emmons, L.K., et al., Climatologies of NO_x and NO_y: A comparison of data and models, *Atmos. Environ. 31*, 1851–1904, 1997.

Fisher, D., T. Duafala, P.M. Midgley, and C. Niemi, Production and Emission of CFCs, Halons, and Related Molecules, *Concentrations, Lifetimes and Trends of CFC's, Halons and Related Species, NASA Tech. Rep. 1339*, 2-1–2-34, 1994.

Fishman, J., and V.G. Brackett, The climatological distribution of tropospheric ozone derived from satellite measurements using version 7 Total Ozone Mapping Spectrometer and Stratospheric Aerosol and Gas experiment data sets, *J. Geophys. Res., 102*, 19,275–19,278, 1997.

Fishman, J., S. Solomon, and P.J. Crutzen, Observational and theoretical evidence in support of a significant in situ photochemical source of tropospheric ozone, *Tellus, 31*, 432–446, 1979.

Fishman, J., C.E. Watson, J.C. Larsen, and J.A. Logan, The distribution of tropospheric ozone obtained from satellite data, *J. Geophys. Res., 95*, 3599–3617, 1990.

Fraser, P.J., P. Hyson, R.A. Rasmussen, A.J. Crawford, and M.A.K. Khalil, Methane, carbon monoxide and methylchloroform in the southern hemisphere, *J. Atmos. Chem., 4*, 3–42, 1986.

Fung, I., J. John, J. Lerner, E. Matthews, M. Prather, L.P. Steele, and P.J. Fraser, Three-dimensional model synthesis of the global methane cycle, *J. Geophys. Res., 96*, 13,033-13,066, 1991.

Goldstein, A.H., S.C. Wofsy, and C.M. Spivakovsky, Seasonal variations of nonmethane hydrocarbons in rural New England: Constraints on OH concentrations in northern midlatitudes, *J. Geophys. Res., 100*, 21,023-21,033, 1995a.

Goldstein, A.H., B.C. Daube, J.W. Munger, and S.C. Wofsy, Automated in situ monitoring of atmospheric non-methane hydrocarbon concentrations and gradients, *J. Atmos. Chem., 21*, 43–59, 1995b.

Greenberg, J.P., P.R. Zimmerman, and R.B. Chatfield, Hydrocarbons and carbon monoxide in African savannah air, *Geophys. Res. Lett., 12*, 113–116, 1985.

Guenther, A., et al., A global model of natural volatile organic compound emissions, *J. Geophys. Res., 100*, 8873–8892, 1995.

Guenther, A., et al., Isoprene fluxes measured by enclosure, relaxed eddy accumulation, surface layer gradient, mixed layer gradient, and mixed layer mass balance techniques, *J. Geophys. Res., 101*, 18,555–18,567, 1996.

Hansen, J., G. Russell, D. Rind, P. Stone, A. Lacis, S. Lebedeff, R. Ruedy, and L. Travis, Efficient three-dimensional global models for climate studies: Models I and II, *Mon. Weather Rev., 111*, 609–662, 1983.

Hao, W.M., M.H. Liu, and P.J. Crutzen, Estimates of annual and regional releases of CO_2 and other trace gases to the atmosphere from fires in the tropics, based on the FAO statistics for the period 1975–1980, in *Proceedings of Third International Symposium on Fire Ecology*, Springer-Verlag, New York, 1990.

Hauglustaine, D.A., G.P. Brasseur, S. Walters, P.J. Rasch, J.-F. Muller, L.K. Emmons, and M.A. Carroll, MOZART, a global chemical transport model for ozone and related chemical tracers, 2, Model results and evaluation, *J. Geophys. Res., 103* , 28,291-28,335, 1998.

Helmig, D., B. Balsey, K. Davis, L.R. Kuck, M. Jensen, J. Bognar, T. Smith Jr., R.V. Arrieta, R. Rodriguez, and J.W. Birks, Vertical profiling and determination of landscape fluxes of biogenic nonmethane hydrocarbons within the planetary boundary layer in the Peruvian Amazon, *J. Geophys. Res., 103*, 25,519–25,532, 1998.

Holton, J.R., P.H. Haynes, M.E. McIntyre, A.R. Douglas, R.B. Rood, and L. Pfister, Stratosphere-troposphere exchange, *Rev. Geophys., 33*, 403–439, 1995.

Horowitz, L.W., and D.J. Jacob, Global impact of fossil fuel combustion on atmospheric NO_x, *J. Geophys. Res., 104*, 23,823–23,840, 1999.

Horowitz, L.W., J. Liang, G.M. Gardner, and D.J. Jacob, Export of reactive nitrogen from North America during summertime: Sensitivity to hydrocarbon chemistry, *J. Geophys. Res., 103*, 13,451–13,476, 1998.

Houweling, S., F. Dentener, and J. Lelieveld, The impact of nonmethane hydrocarbon compounds on tropospheric photochemistry, *J. Geophys. Res., 103*, 10673–10696, 1998.

Jackman, C.H., A.R. Douglass, K.F. Brueske and S.A. Klein, The influence of dynamics on two-dimensional model results: Simulation of ^{14}C and stratospheric aircraft NO_x injections, *J. Geophys. Res., 96*, 22,559–22,572, 1991.

Jacob, D.J., *Introduction to Atmospheric Chemistry*, Princeton Univ. Press, Princeton, N.J., 1999.

Jacob, D.J., and M.J. Prather, Radon-222 as a test of convective transport in a general circulation model, *Tellus, 42*, 118–134, 1990.

Jacob, D.J., and S.C. Wofsy, Photochemistry of biogenic emissions over the Amazon forest, *J. Geophys. Res., 93*, 1477–1486, 1988.

Jacob, D.J., and S.C. Wofsy, Budgets of reactive nitrogen, hydrocarbons and ozone over the Amazon forest during the wet season, *J. Geophys. Res., 95*, 16,737–16,754, 1990.

Jacob, D.J., M.J. Prather, S.C. Wofsy, and M.B. McElroy, Atmospheric distribution of ^{85}Kr simulated with a general circulation model, *J. Geophys. Res., 92*, 6614–6626, 1987.

Jacob, D.J., E.W. Gottlieb, and M.J. Prather, Chemistry of a polluted cloudy boundary layer, *J. Geophys. Res., 94*, 12,975–13,002, 1989.

Jaegle, L., et al., Observed OH and HO_2 in the upper troposphere suggest a major source from convective injection of peroxides, *Geophys. Res. Lett., 24*, 3181–3184, 1997.

Jobson, B.T., Z. Wu, H. Niki, and L.A. Barrie, Seasonal trends of isoprene, C-2-C-5 alkanes, and acetylene at a remote boreal site in Canada, *J. Geophys. Res., 99*, 1589–1599, 1994.

Johnston, H., Evaluation of excess carbon 14 and strontium 90 data for suitability to test two-dimensional stratospheric models, *J. Geophys. Res., 94*, 18,485–18,493, 1989.

Kanakidou, M., F.J. Dentener, and P.J. Crutzen, A global three-dimensional study of the fate of HCFCs and HFC-134A in the troposphere, *J. Geophys. Res., 100*, 18,781–18,801, 1995.

Khalil, M.A.K., and R.A. Rasmussen, The atmospheric lifetime of methylchloroform (CH_3CCl_3), *Tellus, Ser. B, 36*, 317–332, 1984.

Kleinman, L.I., Low and high NO_x tropospheric photochemistry, *J. Geophys. Res., 99*, 16,831–16,838, 1994.

Klinger, L.F., J. Greenberg, A. Guenther, G. Tyndall, P. Zimmerman, M. Mbangui, and J.M. Moutsambote, Patterns in volatile organic compound emissions along a savanna-rainforest gradient in central Africa, *J. Geophys. Res., 103*, 1443–1454, 1998.

Koch, D.M., D.J. Jacob, and W.C. Graustein, Vertical transport of tropospheric aerosols as indicated by BE-7 and PB-210 in a chemical tracer model, *J. Geophys. Res., 101*, 18,651–18,666, 1996.

Kondo, Y., T. Kitada, M. Koike, S. Kawakami, and Y. Makino, Nitric oxide and ozone in the free troposphere over the western Pacific Ocean, *J. Geophys. Res., 98*, 20,527–20,535, 1993.

Koppmann, R., R. Bauer, F.R. Johnen, C. Plass, and J. Rudolph, The distribution of light non-methane hydrocarbons over the mid-Atlantic: Results of the Polarstern cruise ANT VII/1, *J. Atmos. Chem., 15*, 215–234, 1992.

Koppmann, R., F.J. Johnen, C. Plass-Dulmer, and J. Rudolph, Distribution of methylchloride, dichloromethane, trichloroethene and tetrachloroethene over the north and south Atlantic, *J. Geophys. Res. 98*, 20,517–20,526, 1993.

Krol, M., P.J. van Leeuwen, and J. Lelieveld, Global OH trend inferred from methylchloroform measurements, *J. Geophys. Res., 103*, 10,697–10,711, 1998.

Levy, H., II, Normal atmosphere: Large radical and formaldehyde concentrations predicted, *Science, 173*, 141–143, 1971.

Lindskog, A., and J. Moldanova, The influence of the origin, season and time of the day on the distribution of individual NMHC measured at Rorvik, Sweden, *Atmos. Environ., 28*, 2383–2398, 1994.

Lingenfelter, R.E., Production of carbon 14 by cosmic-ray neutrons, *Rev. Geophys., 1*, 35–55, 1963.

Liu, S.C., Possible effects on tropospheric O_3 and OH due to NO emissions, *Geophys. Res. Lett., 4*, 325–328, 1977.

Liu, W.T., and W. Tang, Precipitable water and surface humidity over global oceans from special sensor microwave imager and European Centre for Medium-Range Weather Forecasts, *J. Geophys. Res., 97*, 2251–2264, 1992.

Logan, J.A., Trends in the vertical distribution of ozone: An analysis of ozonesonde data, *J. Geophys. Res., 99*, 25,553-25,585, 1994.

Logan, J.A., An analysis of ozonesonde data for the troposphere: Recommendations for testing 3-D models and development of a gridded climatology for tropospheric ozone, *J. Geophys. Res., 104*, 16,115–16,149, 1999.

Logan, J.A., M.J. Prather, S.C. Wofsy, and M.B. McElroy, Tropospheric chemistry: A global perspective, *J. Geophys. Res., 86*, 7210–7254, 1981.

Lovelock, J. E., Methyl chloroform in the troposphere as an indicator of OH radical abundance, *Nature, 267*, 32–33, 1977.

Mak, J.E., C.A.M. Brenninkmeijer, and M.R. Manning, Evidence for a missing carbon monoxide sink based on tropospheric measurements of ^{14}CO, *Geophys. Res. Lett., 19*, 1467–1470, 1992.

Mak, J.E., C.A.M. Brenninkmeijer, and J. Tamaresis, Atmospheric ^{14}CO observations and their use for estimating carbon monoxide removal rates, *J. Geophys. Res., 99*, 22,915–22,922, 1994.

Makide, Y., and F.S. Rowland, Tropospheric concentrations of methylchloroform, CH_3CCl_3, in January 1978 and estimates of atmospheric residence times for hydrohalocarbons, *Proc. Natl. Acad. Sci. USA, 78*, 5933–5973, 1981.

Manning, M.R., C.A.M. Brenninkmeijer, and W. Allan, Atmospheric carbon monoxide budget of the Southern Hemisphere: Implications of C-13/C-12 measurements, *J. Geophys. Res., 102*, 10,673-10,682, 1997.

Mather, J.H., P.S. Stevens, and W.H. Brune, OH and HO_2 measurements using laser-induced fluorescence, *J. Geophys. Res., 102*, 6427–6436, 1997.

McConnell, J.C., M.B. McElroy, and S.C. Wofsy, Natural sources of atmospheric CO, *Nature, 233*, 187–188, 1971.

McCormick, M.P., E.W. Chiou, L.R. McMaster, W.P. Chu, J.C. Larsen, D. Rind, and S. Oltmans, Annual variation of water vapor in the stratosphere and upper troposphere observed by the Stratospheric Aerosol and Gas Experiment, *J. Geophys. Res., 98*, 4867–4875, 1993.

McCulloch, A., and P.M. Midgley, The production and global distribution of emissions of trichloroethene, tetrachloroethene, and dichloromethane over the period 1988–1992, *Atmos. Environ., 30*, 601–608, 1996.

McCulloch, A., P.M. Midgley, and D.A. Fisher, Distribution of emissions of chlorofluorocarbons (CFCs) 11, 12, 113, 114 and 115 among reporting and non-reporting countries, *Atmos. Environ., 28*, 2567–2582, 1994.

Mckeen, S.A., et al., Photochemical modeling of hydroxyl and its relationship to other species during the tropospheric OH photochemistry experiment, *J. Geophys. Res., 102*, 6467–6493, 1997.

McPeters, R.D., S.M. Hollandsworth, L.E. Flynn, J.R. Herman, and C.J. Seftor, Long term ozone trends derived from the 16-year combined Nimbus 7/Meteor 3 TOMS Version 7 record, *Geophys. Res. Lett., 23*, 3699–3702, 1996.

Michelsen, H.A., R.J. Salawitch, P.O. Wennberg, and J.G. Anderson, Production of $O(^1D)$ from photolysis of O_3, *Geophys. Res. Lett., 21*, 2227–2230, 1994.

Midgley, P.M., and A. McCulloch, The production and global distribution of emissions to the atmosphere of 1,1,1-trichloroethane (methyl chloroform), *Atmos. Environ., 29*, 1601–1608, 1995.

Midgley, P.M., and A. McCulloch, Estimated national releases to the atmosphere of chlorodifluoromethane (HCFC-22) during 1990, *Atmos. Environ., 31*, 809–811, 1997.

Miller, B.R., J. Huang, R.F. Weiss, R.G. Prinn, and P.J. Fraser, Atmospheric trend and lifetime of chlorodifluoromethane (HCFC-22) and the global tropospheric OH concentration, *J. Geophys. Res., 103*, 13,237–13,248, 1998.

Montzka, S.A., R.C. Myers, J.H. Butler, J.W. Elkins, and S.O. Cummings, Global tropospheric distribution and calibration scale of HCFC-22, *Geophys Res. Lett., 20*, 703–706, 1993.

Montzka, S.A., J.H. Butler, R.C. Myers, T.M. Thompson, T.H. Swanson, A.D. Clarke, L.T. Lock, and J.W. Elkins, Decline in the tropospheric abundance of halogen from halocarbons: Implications for stratospheric ozone depletion, *Science, 272*, 1318–1322, 1996.

Mount, G.H., J.W. Brault, P.V. Johnston, E. Marovich, R.O. Jakoubek, C.J. Volpe, J. Harder, and J. Olson, Measurement of tropospheric OH by long-path laser absorption at Fritz Peak observatory, Colorado, during the OH photochemistry experiment, fall 1993, *J. Geophys. Res., 102*, 6393–6413, 1997.

Muller, J.-F., and G. Brasseur, IMAGES: A three-dimen-

sional chemical transport model of the global troposphere, *J. Geophys. Res., 100*, 16,445–16490, 1995.

Munger, J.W., S.M. Fan, P.S. Bakwin, M.L. Goulden, A.H. Goldstein, A.S. Colman, and S.C. Wofsy, Regional budgets for nitrogen oxides from continental sources: Variations of rates for oxidation and deposition with season and distance from source regions, *J. Geophys. Res., 103*, 8355–8368, 1998.

Novelli, P.C., K.A. Masarie, and P.M. Lang, Distributions and recent changes of carbon monoxide in the lower troposphere, *J. Geophys. Res., 103*, 19,015–19,033, 1998.

Nutmagul, W., and D.R. Cronn, Determination of selected atmospheric aromatic hydrocarbons at remote continental and oceanic locations using photoionization/flame-ionization detection, *J. Atmos. Chem., 2*, 415–433, 1985.

O'Brien, K., Secular variations in the productions of cosmogenic isotopes in the Earth's atmosphere, *J. Geophys. Res., 84*, 423–432, 1979.

Peixoto, J.P., and A.H. Oort, *Physics of Climate*, Am. Inst. of Phys., New York, 1992.

Penkett, S.A., N.J. Blake, P. Lightman, A.R.W. Marsh, P. Anwyl, and G. Butcher, The seasonal variation of non-methane hydrocarbons in the free troposphere over the North Atlantic Ocean: Possible evidence for extensive reaction of hydrocarbons with the nitrate radical, *J. Geophys. Res., 98*, 2865–2886, 1993.

Plumb, A.R., and D.D. McConalogue, On the meridional structure of long-lived tropospheric constituents, *J. Geophys. Res., 93*, 15,897–15,913, 1988.

Prather, M.J., Solution of the inhomogeneous Rayleigh scattering atmosphere, *Astrophys. J., 192*, 787–792, 1974.

Prather, M.J., Timescales in atmospheric chemistry: CH_3BR, the ocean, and ozone depletion potentials, *Global Biogeochem. Cycles, 11*, 393–400, 1997.

Prather, M.J., and D.J. Jacob, A persistent imbalance in HO_x and NO_x photochemistry of the upper troposphere driven by deep tropical convection, *Geophys Res. Lett., 24*, 3189–3192, 1997.

Prather, M.J., and E.E. Remsberg, The atmospheric effects of aircraft: Report of the 1992 Models and Measurements Workshop, *NASA Ref. Publ. 1292*, 1993.

Prather, M.J., and C.M. Spivakovsky, Tropospheric OH and the lifetimes of hydrochlorofluorocarbons, *J. Geophys. Res., 95*, 18,723–18,729, 1990.

Prather, M.J., M.B. McElroy, S.C. Wofsy, G. Russell, and D. Rind, Chemistry of the global troposphere: Fluorocarbons as tracers of air motion, *J. Geophys. Res., 92*, 6579–6613, 1987.

Prinn, R.G., R.A. Rasmussen, P.G. Simmonds, F.N. Alyea, D.M. Cunnold, B.C. Lane, C.A. Cardelino, and A.J. Crawford, The atmospheric lifetime experiment, 5, Results for CH_3CCl_3 based on three years of data, *J. Geophys. Res., 88*, 8415–8426, 1983.

Prinn, R.G., D. Cunnold, R. Rasmussen, P. Simmonds, F. Alyea, A. Crawford, P. Fraser, and R. Rosen, Atmospheric trends in methylchloroform and the global average for the hydroxyl radical, *Science, 238*, 945–950, 1987.

Prinn, R.G., D.M. Cunnold, P.G. Simmonds, F.N. Alyea, R. Boldi, D. Gutzler, D. Hartley, R. Rosen, and R.A. Rasmussen, Global average concentration and trend for hydroxyl radicals deduced from ALE/GAGE trichloroethane (methyl chloroform) data for 1978–90, *J. Geophys. Res., 97*, 2445–2461, 1992.

Prinn, R.G., R.F. Weiss, B.R. Miller, J. Huang, F.N. Alyea, D.M. Cunnold, P.J. Fraser, D.E. Hartley, and P.G. Simmonds, Atmospheric trends and lifetime of CH_3CCl_3 and global OH concentrations, *Science, 269*, 187–192, 1995.

Rasmussen, R. A., and M.A.K. Khalil, Atmospheric benzene and toluene, *Geophys. Res. Lett., 10*, 1096–1099, 1983.

Rasmussen, R.A., and M.A.K. Khalil, Isoprene over the Amazon basin, *J. Geophys. Res., 93*, 1417–1421, 1988.

Ravishankara, A.R., and D.L. Albritton, Methyl chloroform and the atmosphere, *Science, 269*, 183–184, 1995.

Ridley, B.A., J.G. Walega, J.E. Dye, and F.E. Grahek, Distributions of NO, NO_x, NO_y, and O_3 to 12 km altitude during the summer monsoon season over New Mexico, *J. Geophys. Res., 99*, 25,519–25,534, 1994.

Rind, D., and J. Lerner, Use of on-line tracers as a diagnostic tool in general circulation model development, *J. Geophys.Res., 101*, 12,667–12,683, 1996.

Rinsland, C.P., et al., Northern and Southern Hemisphere ground-based infrared spectroscopic measurements of tropospheric carbon monoxide and ethane, *J. Geophys. Res., 103*, 28,197–28,219, 1998.

Roelofs, G.J., and J. Lilieveld, Distribution and budget of tropospheric ozone calculated with a chemistry general circulation model, *J. Geophys. Res., 100*, 20,983–20998, 1995.

Rohrer, F., D. Bruning, and D.H. Ehhalt, Tropospheric mixing ratios of NO obtained during TROPOZ II in the latitude region 67°N-56°S, *J. Geophys. Res., 102*, 25,429–25,449, 1997.

Rosenlof, K.H., and J.R. Holton, Estimates of the stratospheric residual circulation using the downward control principle, *J. Geophys. Res., 98*, 10,456–10,479, 1993.

Rossow, W.B., and R.A. Schiffer, ISCCP cloud data products, *Bull. Am. Meteorol. Soc., 72*, 1–20, 1991.

Rudolph, J., The tropospheric distribution and budget of ethane, *J. Geophys. Res., 100*, 11,369–11381, 1995.

Rudolph, J., and F.J. Johnen, Measurements of light hydrocarbons over the Atlantic in regions of low biological activity, *J. Geophys. Res., 95*, 20,583–20,591, 1990.

Rudolph, J., A. Khedim, and B. Bonsag, Light hydrocarbons in the tropospheric boundary layer over tropical Africa, *J. Geophys. Res., 97*, 6181–6186, 1992a.

Rudolph, J., A. Khedim, T. Clarkson, and D. Wagenbach, Long-term measurements of light alkanes and acetylene in the Antarctic troposphere, *Tellus, Ser. B, 44*, 252–261, 1992b.

Rudolph, J., R. Koppmann, and C. Plassdulmer, The budgets of ethane and tetrachloroethene: Is there evidence for an impact of reactions with chlorine atoms in the troposphere, *Atmos. Environ., 30*, 1887–1894, 1996.

Scheel, H.E., E.-G. Brunke, and W. Seiler, Trace gas measurements at the monitoring station Cape Point, South Africa, between 1978 and 1988, *J. Atmos. Chem., 11*, 197–210, 1990.

Shia, R.-L., Y.L. Yung, M. Allen, R. Zurek, and D. Crisp, Sensitivity study of advection and diffusion coefficients in a two-dimensional stratospheric model using excess carbon 14 data, *J. Geophys, Res., 94*, 18,467–18,484, 1989.

Singh, H.B., Atmospheric halocarbons: Evidence in favor of reduced hydroxyl radical concentrations in the troposphere, *Geophys. Res. Lett., 4*, 241–244, 1977a.

Singh, H.B., Preliminary estimation of average tropospheric HO concentrations in the Northern and Southern Hemispheres, *Geophys. Res. Lett., 4*, 453–456, 1977b.

Singh, H.B., W. Viezee and L.J. Salas, Measurements of selected $C_2 - C_5$ hydrocarbons in the troposphere: Latitudinal, vertical and temporal variations, *J. Geophys. Res., 93*, 15,861–15,878, 1988.

Singh, H.B., D. Ohara, D. Herlth, W. Sachse, D.R. Blake, J.D. Bradshaw, M. Kanakidou, and P.J. Crutzen, Acetone in the atmosphere: Distribution, sources, and sinks, *J. Geophys. Res., 99*, 1805–1819, 1994.

Singh, H.B., M. Kanakidou, P.J. Crutzen, and D.J. Jacob, High concentrations and photochemical fate of oxy-

genated hydrocarbons in the global troposphere, *Nature, 378*, 50–54, 1995.

Singh, H.B., et al., Reactive nitrogen and ozone over the western Pacific: Distribution, partitioning, and sources, *J. Geophys. Res., 101*, 1793–1808, 1996a.

Singh, H.B., A.N. Thakur, Y.E. Chen, and M. Kanakidou, Tetrachloroethylene as an indicator of low Cl atom concentrations in the troposphere, *Geophys. Res. Lett., 23*, 1529–1532, 1996b.

Sobolev, V.V., *Light Scattering in Planetary Atmospheres*, Pergamon, Tarrytown, N.Y., 1975.

Soden, B.J., and F.P. Bretherton, Evaluation of water vapor distribution in general circulation models using satellite observations, *J. Geophys, Res., 99*, 1187–1210, 1994.

Spivakovsky, C.M., Reply, *J. Geophys. Res., 96*, 17,395–17,398, 1991.

Spivakovsky, C.M., and Y.J. Balkanski, Tropospheric OH: Constraints imposed by ^{14}CO and CH_3CCl_3, *Report of the WMO-Sponsored Meeting of Carbon Monoxide (CO) Experts*, edited by P.C. Novelli and R.M. Rosson, pp. 73–75, Global Atmos. Watch, World Meteorol. Organ., Geneva, 1994.

Spivakovsky, C.M., R. Yevich, J.A. Logan, S.C. Wofsy, M.B. McElroy, and M.J. Prather, Tropospheric OH in a three-dimensional chemical tracer model: An assessment based on observations of CH_3CCl_3, *J. Geophys. Res., 95*, 18,441–18,471, 1990.

Talukdar, R.K., A. Mellouki, A.-M. Schmoltner, T. Watson, S. Montzka, and A.R. Ravishankara, Kinetics of the OH reaction with methyl chloroform and its atmospheric implications, *Science, 257*, 227–230, 1992.

Talukdar, R.K., J.B. Burkholder, M. Hunter, M.K. Gilles, J.M. Roberts, and A.R. Ravishankara, Atmospheric fate of several alkyl nitrates, 2, UV absorption cross-sections and photodissociation quantum yields, *J. Chem. Soc. Faraday Trans., 93*, 2797–2805, 1997a.

Talukdar, R.K., S.C. Herndon, J.B. Burkholder, J.M. Roberts, and A.R. Ravishankara, Atmospheric fate of several alkyl nitrates, 1, Rate coefficients of the reactions alkyl nitrates with isotopically labeled hydroxyl radicals, *J. Chem. Soc. Faraday Trans. 93*, 2787–2796, 1997b.

Talukdar, R.K., C.A. Longfellow, M.K. Gilles, and A.R. Ravishankara, Quantum yields of $O(^1D)$ in the photolysis of ozone between 289 and 329 nm as a function of temperature, *Geophys. Res. Lett., 25*, 143–146, 1998.

Tanner, D.J., A. Jefferson, and F.L. Eisele, Selected ion chemical ionization mass spectrometric measurement of OH, *J. Geophys. Res., 102*, 6415–6425, 1997.

Thompson, A.M., Aspects of modeling the tropospheric hydroxyl radical concentration, *Isr. J. Chem., 34*, 277–288, 1994.

Thompson, A.M., and R.J. Cicerone, Atmospheric CH_4, CO and OH from 1860–1985, *Nature, 321*, 148–150, 1986a.

Thompson, A.M., and R.J. Cicerone, Possible perturbations to atmospheric CO, CH_4, and OH, *J. Geophys. Res., 91*, 10,853–10,864, 1986b.

Thompson, A.M., M.A. Huntly, and R.W. Stewart, Perturbations to tropospheric oxidants, 1985–2035, 1, Calculations of ozone and OH in chemically coherent regions, *J. Geophys. Res., 95*, 9829–9844, 1990.

Torres, A.L., and H. Buchan, Tropospheric nitric oxide measurements over the Amazon Basin, *J. Geophys. Res., 93*, 1396–1406, 1988.

Torres, A.L., and A.M. Thompson, Nitric oxide in the equatorial Pacific boundary layer: SAGA 3 measurements, *J. Geophys. Res., 98*, 16,949–16,954, 1993.

Trenberth, K.E., Global analyses from ECMWF and atlas of 1000 to 10 mb circulation statistics, *NCAR/TN-373+STR*, Natl. Cent. for Atmos. Res., Boulder, Colo., 1992.

Volk, C.M., J.W. Elkins, D.W. Fahey, G.S. Dutton, J.M. Gilligan, M. Loewenstein, J.R. Podolske, K.R. Chan, and M.R. Gunson, Evaluation of source gas lifetimes from stratospheric observations, *J. Geophys. Res., 102*, 25,543–25,564, 1997.

Volz, A., D.H. Ehhalt, and R.G. Derwent, Seasonal and latitudinal variation of ^{14}CO and the tropospheric concentration of OH radicals, *J. Geophys. Res., 86*, 5163–5171, 1981.

Wang, Y. H., and D.J. Jacob, Anthropogenic forcing on tropospheric ozone and OH since preindustrial times, *J. Geophys. Res., 103*, 31,123–31,135, 1998.

Wang, Y.H., D.J. Jacob, and J.A. Logan, Global simulation of tropospheric O_3-NO_x-hydrocarbon chemistry, 1, Model formulation, *J. Geophys. Res., 103*, 10,713–10,726, 1998a.

Wang, Y.H., J.A. Logan, and D.J. Jacob, Global simulation of tropospheric O_3-NO_x-hydrocarbon chemistry, 2, Model evaluation, *J. Geophys. Res., 103*, 10,727–10,756, 1998b.

Wang, Y.H., D.J. Jacob, and J.A. Logan, Global simulation of tropospheric O_3-NO_x-hydrocarbon chemistry, 3, Origin of tropospheric ozone and effects of nonmethane hydrocarbons, *J. Geophys. Res., 103*, 10,757–10,768, 1998c.

Warneck, P., On the role of OH and HO_2 radicals in the troposphere, *Tellus, 26*, 39–46, 1974.

Weinstock, B., and H. Niki, Carbon monoxide balance in nature, *Science, 176*, 290–292, 1972.

Weiss, W., A. Sittkus, H. Stockburger, and H. Sartorious, Large-scale atmospheric mixing derived from meridional profiles of krypton 85, *J. Geophys. Res., 88*, 8574–8578, 1983.

Wennberg, P.O., et al., Removal of stratospheric O_3 by radicals: In situ measurements of OH, HO_2, NO, NO_2, ClO, and BrO, *Science, 266*, 398–404, 1994.

Wennberg, P.O., et al., Hydrogen radicals, nitrogen radicals, and the production of O_3 in the upper troposphere, *Science, 279*, 49–53, 1998.

Wofsy, S.C., Interactions of CH_4 and CO in the Earth's atmosphere, *Annu. Rev. Earth Planet. Sci., 4*, 441–469, 1976.

Wofsy, S.C., Temporal and latitudinal variations of stratospheric trace gases: A critical comparison between theory and experiment, *J. Geophys. Res., 83*, 364–378, 1978.

Yang, H., and K.K. Tung, Cross-isentropic stratosphere-troposphere exchange of mass and water vapor, *J. Geophys. Res., 101*, 9413-9423, 1996.

Zander, R., P. Demoulin, D.H. Ehhalt, U. Schmidt, and C.P. Rinsland, Secular increase of the total vertical column abundance of carbon monoxide above central Europe since 1950, *J. Geophys. Res., 94*, 11,021–11,028, 1989.

Zimmerman, P.R., J.P. Greenburg, and C.E. Westberg, Measurements of atmospheric hydrocarbons and biogenic emission fluxes in the Amazon boundary layer, *J. Geophys. Res., 93*, 1407–1416, 1988.

Y. J. Balkanski, Laboratoire des Sciences du Climat et de l'Environnement, U.M.R. CEA-CNRS, L'Orme des Merisiers, Bat. 709, 91191 Gif-sur Yvette, Cedex, France. (ybalkanski@cea.fr)

C. A. M. Brenninkmeijer, Max Planck Institute for Chemistry, P.O. Box 3060, 55060 Mainz, Germany. (carlb@mpch-mainz.mpg.de)

M. Foreman-Fowler, Steelhead Machine and Design, 822 La Luz, Albuquerque, NM 87107. (mfowler@lgmtech.com)

A. C. Fusco, D. B. A. Jones, J. A. Logan, M. B. McElroy, C. M. Spivakovsky, and S. C. Wofsy, Harvard Uni-

versity, 29 Oxford Street, DEAS, Pierce Hall, Cambridge, MA 02138. (acf@io.harvard.edu; dbj@io.harvard.edu; jal@io.harvard.edu; mbm@io.harvard.edu; cms@io.harvard.edu; scw@io.harvard.edu)

L. W. Horowitz, GFDL/NOAA, P.O. Box 308, Princeton University, Princeton, NJ 08542. (lwh@gfdl.gov)

S. A. Montzka, NOAA Climate Monitoring and Diagnostics Laboratory, R/E/CG1, 325 Broadway, Boulder, CO 80303. (smontzka@cmdl.noaa.gov)

M. J. Prather, Department of Geoscience, University of California, Irvine, CA 92717-3100. (mprather@uci.edu)

(Received March 24, 1999; revised September 10, 1999; accepted September 20, 1999.)